

# **Evaluation and Detection of Exosomes and Exosomal microRNAs in Breast Cancer**

Dissertation

with the aim of obtaining a doctoral degree (Dr. rer. nat.)

at the Department of Biology

Faculty of Mathematics, Informatics and Natural Sciences

University of Hamburg

Submitted by

Ines Stevic

Hamburg, 2019

Reviewers of the dissertation:

PD. Dr. Heidi Schwarzenbach

University Medical Center Hamburg-Eppendorf (UKE)

Institute of Tumor Biology

Campus Forschung N27

Martinistraße 52

20246 Hamburg

Prof. Dr. Julia Kehr

University of Hamburg

Faculty of Mathematics, Informatics and Natural Sciences

Department of Biology

Institute of Plant Science and Microbiology

Molecular Plant Genetics

Otto-Warburg-Haus

Ohnhorststr. 18

22609 Hamburg

Date of the disputation: 18.01.2019



Institut für Tumorbiologie

Universitätsklinikum Hamburg-Eppendorf  
Institut für Tumorbiologie  
Martinistraße 52 20246 Hamburg

Zentrum für Experimentelle Medizin

Dr. Linda Scarrott

Visiting scientist from

Boehringer Ingelheim Pharma GmbH & Co. KG

Transl. Medicine + Clin. Pharmacology

Tel.: +49 (7351) 54-187716

Fax: +49 (7351) 83-187716

Hamburg, 28. September 2018

Subject: **English Language Thesis Certification for Ines Stevic**

To whom it may concern,

Ines Stevic, who was born on 20.01.1990 in Sarajevo, Bosnia and Herzegovina, is submitting her doctoral dissertation in English. The title of the thesis is „Evaluation and Detection of Exosomes and Exosomal microRNAs in Breast Cancer”.

I hereby certify as a native English speaker and molecular biologist that I have read the thesis and that the English language used in this thesis is sufficiently correct for submission.

Yours Sincerely,

Dr. Linda Scarrott

Universitätsklinikum Hamburg-Eppendorf  
Zentrum für Experimentelle Medizin  
Institut für Tumorbiologie  
Martinistraße 52, 20246 Hamburg  
Tel. +49 40-74 103-2553, Fax: +49 40-74 103-4546

Gerrichtsbekand: Hamburg

Körperschaft des öffentlichen Rechts

USI-Id: DE 23 8638 948

Bank: HSH Nordbank | BIC: HSHNDE33

PLZ: 210 500 00 | Konto: 104 364 000

IBAN: 019 721 0500 0001 0436 4000

Vorstandsmitglieder:

Prof. Dr. Burkhard Goke (Vorstandsvorsitzender)

Prof. Dr. Dr. Uwe Rich-Gromus | Joachim Proß | Rainer Schöppik



Universitätsklinikum  
Hamburg-Eppendorf

Part of this thesis is was already accepted for publishing in BMC Medicine:

Stevic I, Müller V, Weber K, Fasching PA, Karn T, Marmé F, Schem C, Stickeler E , Denkert C, van Mackelenbergh M, Salat C, Schneeweiss A, Pantel K ,Loibl S, Untch M, Schwarzenbach H. "Specific microRNA signatures in exosomes of triple-negative and HER2-positive breast cancer patients undergoing neoadjuvant therapy within the GeparSixto trial". **BMC Medicine**, accepted on 30. August.

## Table of Contents

Table of Tables.....	IX
Table of Figures .....	X
<b>1. Introduction.....</b>	<b>11</b>
1.1. Mammary gland.....	11
1.2. Breast cancer.....	12
1.3. Histological classification of breast cancer .....	13
1.4. TNM classification and stages of breast cancer .....	15
1.5. Molecular classification of breast cancer .....	16
1.6. Breast cancer metastases .....	17
1.7. Breast cancer therapy.....	18
1.8. Neoadjuvant treatment.....	18
1.8.1. Neoadjuvant treatment in TNBC patients .....	19
1.8.2. Neoadjuvant treatment in HER2-positive patients.....	20
1.9. Extracellular vesicles .....	21
1.10. Exosome biogenesis.....	22
1.11. MiRNAs.....	23
1.11.1. Canonical and non-canonical miRNAs biogenesis .....	24
1.12. History of detection of miRNAs .....	27
1.13. Exosomal miRNAs .....	27
<b>2. Aim of the study .....</b>	<b>30</b>
<b>3. Materials .....</b>	<b>32</b>

3.1.	Commercially available kits .....	32
3.2.	Chemicals and solutions .....	33
3.3.	Antibodies.....	34
3.3.1.	Primary antibodies.....	34
3.3.2.	Secondary antibodies.....	34
3.4.	Buffers and Solutions .....	35
3.5.	Devices .....	37
3.6.	List of 384 miRNAs .....	38
3.7.	Design of hsa-miR-376c-3p oligos.....	42
3.8.	RT <sup>2</sup> Profiler™ PCR Array Human BC .....	42
	The gene list containing following mRNA and controls used in this study: .....	42
3.9.	Triple negative BC cell lines .....	45
3.10.	Study populations.....	45
<b>4.</b>	<b>Methods</b> .....	<b>46</b>
4.1.	Verification of hemolysis in plasma samples .....	46
4.2.	Isolation of total exosomes from plasma samples using ExoQuick .....	46
4.3.	Visualization of exosomes using confocal microscope .....	47
4.4.	ELISA.....	47
4.5.	Western blotting .....	48
4.6.	Extraction of miRNAs and conversion into cDNA .....	51
4.7.	Preamplification of miRNAs .....	52
4.8.	MiRNAs expression profiling .....	53

4.9.	Cell line cultures .....	54
4.10.	Identification of mRNA targets of miR-376c using MirTrap system.....	54
4.11.	Isolation of EVs from cell lines using ultracentrifugation.....	60
4.12.	Nanoparticle tracking analysis .....	61
4.13.	Live imaging of EV shuttle.....	62
4.14.	Transient transfection of cell lines .....	63
4.15.	MTT .....	63
4.16.	Apoptosis measured by FACS .....	64
4.17.	Data normalization and statistical analyses .....	65
<b>5.</b>	<b>Results</b> .....	<b>68</b>
5.1.	Study workflow .....	68
5.2.	Measurement of hemolysis .....	68
5.3.	Patient characteristics comprising categorial and continuous variables.....	69
5.4.	Higher levels of exosomes in the blood circulation of breast cancer patients.....	71
5.5.	Different exosomal miRNA signatures in HER2-positive and TNBC patients .....	74
5.6.	Exosomal miRNA levels after neoadjuvant therapy .....	79
5.7.	Associations of exosomal miRNA levels with the established risk factors .....	80
5.8.	Associations of exosomal miRNA levels with pCR and treatment arm.....	84
5.9.	Identification of potential mRNAs targets of miR-376c .....	87
5.10.	No impact of miR-376c on cell proliferation.....	89
5.11.	No impact of miR-376c on apoptosis .....	90
5.12.	Size distribution of EVs determined by nanoparticles tracking analysis.....	91

5.13.	Shuttle of EV visualized by confocal microscopy .....	92
6.	<b>Discussion</b> .....	95
6.1.	Quantification of exosomal miRNA in BC patients .....	95
6.2.	Potential mRNA targets of miR-376c .....	100
6.3.	Impact of miR-376c on cell proliferation and apoptosis .....	101
6.4.	EV shuttle .....	102
7.	<b>Conclusion</b> .....	104
8.	<b>Future perspectives</b> .....	105
9.	<b>Summary</b> .....	106
10.	<b>Zusammenfassung</b> .....	108
11.	<b>List of Abbreviations</b> .....	110
12.	<b>References</b> .....	115
13.	<b>Acknowledgments</b> .....	129
14.	<b>Eidesstattliche Versicherung</b> .....	131
15.	<b>Declaration on oath</b> .....	132



## Table of Tables

Table 1: Ten most common cancer types grouped by sex .....	10
Table 2: Overview of TNM classification of breast cancer according to the American Joint Committee on Cancer (AJCC), 7th edition, 2010 .....	15
Table 3: Stages of breast cancer according to the American Joint Committee on Cancer (AJCC), 7th edition 2010 .....	16
Table 4: Breast cancer patient characteristics (categorical variables) .....	70
Table 5: Patient characteristics at the time of primary diagnosis of breast cancer (continuous variables) .....	71
Table 6: Significantly deregulated exosomal miRNAs in plasma of HER2-positive and TNBC patients .....	77
Table 7: Significant associations between the plasma levels of exosomal miRNAs and clinicopathological/risk parameters (categorical variables).....	82
Table 8: Significant associations between the plasma levels of exosomal miRNAs and clinicopathological risk parameters (continuous variables) .....	83
Table 9: Logistic regression models for pCR with p-values odd ratio and confidence intervals .....	85
Table 10: Predicted mRNA targets with fold enrichments and function of the gene. ....	88

## Table of Figures

Figure 1: Anatomy of the mammary gland .....	11
Figure 2: Histological subtypes of ER- positive breast cancer .....	13
Figure 3: Histological types of ER-negative breast cancer .....	14
Figure 4: Metastasis .....	17
Figure 5: TNBC subtypes and suggested therapy .....	20
Figure 6: Exosome biogenesis.....	23
Figure 7: MiRNA biogenesis and function .....	26
Figure 8: Release of miRNAs into the blood .....	28
Figure 9: Schematic representation of the gel membrane assembly .....	50
Figure 10: MirTrap system.....	55
Figure 11: Workflow of the study .....	68
Figure 12: Levels of free hemoglobin measured in plasma samples .....	69
Figure 13: Verification and quantification of exosomes .....	73
Figure 14: Hierarchical cluster of 48 exosomal miRNAs .....	75
Figure 15: Volcano plot of 45 exosomal miRNAs.....	76
Figure 16: Exosomal miRNAs differ between HER2-positive and TNBC patients .....	79
Figure 17: Exosomal miRNA levels before and after neoadjuvant therapy.....	80
Figure 18: MiR-376c has no effect on cell proliferation in breast cancer cell lines .....	89
Figure 19: miR-376c impact on apoptosis in MDA-MB-231 and MDA-MB-468 .....	90
Figure 20: Size distribution of EVs determined by NTA.....	91
Figure 21: EVs are localized in the cell membrane.....	92
Figure 22: EVs released from cells .....	93
Figure 23: EVs shuttle from inside of the cell to outside.....	94

## 1. Introduction

### 1.1. Mammary gland

The mammary gland is an organ present exclusively in mammals, and it is responsible for providing nutrition to the newborn. Mammary development begins during embryogenesis and subsequent growth begins in female puberty, and is dependent on the high levels of estrogen (ER) produced by the ovary, as well as the levels of progesterone (PR) (Ali and Coombes, 2002).

The breast epithelium is composed of two cell types, an inner layer of secretory luminal cells and an outer layer of basal/myoepithelial cells. Mammary gland forms a ductal network embedded in an adipose tissue that connects the nipple through collecting ducts to an intricate system of 12-20 lobes (Visvader and Stingl, 2014).

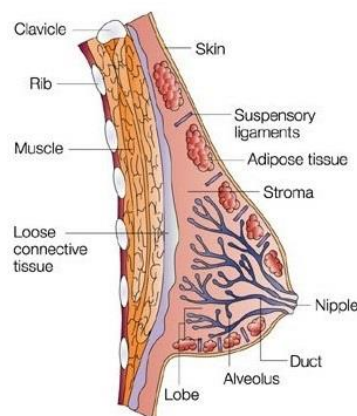




**Figure 1: Anatomy of the mammary gland** (taken from Ali and Coombes, 2002)

The mammary gland is located in the breast covering the pectoralis major, a fan-shaped muscle positioned at the chest. A developed mammary gland comprises alveoli that are surrounded by myoepithelial cells. The alveoli form a complex network of branching ducts. Each duct is lined with a layer of epithelial cells, responsible for milk production under the influence of ER. Each lobule has a lactiferous duct, which opens into the nipple of the breast. The alveoli transport milk from the lobules to the nipple, which is sucked by the infant during breastfeeding.

## 1.2. Breast cancer

Breast cancer (BC) is the second most common cancer in the world, and so far the most frequent cancer among women (Ferlay et al., 2015). BC is the leading cause of cancer deaths in women (Siegel et al., 2017).

**Table 1: Ten most common cancer types grouped by sex** (taken from and adapted according to Siegel et al., 2017)

Estimated new cases			Males	Females			
Prostate	161.360	19%		Breast	252.710	30%	
Lung and bronchus	116.990	14%		Lung and bronchus	105.510	12%	
Colon and rectum	71.420	9%		Colon and rectum	64.010	8%	
Urinary bladder	60.490	7%		Uterine corpus	61.380	7%	
Melanoma of the skin	52.170	6%		Thyroid	42.470	5%	
Kidney and renal pelvis	40.610	5%		Melanoma of the skin	34.940	4%	
Non-Hodgkin lymphoma	40.080	5%		Non-Hodgkin lymphoma	32.160	4%	
Leukemia	36.290	4%		Leukemia	25.840	3%	
Oral cavity and pharynx	35.720	4%		Pancreas	25.700	3%	
Liver and intrahepatic bile duct	29.200	3%		Kidney and renal pelvis	23.380	3%	
<b>All sites</b>	<b>836.150</b>	<b>100%</b>		<b>All sites</b>	<b>852.630</b>	<b>100%</b>	
Estimated Deaths			Males	Females			
Lung and bronchus	84.590	27%		Lung and bronchus	71.280	25%	
Colon and rectum	27.150	9%		Breast	40.610	14%	
Prostate	26.730	8%		Colon and rectum	23.110	8%	
Pancreas	22.300	7%		Pancreas	20.790	7%	
Liver and intrahepatic bile duct	19.610	6%		Ovary	14.080	5%	
Leukemia	14.300	4%		Uterine corpus	10.920	4%	
Esophagus	12.720	4%		Leukemia	10.200	4%	
Urinary bladder	12.240	4%		Liver and intrahepatic bile duct	9.310	3%	
Non-Hodgkin lymphoma	11.450	4%		Non-Hodgkin lymphoma	8.690	3%	
Brain and other nervous system	9.620	3%		Brain and other nervous system	7.080	3%	
<b>All sites</b>	<b>318.420</b>	<b>100%</b>		<b>All sites</b>	<b>282.500</b>	<b>100%</b>	

Estimated new cases of cancers in males and females with estimated deaths cases in the United States.

BC develops from the cells of mammary gland, exhibiting different morphological features, immunohistochemical profiles, and distinctive histopathological subtypes (Makki, 2015).

Nowadays, the wide and regular use of mammography as a screening tool, has improved the early detection of breast lesions (Bocker, 2002).

The incidence of BC increases with genetic predisposition, age and life style factors like weight, alcohol and use of oral contraceptive (McPherson et al., 2000). About 5-10% of all BC cases are hereditary caused by mutations in the tumor suppressor genes BRCA1 and BRCA2 (Walsh et al., 2010). BRCA1 and BRCA2 are tumor suppressors which are essential for the repair of double-strand DNA breaks by homologous recombination and the control of the cell cycle (Narod and Foulkes, 2004; Venkitaraman, 2001).

### 1.3. Histological classification of breast cancer

Breast tumours are categorized into *in situ* carcinoma and invasive (infiltrating) carcinoma.

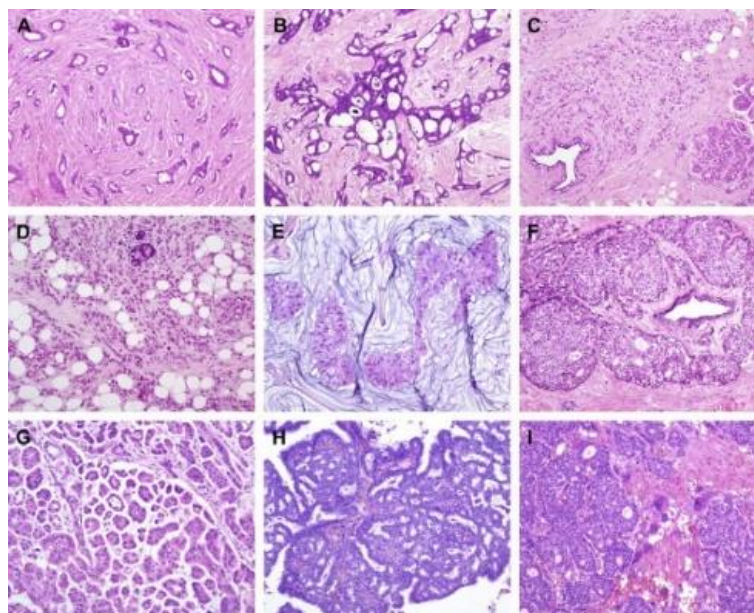


**Figure 2: Histological subtypes of ER- positive BC** (taken from Malhotra et al., 2010)

(A) Tubular carcinoma, (B) cribriform carcinoma, (C) classic invasive lobular carcinoma, (D) pleomorphic invasive lobular carcinoma, (E) mucinous carcinoma, (F) neuroendocrine carcinoma, (G) micropapillary carcinoma, (H) papillary carcinoma, (I) low grade invasive ductal carcinoma with osteoclast-like giant cells.

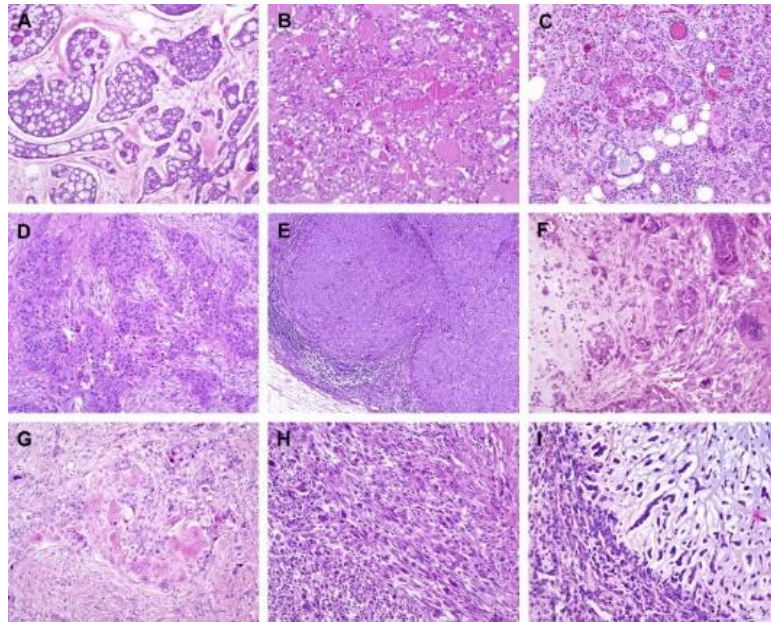


**Figure 3: Histological types of ER-negative BC** (taken from Malhotra et al., 2010)

(A) Adenoid cystic carcinoma, (B) secretory carcinoma, (C) acinic-cell carcinoma, (D) apocrine carcinoma, (E) medullary carcinoma, (F) metaplastic carcinoma with heterologous elements, (G) metaplastic carcinoma with squamous metaplasia, (H) metaplastic spindle cell carcinoma, (I) metaplastic matrix-producing carcinoma.

Breast carcinoma *in situ* is further sub-classified as ductal or lobular tumours. Ductal carcinoma *in situ* (DCIS) is more common than lobular carcinoma *in situ* (LCIS) (Malhotra et al., 2010). DCIS accounts for about 20%–25% of all newly diagnosed cases of BC in the United States and for 17% to 34% of mammography-detected cases (Ernster et al., 2002; May et al., 2000). Lobular carcinomas *in situ* (LCIS) accounts for 1-2% of all BCs (Cutuli et al., 2015). DCIS has traditionally been further sub-classified based on the architectural features of the tumor which has given rise to five well recognized subtypes: comedo, cribriform, micropapillary, papillary and solid (Makki, 2015; Malhotra et al., 2010).

Invasive BCs account for 25% of all BCs and the latest edition of the classification by the World Health Organisation reveals the existence of at least 17 distinct histological subtypes (Figure 2 and Figure 3) (Malhotra et al., 2010).

#### 1.4. TNM classification and stages of breast cancer

The most widely used staging system is the TNM system approved by the American Joint Committee on Cancer (AJCC) and the International Union for Cancer Control (UICC). This system describes the stages of the primary tumor (T), the presence of regional lymph nodes (N), and the occurrence of distant metastases (M) (Edge and Compton, 2010).

**Table 2: Overview of TNM classification of BC according to the American Joint Committee on Cancer (AJCC), 7th edition, 2010**

<b>Primary Tumor (T)</b>	
TX	Primary tumor cannot be assessed
T0	No evidence of primary tumor
Tis (DCIS)	Ductal carcinoma <i>in situ</i>
Tis (LCIS)	Lobular carcinoma <i>in situ</i>
T1	Tumor $\leq$ 2.0 cm
T1mic	Microinvasion $\leq$ 0.1
T1a	Tumor $>$ 0.1 cm but $\leq$ 0.5 cm
T1b	Tumor $>$ 0.5 cm but $\leq$ 1.0 cm
T1c	Tumor $>$ 1.0 cm but $\leq$ 2.0 cm
T2	Tumor $>$ 2.0 cm but $\leq$ 5.0 cm
T3	Tumor $>$ 5.0 cm
T4	Tumor of any size with direct extension to the chest wall or skin
T4a	Extension to the chest wall, do not include pectoralis muscle
T4b	Edema (with peau d'orange) or ulceration of the skin of the breast, or satellite skin nodules confined to the same breast
<b>Regional Lymph Nodes (N)</b>	
NX	Regional lymph nodes cannot be assessed
N0	No regional lymph node metastasis
N1	Metastasis to movable ipsilateral axillary lymph node
N2	Metastasis to ipsilateral axillary lymph node fixed or matted, or in clinically apparent ipsilateral internal mammary nodes in the absence of clinically evident axillary lymph node metastasis
N3	Metastasis in ipsilateral infraclavicular lymph node with or without axillary lymph node involvement or metastasis in ipsilateral supraclavicular lymph node with or without axillary or internal mammary lymph node involvement
<b>Distant Metastasis (M)</b>	
MX	Distant metastasis cannot be assessed
M0	No distant metastasis
M1	Distant metastasis

**Table 3: Stages of breast cancer according to the American Joint Committee on Cancer (AJCC), 7th edition 2010**

<b>Stage 0</b>	Tis	N0	M0
<b>Stage I</b>	T1	N0	M0
<b>Stage IIA</b>	T0	N1	M0
	T1	N1	M0
	T2	N0	M0
<b>Stage IIB</b>	T2	N1	M0
	T3	N0	M0
<b>Stage IIIA</b>	T0	N2	M0
	T1	N2	M0
	T2	N2	M0
	T3	N1	M0
	T3	N2	M0
<b>Stage IIIB</b>	T4	N0	M0
	T4	N1	M0
	T4	N2	M0
<b>Stage IIIC</b>	Any T	N3	M0
<b>Stage IV</b>	Any T	Any N	M1

### 1.5. Molecular classification of breast cancer

BC is a strikingly heterogeneous disease with different clinical, pathological, and molecular features. Molecular classification relies on the characterization of the ER, PR and human epidermal growth factor (HER2) protein expression (Rivenbark et al., 2013) . In 2011, the St. Gallen International Expert Consensus introduced a new classification system for BC consisting of five subgroups. The criteria to identify these subtypes were further refined at the Conference in 2013 where a moderate or strong expression of PR and levels of the proliferative Ki-67 factor were also recognized as being important. According to these criteria, the subtypes have been defined as: Luminal A (ER-positive, HER2-negative, Ki-67 low and PR high), Luminal B (HER2-negative, ER-positive, and either Ki-67 high or PR low), Luminal B-like (HER2-positive, ER-positive, Ki-67 high, and PR high), HER2-positive (ER- and PR-negative) and triple-negative (ER- PR- and HER2-negative) (Goldhirsch et al., 2013; Goldhirsch et al., 2011).



## 1.6. Breast cancer metastases

Metastases arise from cells that have detached from the primary tumor and spread into the blood circulation, forming secondary tumours in distant organs (Chambers et al., 2002). The ability of tumor cells to invade surrounding tissue and migrate through the blood circulation appears to be associated with the epithelial-mesenchymal transition (EMT) (Joosse et al., 2015; Tsai and Yang, 2013). EMT leads to cell dedifferentiation and promotes motility of tumor cells. It is associated with loss of cell-cell contacts, apical-basal polarization, altered adhesion, rearrangement of molecular markers and cytoskeleton organization (Tsai and Yang, 2013). In particular, there is a loss of epithelial cadherin (E-cadherin) expression and the expression of vimentin and neural cadherin (N-cadherin) (Lamouille et al., 2014). When undergoing EMT, tumor cells change partially or fully their epithelial phenotype into a mesenchymal organization. When cells settle down at secondary site, tumor cells can become epithelial. They undergo mesenchymal-epithelial transition, (MET) a reversible processes of EMT (Tsai and Yang, 2013).

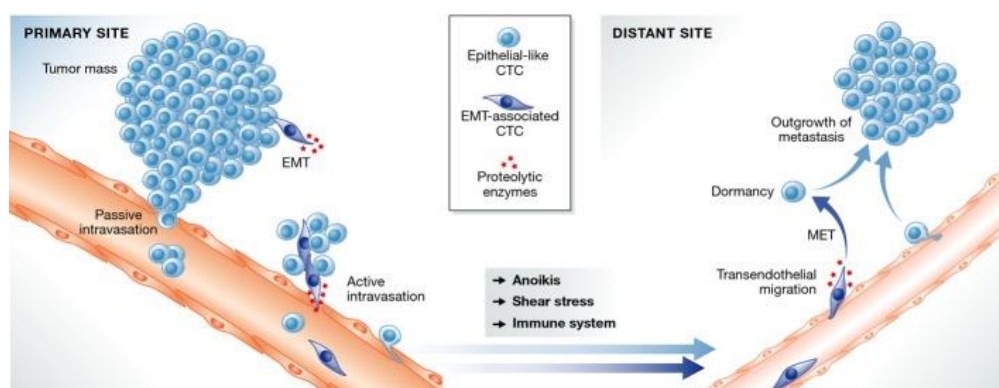


**Figure 4: Metastasis** (taken from Joosse et al., 2015)

Epithelial cancer cells undergo epithelial-mesenchymal transition (EMT) and become mesenchymal. They detach from the primary tumor and migrate through the extracellular matrix into the blood circulation. Once, the cancer cells reach a distant site, undergo mesenchymal-epithelial transition (MET), it enter the state of dormancy and/or grow to become metastasis.

### **1.7. Breast cancer therapy**

Since 2011, the St. Gallen Consensus has been aiming at standardizing a treatment tailored toward clinical and biological subgroups of BC. There are five subtypes of BC that demand individual treatment approaches. TNBC for which chemotherapy is the only option, HER2-positive tumours, for which anti-HER2 therapy and chemotherapy are applied and luminal BC types which are treated with endocrine therapy. The majority of the patients who are hormone receptor positive do not need chemotherapy. The receptor status is determined by immunohistochemistry (IHC) and/or *in situ* hybridization assays. In addition, tumours are characterized by grade and proliferative factors (usually by Ki-67 immunostaining) that may facilitate the decision for an additional chemotherapy in ER positive patients (Curigliano et al., 2017). TNBC is an aggressive subtype with a higher incidence of relapse and death. Even with an adjuvant chemotherapy, the 5-year disease free survival rate remains low (Biswas et al., 2017).

### **1.8. Neoadjuvant treatment**

Neoadjuvant treatment describes a therapeutic intervention prior to surgery. In BC, the aim of neoadjuvant treatment is to reduce the size of unresectable tumours, to enable surgery to be performed. For operable tumours, neoadjuvant treatment allows for higher conservation of the breast by decreasing the need for mastectomy. Today, neoadjuvant therapy is also increasingly considered a platform for testing novel therapies (von Minckwitz and Martin, 2012).

### 1.8.1. Neoadjuvant treatment in TNBC patients

TNBC is the BC subtype with the poorest prognosis. The heterogeneous nature and loss of ER, PR and HER2 in TNBC tumours may explain the difficulty in treating this BC subtype (Omarini et al., 2018). Lehmann et al. Have shown that TNBC is a highly diverse group of cancers and using cluster analysis they identified 6 TNBC subtypes with unique gene expression patterns including 2 basal-like (BL1 and BL2), an immunomodulatory (IM), a mesenchymal (M), a mesenchymal stem-like (MSL), and a luminal androgen receptor (LAR) subtype (Lehmann et al., 2011).

The combination of new therapeutic agents with standard neoadjuvant anthracycline/taxane therapies are currently being investigated as novel treatments strategies for TNBC patients. As shown in Figure 5, a promising therapy with different agents is proposed for each subtype (Omarini et al., 2018). The agents being included can be DNA-damaging agents (e.g. platinum), as well as potentiators of DNA damage, an investigational agent iniparib, and inhibitors of poly-ADP ribose polymerase, such as olaparib. The use of neoadjuvant treatment and the determination of pCR as a surrogate of overall survival will allow the rapid evaluation of these novel combination therapies (von Minckwitz and Martin, 2012).

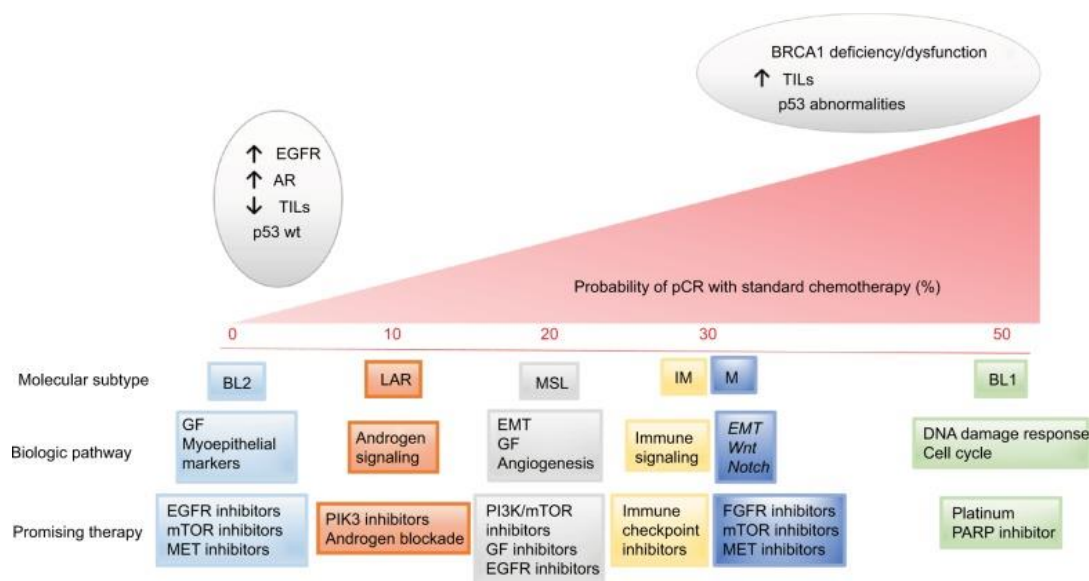


**Figure 5: TNBC subtypes and suggested therapy** (taken from Omarini et al., 2018)

TNBC molecular subtypes (BL1 and BL2, basal like; IM, immunomodulatory; M, mesenchymal; MSL, mesenchymal stem-like; LAR, luminal androgen receptor) are shown with their main biological pathways and suggested therapy regimens. Each of these subtypes shows a different pCR rate to the standard neoadjuvant chemotherapy.

### 1.8.2. Neoadjuvant treatment in HER2-positive patients

In early HER2-positive BC patients, neoadjuvant treatment with a combination of sequential chemotherapy and HER2-targeted therapy is currently the standard of care (Harbeck and Gluz, 2017). This is followed by breast surgery, radiotherapy, completion of 1 year of HER2-directed therapy, and – depending on the tumor biology – endocrine adjuvant therapy (Wuerstlein and Harbeck, 2017).

The anthracycline-taxane based neoadjuvant chemotherapy consists of anthracyclines (e.g. doxorubicin, epirubicin, liposomal doxorubicin) and taxanes (e.g. docetaxel, paclitaxel, nab-paclitaxel).

The anthracycline form irreversible complexes with DNA and topoisomerase II to induce apoptosis thus, inhibit DNA and RNA synthesis. By stabilising microtubules taxane inhibit cell

division. The randomized phase III GeparQuattro study carried out by the German Breast Group/Gynecologic Oncology Study Group revealed that combining trastuzumab (a monoclonal antibody to HER2) with anthracycline-taxane –based neoadjuvant chemotherapy results in a high positive pCR rate without clinically relevant, early toxicity in HER2-positive patients (Untch et al., 2010). Also, the administration of carboplatin improves pCR rates regardless of patients’ BRCA status. Whether or not this treatment will translate into a survival benefit remains unclear (Harbeck and Gluz, 2017).

The 10-year survival rates in the HER2-positive BC subgroup do reach now more than 75% since the introduction of the first adjuvant and later neoadjuvant HER2-targeted therapies in the last years (Wuerstlein and Harbeck, 2017).

### **1.9. Extracellular vesicles**

Extracellular vesicles (EVs) were first observed in 1967 by Peter Wolf who referred them as “platelet dust” and characterized them as platelet-secreted vesicles during blood coagulation (Wolf, 1967). EVs are a heterogeneous population of lipid bilayer membrane vesicles and range in size from 30 to 10000 nm in diameter. EVs are shed from the surface of cells into the extracellular environment in a highly regulated process (Tricarico et al., 2017). They have emerged as a novel and important player in intercellular communication, mainly through their ability to transfer their biological content, consisting of proteins, lipids, and nucleic acids, to recipient cells (Colombo et al., 2014; Wen et al., 2017; Willms et al., 2018). This EV shuttle may modify the behaviour of target cells at close or distant sites. Regardless of their origin, all EVs include RNA, lipids, proteins and possibly DNA (Bebelman et al., 2018). *In vivo*, EVs are found in blood, urine, amniotic fluid, breast milk, seminal fluid, saliva and malignant effusions. Based on their origin, EVs can be divided into subgroups of “small” vesicles and “big” vesicles (Bebelman et al., 2018). Exosomes belong to the small membrane vesicles, 40–100 nm in

diameter, secreted when multivesicular bodies (MVBs) fuse with the plasma membrane (Hessvik et al., 2012). In 1987 Rose Johnstone, a pioneer in this field, chose the term “exosome” and emphasized that “the process seemed to be akin to reverse endocytosis, with internal vesicular contents released in contrast to external molecules internalized in membrane-bound structures” (Hessvik and Llorente, 2018; Johnstone et al., 1987). In 2007 a breakthrough in the field was made when exosomes were detected to carry nucleic acids, namely mRNA and miRNA (Valadi et al., 2007a).

### **1.10. Exosome biogenesis**

Exosome biogenesis starts within the endosomal system. First, early endosomes mature into late endosomes or MVBs (Bellingham et al., 2012). During this process, the endosomal membrane invaginates to generate intraluminal vesicles (ILVs) in the lumen of the organelles (Huotari and Helenius, 2011). The components of the endosomal sorting complex required for transport (ESCRT) are involved in MVB and internal luminal vesicle (ILV) biogenesis. ESCRTs consist of approximately 20 proteins that assemble into 4 complexes (ESCRT-0, -I, -II and -III) and are conserved from yeast to mammals (Henne et al., 2011).

The ESCRT pathway is subdivided into early stages where cargo is recognized and potentially clustered (ESCRT-0, -I, and -II) until it is corralled by the downstream ESCRT-III complex, which lacks ubiquitin binding, but is able to couple ESCRT-III assembly with cargo deubiquitination and vesicle budding (Henne et al., 2011). Each ESCRT orchestrates a discrete step in MVB vesicle formation. ESCRT-0, together with flat clathrin coats, forms a protein network on endosomal membranes, capturing ubiquitinated cargo proteins and initiating their sorting into the MVB pathway (Ren et al., 2009). After initial involution of the limiting membrane into the MVB lumen triggered by ESCRT-I/II, ESCRT-III forms a spiral-shaped

structure that constricts the budding neck, and the ATPase VPS4 drives membrane scission (Henne et al., 2011).

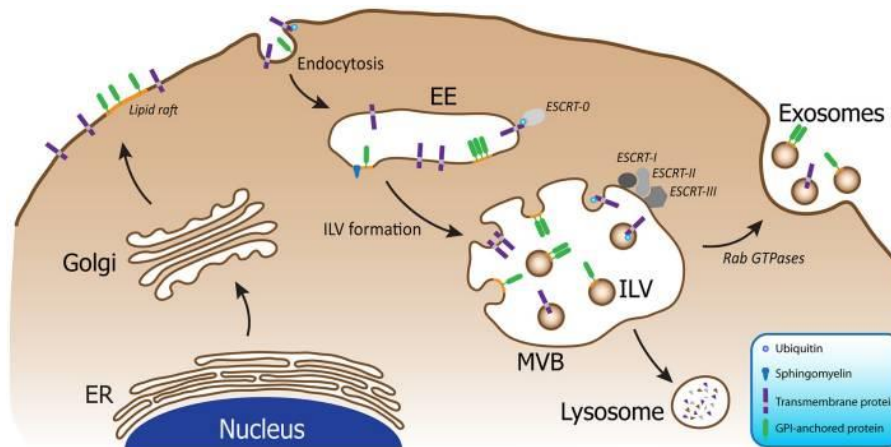


**Figure 6: Exosome biogenesis** (taken from Bellingham et al., 2012)

The biogenesis of exosomes starts with the endocytosis of microvesicles that fuse to an early endosome (EE). EE serve as initial sorting endosomes where cargo is packaged into internal luminal vesicle (ILVs) within MVBs upon inward budding of the membrane. MVBs can then fuse with lysosomes. In this case, the cargo is degraded or the MVBs can fuse with the plasma membrane, resulting in release of ILVs as exosomes. This process is regulated by Rab GTPases.

### 1.11. MiRNAs

MicroRNAs (miRNAs) are a class of small non-coding RNA molecules with approximately 18-25 nucleotides in length. They regulate gene expression post-transcriptionally by binding to the 3' untranslated region (UTR), coding sequences or 5' UTR of target mRNAs, leading to inhibition of translation or mRNA degradation (Filipowicz et al., 2008; Krek et al., 2005). MiRNAs may have dual functions and be both, tumor suppressors and oncogenes. Numerous studies have shown that miRNAs act as oncogenes by downregulating the protein expression of tumor suppressor genes and thereby, contributing to tumor formation by stimulating cell

proliferation, angiogenesis and/or tumor invasion. Conversely, miRNAs can also act as tumor suppressors by downregulating proteins with oncogenic activity (Garzon et al., 2010; Shenouda and Alahari, 2009).

MiRNAs are involved in biological and pathological processes, including tumorigenesis, and have important regulatory roles in cell development, differentiation, proliferation and apoptosis (Filipowicz et al., 2008; Krek et al., 2005; Slaby et al., 2009). The binding of miRNAs to the target mRNA is critical for regulating the mRNA level and protein expression. Since there are more than 2000 miRNAs (Friedlander et al., 2014) and a single miRNA can bind to at least 100 different target transcript, (Filipowicz et al., 2008) it has been estimated that miRNAs are able to modulate up to 60% of protein-coding genes in the human genome at the translational level (Friedman et al., 2009).

MiRNAs could be an ideal class of blood-based biomarkers for cancer detection because miRNAs expression is frequently dysregulated in different cancers and appears to be tissue-specific (Ludwig et al., 2016). Therefore, circulating miRNAs may be useful as diagnostic, prognostic, and/or predictive biomarkers, and may also have relevance as new therapeutic targets.

### **1.11.1. Canonical and non-canonical miRNAs biogenesis**

The first step in miRNAs synthesis begins in the nucleus with a long primary miRNA (pri-miRNA). The pri-miRNA has an hairpin stem length of approximately 35 nucleotides and apical loop sizes of approximately 3-23 nucleotides with a presence of primary sequence motifs e.g. the CNNC motif and the UG motif (Adams, 2017). The pri-miRNA is produced after miRNA gene transcription by RNA polymerase II or, less commonly, by RNA polymerase III (Bartels and Tsongalis, 2009; Borchert et al., 2006; Lee et al., 2004). The initial processing step of pri-miRNA is mediated by the microprocessor complex. This complex comprises the double-



stranded RNA-specific ribonuclease III-type endonuclease, Drosha, with its cofactor DGCR8, a double-stranded RNA-binding protein responsible for recognizing the hairpin loop of the pre-miRNA and ensuring correct cleavage by Drosha. A hairpin-shaped precursor miRNA of approximately 70 nucleotides in length is formed. Subsequently, the pre-miRNA, is exported from the nucleus by Exportin-5–Ran-GTP. In the cytoplasm, Rnase Dicer in complex with the double-stranded RNA-binding protein TRBP cleaves the pre-miRNA hairpin to its mature length of approximately 22 nucleotides. The miRNA duplexes then form complexes with the RNA-induced silencing complex (RISC), leading to unwinding of the miRNAs duplexes to form single-stranded miRNAs. Important components of this complex are proteins of the Argonaute family, such as AGO1, AGO2, AGO3 and AGO4 (Corcoran et al., 2011; Filipowicz et al., 2008; Winter et al., 2009). The AGO2-bound mature miRNA is subsequently assembled into effector complexes termed miRNA-containing ribonucleoprotein particles (Heman-Ackah et al., 2013).

Within the RISC, miRNAs pair to an mRNA usually through imperfect base pairing within the 3'UTR. The “seed” region (nucleotides 2–7) at the 5' end of the miRNA is sufficient for the specificity and functionality of the negative posttranscriptional regulation of gene expression. However, miRNAs have also been implicated in regulating mRNA degradation by accelerating decapping, deadenylation and compartmentalization of the mRNA (Corcoran et al., 2011).

Non-canonical miRNAs are a subset of miRNAs, including snoRNAs, endogenous shRNAs and tRNAs. They structurally and functionally resemble canonical miRNAs, but they were found to follow distinct maturation pathways, typically bypassing one or more steps of the classic canonical biogenesis pathway (Abdelfattah et al., 2014).

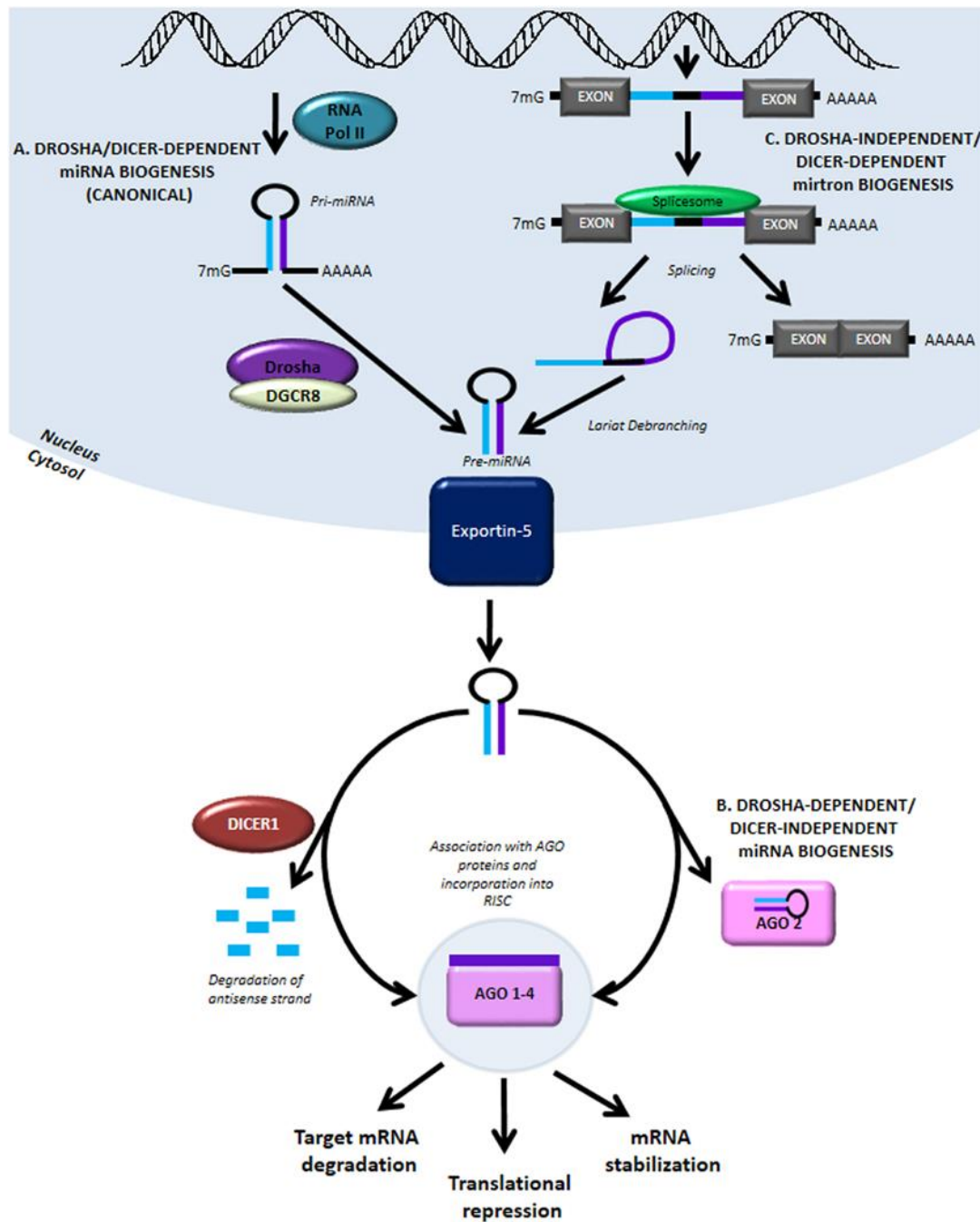


**Figure 7: MiRNAs biogenesis and function** (taken from Heman-Ackah et al., 2013)

(A) The canonical miRNAs biogenesis pathway is Drosha- and Dicer-dependent. The pri-miRNA is initially transcribed by RNA polymerase II, and then cleaved by Drosha with DGCR8 to generate a hair-pin-folded pre-miRNA. Following the transport to the cytoplasm by Exportin 5, the pre-miRNA is processed by Dicer and TRBP to the double-stranded mature miRNA (B) In a Drosha-dependent and Dicer-independent non-canonical pathway the cytoplasmic pri-miRNA is bound by AGO2 (C) A further non-canonical pathway involves Drosha-independent and Dicer-dependent biogenesis and generates mirtrons, transcribed from intronic sequences and obtained by splicing and lariat-debranching.

### **1.12. History of detection of miRNAs**

First characterized in 1993, miRNAs *lin-4* and *let-7* were initially shown to be involved in the control of developmental timing in *Caenorhabditis elegans*. When *lin-4* or *let-7* were inactivated, specific epithelial cells underwent additional cell divisions instead of their normal differentiation process. Based on this observation that miRNAs control cell proliferation and apoptosis in *C. Elegans* and *Drosophila* (Fu et al., 2011), it was assumed that miRNAs play a role in cancer.

Then in 2002, the first report was published suggesting the important function of miRNAs in cancer. In this regard, Calin et al. Discovered that miR-15 and miR-16 located at chromosome 13q14 are deleted or downregulated in over 60% of B-cell in chronic lymphocytic leukemia (CLL) (Calin et al., 2002). In 2004, the same group identified a significant percentage of miRNAs to be located at fragile sites that harboured amplification, loss of heterozygosity (LOH) or breakpoints (Calin et al., 2004).

### **1.13. Exosomal miRNAs**

Besides the release of miRNAs by apoptosis and necrosis, miRNAs are actively secreted into the peripheral blood circulation and other body fluids where they are protected from enzymatic degradation by the surrounding phospholipid membrane of exosomes (Schwarzenbach et al., 2014).

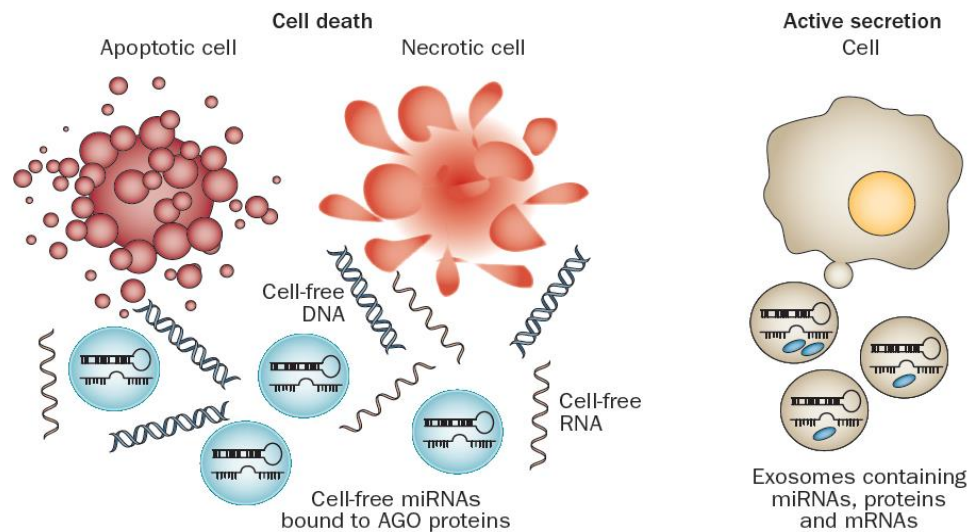


**Figure 8: Release of miRNAs into the blood** (taken from Schwarzenbach et al., 2014)

MiRNAs can be released into the blood by cell death (apoptosis and necrosis) or active secretion (exosomes). Apoptosis leads to cell shrinkage and releases fragmented cell remnants and apoptotic bodies, including RNA transcripts and short DNA fragments. Necrosis leads to cell swells and releases long DNA strands. RNA transcripts released by apoptotic and necrotic cells form complexes with specific RNA-binding proteins (e.g. AGO proteins). Living cells can actively secrete miRNA-containing exosomes into the extracellular space through the fusion of MVBs with the plasma membrane.

Currently, there are some studies that have analysed circulating exosomal miRNAs in plasma or serum from BC patients. Eichelser et al. Showed that a prevalence of miR-101, miR-372 and miR-373 were found in exosomes and not cell free in the plasma. The levels of circulating exosomal miR-373 were higher in TNBC than luminal carcinomas. ER-and PR-negative tumours displayed higher concentrations of exosomal miR-373 than patients with hormone-receptor positive tumours (Eichelser et al., 2014). Moreover, Yoshikawa et al. Showed that exosomal miR-223-3p may be useful as a minimally invasive biomarker for DSIC patients diagnosed by biopsy (Yoshikawa et al., 2018).

Exosomes can also transmit drug resistance through delivering miRNAs. Zhong et al. Analysed changes of exosomal miRNA levels in BC MDA-MB-231 sublines that developed resistance to docetaxel, epirubicin or vinorelbine. Different miRNAs were found to be upregulated as well

as loaded at an increased copy number into exosomes from the different resistant cell lines. (Zhong et al., 2016). These findings suggest that miRNAs are selectively packed in exosomes, although the underlying mechanism remains largely unclear (Zhang et al., 2015).

Hannafon et al. showed that cancer cell derived exosomes can modulate angiogenesis. Docosahexaenoic acid (DHA) is a natural compound with anti-angiogenic properties, currently under investigation as a dietary supplement for BC prevention and treatment. *In vitro* treatment of BC cells with DHA altered exosome secretion rate, and miRNAs, such as let-7a, miR-23b, miR-27a/b, miR-21, let-7, and miR-320b known to have anti-cancer and/or anti-angiogenic activity, were increasingly enriched in the exosomes from BC lines but not in exosomes from normal breast cells (Hannafon et al., 2015).

## 2. Aim of the study

The aim of this study was to analyse which miRNAs play a role in cell to cell shuttle of exosomes in breast cancer along with the determination of their potential target mRNAs whose protein products participate in signalling pathways.

The study consisted of four subparts, each performed based on the previous project part.

### Quantification of circulating exosomal miRNAs in the plasma of BC patients

Triple-negative and HER2-positive tumours are the most aggressive forms of BC. Despite of systemic therapy in the (neo)adjuvant setting, these tumours progress, metastasize and develop resistance in a considerable number of patients, thus emphasizing the need for monitoring of treatment and a better understanding of resistance. Therefore, the aim of this study was to identify particular miRNA signatures in exosomes of these two subgroups, and to examine their clinical relevance, to distinguish BC patients who respond to carboplatin therapy from resistant patients.

The deregulation of exosomal miRNAs was determined in 15 patients before neoadjuvant therapy, using quantitative TaqMan real-time PCR-based miRNAs array cards containing 384 different miRNAs. Afterwards, 45 most clinically relevant exosomal miRNAs were selected and quantified in plasma of 211 HER2-positive and 224 TNBC patients before neoadjuvant therapy, 20 healthy women, and in plasma samples of 4 HER2-positive and 5 TNBC patients after therapy. The data were compared with clinical parameters and statistically evaluated.

### Identification potential mRNA targets of miR-376c

The second aim was to identify potential mRNAs targets of one of those most deregulated exosomal miRNAs (miR-376c) that has been detected in the first part of the project.

The screening was carried out by the MirTrap system containing the RISC complex which is expressed by the pMirTrap vector, and is able to bind miRNAs to its targets mRNAs. Then the targeted mRNAs were identified by immunoprecipitation and mRNA array.

#### Functional analysis of miR-376c

The focus of this part of the study was to check whether miR-376c effects cell proliferation and apoptosis. BC cells were transfected with mimics and inhibitors of miR-376c. Cell proliferation was tested using MTT assay, and apoptosis was measured using FACS.

#### Characterization of EVs and EV shuttle using confocal microscopy

The final aim of this study was to characterize EVs and visualize EVs shuttle between cells in a live cell imaging experiment. EVs shuttle was monitored using red fluorescent stained EVs under a confocal microscope. Nanoparticle tracking analysis (NTA) was used for determining size and concentrations of EVs isolated by ultracentrifugation.

### 3. Materials

#### 3.1. Commercially available kits

AllStars Negative Control siRNA	Qiagen, Hilden, Germany
DC Protein Assay Kit	Bio-Rad, Hercules, USA
ExoELISA Complete Kit (CD63 Detection)	System Biosciences, Palo Alto USA
Exo-Glow™-Exosome Labeling Kits	BioCat, Heidelberg, Germany
ExoQuick exosome precipitation solution	BioCat, Heidelberg, Germany
ExoQuick TC	BioCat, Heidelberg, Germany
Exosome Antibodies & ELISA Kit	System Bioscience
FITC Annexin V Apoptosis Detection Kit with 7-AAD	BioLegend, San Diego, USA
HiPerFect Transfection Reagent	Qiagen, Hilden, Germany
hsa-miR-376c inhibitor	Qiagen, Hilden, Germany
hsa-miR-376c mimics	Qiagen, Hilden, Germany
MirTrap Control Kit	Takara BioCat,
MirTrap Isolation Kit	Takara BioCat,
miScript Inhibitor Negative Control	Qiagen, Hilden, Germany
NucleoSpin RNA XS Kit	Macherey-Nagel Düren, Germany
One-Step SYBR® PrimeScript™ RT-PCR Kit II	Takara, Kusatsu, Shiga Prefecture, Japan
PKH26 Red Fluorescent Cell Linker Kit for General Cell Membrane Labeling	Sigma Aldrich, Munich, Germany
pMirTrap Vector	Takara, Kusatsu, Shiga Prefecture, Japan
RT PreAMP cDNA Synthesis kit	Qiagen, Hilden, Germany
RT <sup>2</sup> Profiler™ PCR Array Human Breast Cancer	Qiagen, Hilden, Germany
TaqMan miRNA ABC Purification Kit	Thermo Fisher Scientific, Massachusetts
TaqMan MiRNA Reverse Transcription kit	Thermo Fisher Scientific, Massachusetts
TaqMan PreAmplification kit	Thermo Fisher Scientific, Massachusetts
TaqMan® Universal Master Mix II	Thermo Fisher Scientific, Massachusetts
Venor® GeM Classic Kits	Minerva-Biolabs, Berlin Germany
Xfect MiRNA Transfection Reagent	Takara, Kusatsu, Shiga Prefecture, Japan



### 3.2. Chemicals and solutions

BSA (Bovines Serum Albumin)	Sigma-Aldrich, Munich, Germany
Camptothecin	Biovision , San Francisco, USA
DMEM-(Dulbecco's Modified Eagle's Medium)	Thermo Fisher Scientific, Massachusetts
DPBS (Dulbecco's Phosphate Buffered Saline)	Gibco Life Technologies
EASY Dilution solution for Real-time PCR	Takara Bio, Cat
Ethanol	J.T. Baker, Deventer, NL
Ethidiumbromid	Sigma-Aldrich, Munich, Germany
Fetal bovine serum (FBS)	Capricorn Scientific, Ebsdorfergrund Germany
H <sub>2</sub> O <sub>2</sub>	Carl Roth, Karlsruhe
HCl	Sigma-Aldrich, Munich, Germany
HEPES	Carl Roth, Karlsruhe
Immobilon-P Membran, PVDF, 0.45 µm	Merck, Darmstadt
Isopropanol (2-Propanol)	Sigma-Aldrich, Munich
L-Glutamine 200 mM	Thermo Fisher Scientific, Massachusetts
Loading Buffer (6x)	Fisher Scientific, Schwerte
Luminol	Sigma-Aldrich, Munich
Methanol	J.T. Baker, Deventer, NL
MTT(3-(4,5-Dimethylthiazol-2-yl)-2,5-Diphenyl tetrazolium Bromide)	Sigma-Aldrich, Munich, Germany
NaCl	Carl Roth, Karlsruhe
NaOH	Carl Roth, Karlsruhe
Nuclease free Water	Qiagen, Hilden, Germany
p-Cumarsäure Sigma-Aldrich	Sigma-Aldrich, Munich
Powdered milk, blotting grade	Carl Roth, Karlsruhe
Protease Inhibitor Cocktail Tablets: Complete, Mini, EDTA-free	Roche Applied Science,
ProtoGel 30%	National Diagnostics, Atlanta
RIPA buffer (Radio immunoprecipitation assay buffer)	Merck, Darmstadt
GelRed® Nucleic Acid Gel Stain	Biotium, USA
SDS (Sodium dodecyl 33ulphate)	Affymetrix USB, Santa Clara
Streptomycin/Penicillin (200 U/mL)	Thermo Fisher Scientific, Massachusetts
TEMED (Tetramethylethylenediamine)	Sigma-Aldrich, Munich, Germany
Thrombin	BioCat, Heidelberg, Germany

---

Transfer membrane FlouoroTrus PVDF, 0.2 $\mu$ m	Pall Laboratory
Trizma Base	Sigma-Aldrich, Munich, Germany
Trypsin/ EDTA (25%)	Thermo Fisher Scientific, Massachusetts
Tween 20	Merck, Darmstadt, Germany

### 3.3. Antibodies

#### 3.3.1. Primary antibodies

CD63	1:1000	ABGENT, San Diego, California, USA
CD81	1:500	Invitrogen, Darmstadt, Germany
AGO2	1:2000	TAKARA BIO INC, Shiga, Japan

#### 3.3.2. Secondary antibodies

Anti-mouse immunoglobulins HRP	1:2000	Dako, Glostrup, Denmark
Anti-rabbit immunoglobulins HRP	1:2000	Dako, Glostrup, Denmark

### 3.4. Buffers and Solutions

#### Erythrocyte lysis buffer

Sucrose	0.3 M
Tris pH 7.5	10 mM
MgCl <sub>2</sub>	5 mM
Triton X100	1%

#### Lysis buffer

HCl	4 mM
0.1% NP-40 in isopropanol	

#### 4x SDS Sample buffer

Tris (pH 6.8)	240 mM
Glycerol	40% (v/v)
Bromphenolblue	0.1% (w/v)
SDS	4% (w/v)

#### 10x TBS

Tris	50 mM
NaCl	150 mM
pH	set to 7.6
H <sub>2</sub> O	add up to 1 L

#### 1x TBST

10x TBS	100 mL
H <sub>2</sub> O	900 mL
Tween 20	1000 µl

#### 5x Laemmli

Glycin	960 mM
Tris	125 mM
SDS	17 mM
H <sub>2</sub> O	add up to 1 L

## 1x Transfer Buffer

Tris	48 mM
Glycin	39 mM
SDS	0.037% (v/v)
MeOH	20%
H <sub>2</sub> O	add up to 1 L

## Detection solution for Western blot

## Solution A

p-Cumarsäure	0.2 mM
Luminol	1.25 mM
Tris (pH 8.5)	100 mM
H <sub>2</sub> O	8.85 mL

## Solution B

H <sub>2</sub> O <sub>2</sub>	0.06% (v/v)
Tris (pH 8.5)	100 mM
H <sub>2</sub> O	9 mL

## Mix Solution A and Solution B

## Medium for Agar plates

LB-Agar (Luria Miller)	40 g
Ampicillin	100 µg/mL
H <sub>2</sub> O	add up to 1 L

### 3.5. Devices

7300 HT Real-Time PCR System 384 block	Thermofisher Scientific, Massachusetts, USA
Analysenwaage BP610	Sartorius, Göttingen
Analysenwaage CPA224S-0CE	Sartorius, Göttingen
Automatic-Sarpette®	Sarstedt, Nümbrecht
Dokumentation Mikroskop-AxioCam MRc	Carl Zeiss (Oberkochen)
Electronic Hemocytometer Vi-CELL™XR	Beckman Coulter (Brea, CA, USA)
FACS Canto II	BD Biosciences, Heidelberg
Fridge -20	Liebherr, Kirchdorf
Fridge -80	Kryotec-Kryosafe, Hamburg
Heidolph magnetic stirrers	Merck, Darmstadt
Heidolph™ Rotamax Orbital Platform Shaker	Fisher Scientific, Hampshire, USA
Inkubator HerraCell 150i	Thermofisher Scientific, Massachusetts, USA
Leica TCS SP5	Wetzlar, Germany
Leica TCS SP8	Wetzlar, Germany
MC 6, Centrifuge	Sarstedt, Nümbrecht
Microcentrifuge, MiniStar	VWR Radnor, Pennsylvania, United States
Microplate reader	Tecan, Männerdorf, Switzerland)
MJ Research PTC-200 Peltier Thermal Cycler	Global Medical Instrumentation
NanoSight LM10instrument	NanoSight Technology, Malvern, UK
Optima LE-80K Ultracentrifuge	Beckman Coulter (Brea, CA, USA)
peqSTAR 96 Universal Gradient	Isogen Life science, Utrecht, Netherlands
pH-Meter	InoLab WTW, Weilheim
qPCR CFX96	Bio-Rad, Hercules, USA
Qubit 2.0	Invitrogen by life technologies
Real time PCR 7300 HT 384 block	Applied Biosystems
Roller, SRT 6	Bibby Scientific, Staffordshire, UK
Sonicator UP50H	Hielscher Ultrasonics, Teltow
Spectrophotometric plate reader	Tecan, Männerdorf
Table centrifuge 5415R	Eppendorf, Hamburg
Thermomixer comfort	Eppendorf, Hamburg
Vortex-Genie 2	Scientific industries inc, New York USA
Watterbath 1003 GFL	GmbH für Labortechnik, Burgwedel
XCell SureLock® Mini- Cell device	Thermofisher Scientific, Massachusetts, USA
X-ray developer Curix60	AGFA, Mortsel, Belgium

### 3.6. List of 384 miRNAs

hsa-let-7a-5p	hsa-miR-33b-5p	hsa-miR-139-3p
hsa-let-7c	hsa-miR-34a-5p	hsa-miR-139-5p
hsa-let-7d-5p	hsa-miR-34c-5p	hsa-miR-140-3p
hsa-let-7e-5p	hsa-miR-92a-3p	hsa-miR-140-5p
hsa-let-7f-5p	hsa-miR-93-5p	hsa-miR-141-3p
hsa-let-7g-5p	hsa-miR-95	hsa-miR-142-3p
hsa-miR-1	hsa-miR-96-5p	hsa-miR-142-5p
hsa-miR-9-5p	hsa-miR-98	hsa-miR-143-3p
hsa-miR-10a-5p	hsa-miR-99a-5p	hsa-miR-145-5p
hsa-miR-10b-5p	hsa-miR-99b-5p	hsa-miR-146a-5p
hsa-miR-15a-5p	hsa-miR-100-5p	hsa-miR-146b-3p
hsa-miR-15b-5p	hsa-miR-101-3p	hsa-miR-146b-5p
hsa-miR-16-5p	hsa-miR-103a-3p	hsa-miR-147b
hsa-miR-17-5p	hsa-miR-105-5p	hsa-miR-148a-3p
hsa-miR-18a-5p	hsa-miR-106a-5p	hsa-miR-148b-3p
hsa-miR-18b-5p	hsa-miR-106b-5p	hsa-miR-149-5p
hsa-miR-19a-3p	hsa-miR-107	hsa-miR-150-5p
hsa-miR-19b-3p	hsa-miR-122-5p	hsa-miR-152
hsa-miR-20a-5p	hsa-miR-124-3p	hsa-miR-153
hsa-miR-20b-5p	hsa-miR-125a-3p	hsa-miR-154-5p
hsa-miR-21-5p	hsa-miR-125a-5p	hsa-miR-181a-5p
hsa-miR-22-3p	hsa-miR-125b-5p	hsa-miR-181c-5p
hsa-miR-23a-3p	hsa-miR-126-3p	hsa-miR-182-5p
hsa-miR-23b-3p	hsa-miR-127-3p	hsa-miR-183-5p
hsa-miR-24-3p	hsa-miR-127-5p	hsa-miR-184
hsa-miR-25-3p	hsa-miR-128	hsa-miR-185-5p
hsa-miR-26a-5p	hsa-miR-129-2-3p	hsa-miR-186-5p
hsa-miR-26b-5p	hsa-miR-129-5p	hsa-miR-187-3p
hsa-miR-27a-3p	hsa-miR-130a-3p	hsa-miR-188-3p
hsa-miR-27b-3p	hsa-miR-130b-3p	hsa-miR-190a
hsa-miR-28-3p	hsa-miR-132-3p	hsa-miR-191-5p

hsa-miR-28-5p	hsa-miR-133a	hsa-miR-192-5p
hsa-miR-29a-3p	hsa-miR-133b	hsa-miR-193a-3p
hsa-miR-29b-3p	hsa-miR-134	hsa-miR-193a-5p
hsa-miR-29c-3p	hsa-miR-135a-5p	hsa-miR-193b-3p
hsa-miR-30b-5p	hsa-miR-135b-5p	hsa-miR-194-5p
hsa-miR-30c-5p	hsa-miR-136-5p	hsa-miR-195-5p
hsa-miR-31-5p	hsa-miR-137	hsa-miR-196b-5p
hsa-miR-32-5p	hsa-miR-138-5p	hsa-miR-197-3p
hsa-miR-198	hsa-miR-329	hsa-miR-409-5p
hsa-miR-199a-5p	hsa-miR-330-3p	hsa-miR-410
hsa-miR-199a-3p	hsa-miR-330-5p	hsa-miR-411-5p
hsa-miR-199b-5p	hsa-miR-331-3p	hsa-miR-422a
hsa-miR-200a-3p	hsa-miR-331-5p	hsa-miR-423-5p
hsa-miR-200b-3p	hsa-miR-335-5p	hsa-miR-424-5p
hsa-miR-200c-3p	hsa-miR-337-5p	hsa-miR-425-5p
hsa-miR-202-3p	hsa-miR-338-3p	hsa-miR-429
hsa-miR-203	hsa-miR-339-3p	hsa-miR-431-5p
hsa-miR-204-5p	hsa-miR-339-5p	hsa-miR-433
hsa-miR-205-5p	hsa-miR-340-5p	hsa-miR-449a
hsa-miR-208b	hsa-miR-155-5p	hsa-miR-449b-5p
hsa-miR-210	hsa-let-7b-5p	hsa-miR-450a-5p
hsa-miR-214-3p	hsa-miR-342-3p	hsa-miR-450b-3p
hsa-miR-215	hsa-miR-342-5p	hsa-miR-450b-5p
hsa-miR-216a	hsa-miR-345-5p	hsa-miR-451a
hsa-miR-216b	hsa-miR-361-5p	hsa-miR-452-5p
hsa-miR-217	hsa-miR-362-3p	hsa-miR-323b-5p
hsa-miR-218-5p	hsa-miR-362-5p	hsa-miR-454-3p
hsa-miR-219-5p	hsa-miR-363-3p	hsa-miR-455-3p
hsa-miR-221-3p	hsa-miR-365a-3p	hsa-miR-455-5p
hsa-miR-222-3p	hsa-miR-367-3p	hsa-miR-483-5p
hsa-miR-223-3p	hsa-miR-369-3p	hsa-miR-484
hsa-miR-224-5p	hsa-miR-369-5p	hsa-miR-485-3p
hsa-miR-296-3p	hsa-miR-370	hsa-miR-485-5p
hsa-miR-296-5p	hsa-miR-371-3p	hsa-miR-486-3p

hsa-miR-299-3p	hsa-miR-372	hsa-miR-486-5p
hsa-miR-299-5p	hsa-miR-373-3p	hsa-miR-487a
hsa-miR-301a-3p	hsa-miR-374a-5p	hsa-miR-487b
hsa-miR-301b	hsa-miR-374b-5p	hsa-miR-488-3p
hsa-miR-302a-3p	hsa-miR-375	hsa-miR-489
hsa-miR-302b-3p	hsa-miR-376a-3p	hsa-miR-490-3p
hsa-miR-302c-3p	hsa-miR-376b	hsa-miR-491-3p
hsa-miR-320a	hsa-miR-377-3p	hsa-miR-491-5p
hsa-miR-323-3p	hsa-miR-379-5p	hsa-miR-493-3p
hsa-miR-324-3p	hsa-miR-380-3p	hsa-miR-494
hsa-miR-324-5p	hsa-miR-381	hsa-miR-495
hsa-miR-326	hsa-miR-382-5p	hsa-miR-496
hsa-miR-328	hsa-miR-383	hsa-miR-499a-3p
hsa-miR-499a-5p	hsa-miR-522-3p	hsa-miR-616-3p
hsa-miR-500a-5p	hsa-miR-523-3p	hsa-miR-618
hsa-miR-501-3p	hsa-miR-524-5p	hsa-miR-624-3p
hsa-miR-501-5p	hsa-miR-525-3p	hsa-miR-625-5p
hsa-miR-502-3p	hsa-miR-525-5p	hsa-miR-627
hsa-miR-502-5p	hsa-miR-526b-5p	hsa-miR-628-5p
hsa-miR-503	hsa-miR-532-3p	hsa-miR-629-5p
hsa-miR-504	hsa-miR-532-5p	hsa-miR-636
hsa-miR-505-3p	hsa-miR-539-5p	hsa-miR-642a-5p
hsa-miR-507	hsa-miR-541-3p	hsa-miR-651
hsa-miR-508-3p	hsa-miR-542-3p	hsa-miR-652-3p
hsa-miR-508-5p	hsa-miR-542-5p	hsa-miR-653
hsa-miR-509-5p	hsa-miR-544a	hsa-miR-654-3p
hsa-miR-510	hsa-miR-545-3p	hsa-miR-654-5p
hsa-miR-512-3p	hsa-miR-548a-3p	hsa-miR-655
hsa-miR-512-5p	hsa-miR-548a-5p	hsa-miR-660-5p
hsa-miR-513-5p	hsa-miR-548b-3p	hsa-miR-671-3p
hsa-miR-515-3p	hsa-miR-548b-3p	hsa-miR-672
hsa-miR-515-5p	hsa-miR-548c-3p	hsa-miR-674
hsa-miR-516a-5p	hsa-miR-548c-5p	hsa-miR-708-5p
hsa-miR-516b-5p	hsa-miR-548d-3p	hsa-miR-744-5p



hsa-miR-517a-3p	hsa-miR-548d-5p	hsa-miR-758
hsa-miR-517c-3p	hsa-miR-551b-3p	hsa-miR-871
hsa-miR-518a-3p	hsa-miR-556-3p	hsa-miR-872
hsa-miR-518a-5p	hsa-miR-556-5p	hsa-miR-873-5p
hsa-miR-518b	hsa-miR-561-3p	hsa-miR-874
hsa-miR-518c-3p	hsa-miR-570-3p	hsa-miR-875-3p
hsa-miR-518d-3p	hsa-miR-574-3p	hsa-miR-876-3p
hsa-miR-518d-5p	hsa-miR-576-3p	hsa-miR-876-5p
hsa-miR-518e-3p	hsa-miR-576-5p	hsa-miR-885-3p
hsa-miR-518f-3p	hsa-miR-579	hsa-miR-885-5p
hsa-miR-519a-3p	hsa-miR-582-3p	hsa-miR-886-3p
hsa-miR-519d	hsa-miR-582-5p	hsa-miR-886-5p
hsa-miR-519e-3p	hsa-miR-589-5p	hsa-miR-887
hsa-miR-520a-3p	hsa-miR-590-5p	hsa-miR-888-5p
hsa-miR-520a-5p	hsa-miR-597	hsa-miR-889
hsa-miR-520d-5p	hsa-miR-598	hsa-miR-890
hsa-miR-520g	hsa-miR-615-3p	hsa-miR-891a
hsa-miR-521	hsa-miR-615-5p	hsa-miR-891b
hsa-miR-892a	hsa-miR-376c	Exogenous ath-miR159a
hsa-miR-147a	hsa-miR-384	Endogenous RNU44
hsa-miR-208a	hsa-miR-412	Endogenous RNU48
hsa-miR-211-5p	hsa-miR-448	4x Endogenous U6 snRNA
hsa-miR-212-3p	hsa-miR-492	Exogenous cel-miR-39-3p
hsa-miR-219-1-3p	hsa-miR-506-3p	
hsa-miR-219-2-3p	hsa-miR-509-3-5p	
hsa-miR-220a	hsa-miR-511	
hsa-miR-220b	hsa-miR-517b	
hsa-miR-220c	hsa-miR-519c-3p	
hsa-miR-298	hsa-miR-520b	
hsa-miR-325	hsa-miR-520e	
has-miR-346	has-miR-520F	

### 3.7. Design of hsa-miR-376c-3p oligos

Guide Strand: 5'/Phos AACAUAGAGGAAAUUCCACGUCG 3'

Passenger Strand: 5'/Phos ACGUGGAAUUUCCUCUAUGUCUAG 3'

### 3.8. RT<sup>2</sup> Profiler™ PCR Array Human BC

The gene list containing following mRNA and controls used in this study:

1. ABCB1-ATP-binding cassette, sub-family B (MDR/TAP), member 1
2. ABCG2- ATP-binding cassette, sub-family G (WHITE), member 2
3. ADAM23 -ADAM metalloproteinase domain 23
4. AKT1- V-akt murine thymoma viral oncogene homolog 1
5. APC -Adenomatous polyposis coli)
6. AR -Androgen receptor
7. ATM-Ataxia telangiectasia mutated
8. BAD -BCL2-associated agonist of cell death
9. BCL2- B-cell CLL/lymphoma 2
10. BIRC5 -Baculoviral IAP repeat containing 5
11. BRCA1 -Breast cancer 1
12. BRCA2- Breast cancer 2
13. CCNA1- Cyclin A1
14. CCND1 -Cyclin D1
15. CCND2 -Cyclin D2
16. CCNE1 -Cyclin E1
17. CDH1 -Cadherin 1, type 1, E-cadherin (epithelial)
18. CDH13- Cadherin 13, H-cadherin
19. CDK2- Cyclin-dependent kinase 2
20. CDKN1A- Cyclin-dependent kinase inhibitor 1A (p21, Cip1)
21. CDKN1C- Cyclin-dependent kinase inhibitor 1C (p57, Kip2)
22. CDKN2A- Cyclin-dependent kinase inhibitor 2A (melanoma, p16, inhibits CDK4)
23. CSF1- Colony stimulating factor 1 (macrophage)
24. CST6 -Cystatin E/M

25. CTNNB1- Catenin (cadherin-associated protein), beta 1, 88kDa
26. CTSD- Cathepsin D
27. EGF- Epidermal growth factor
28. EGFR -Epidermal growth factor receptor
29. ERBB2 - V-erb-b2 erythroblastic leukemia viral oncogene homolog 2
30. ESR1- Estrogen receptor 1
31. ESR2- Estrogen receptor 2 (ER beta)
32. FOXA1- Forkhead box A1
33. GATA3 -GATA binding protein 3
34. GLI1 -GLI family zinc finger 1
35. GRB7 -Growth factor receptor-bound protein 7
36. GSTP1- Glutathione S-transferase pi 1
37. HIC1- Hypermethylated in cancer 1
38. ID1- Inhibitor of DNA binding 1, dominant negative helix-loop-helix protein
39. IGF1- Insulin-like growth factor 1 (somatomedin C)
40. IGF1R- Insulin-like growth factor 1 receptor
41. IGFBP3- Insulin-like growth factor binding protein 3
42. IL6 -Interleukin 6 (interferon, beta 2)
43. JUN- Jun proto-oncogene
44. KRT18 Keratin 18
45. KRT19-Keratin 19
46. KRT5 -Keratin 5
47. KRT8 Keratin 8
48. MAPK1 Mitogen-activated protein kinase 1
49. MAPK3- Mitogen-activated protein kinase 3
50. MAPK8- Mitogen-activated protein kinase 8
51. MGMT -O-6-methylguanine-DNA methyltransferase
52. MKI67- Antigen identified by monoclonal antibody Ki-67
53. MLH1- MutL homolog 1, colon cancer, nonpolyposis type 2 (E. coli)
54. MMP2 -Matrix metalloproteinase 2 (gelatinase A, 72kDa gelatinase, 72kDa type IV collagenase),
55. MMP9-Matrix metalloproteinase 9 (gelatinase B, 92kDa gelatinase, 92kDa type IV collagenase)
56. MUC1- Mucin 1, cell surface associated

57. MYC -V-myc myelocytomatosis viral oncogene homolog (avian)
58. NME1 -Non-metastatic cells 1, protein
59. NOTCH1- Notch 1
60. NR3C1- Nuclear receptor subfamily 3, group C, member 1 (glucocorticoid receptor),
61. PGR -Progesterone receptor
62. PLAU- Plasminogen activator, urokinase
63. PRDM2- PR domain containing 2, with ZNF domain
64. PTEN- Phosphatase and tensin homolog
65. PTGS2-Prostaglandin-endoperoxide synthase 2 (prostaglandin G/H synthase and cyclooxygenase)
66. PYCARD -PYD and CARD domain containing
67. RARB -Retinoic acid receptor, bet
68. RASSF1 - Ras association (RalGDS/AF-6) domain family member 1
69. RB1- Retinoblastoma 1
70. SERPINE1- Serpin peptidase inhibitor, clade E (nexin, plasminogen activator inhibitor type1), member 1
71. SFN- Stratifin
72. SFRP1 -Secreted frizzled-related protein 1
73. SLC39A6 -Solute carrier family 39 (zinc transporter), member 6
74. SLIT2 -Slit homolog 2
75. SNAI2- Snail homolog 2
76. SRC -V-src sarcoma (Schmidt-Ruppin A-2) viral oncogene homolog (avian)
77. TFF3- Trefoil factor 3 (intestinal)
78. TGFB1- Transforming growth factor, beta 1
79. THBS1 -Thrombospondin 1
80. TP53 -Tumor protein p53
81. TP73 -Tumor protein p73
82. TWIST1 -Twist homolog 1
83. VEGFA- Vascular endothelial growth factor A
84. XBP1 -X-box binding protein 1
85. ACTB - Actin, beta
86. B2M- Beta-2-microglobulin
87. GAPDH- Glyceraldehyde-3-phosphate dehydrogenase
88. HPRT1-Hypoxanthine phosphoribosyltransferase 1

89. RPLP0- Ribosomal protein, large, P0.
90. human genomic DNA contamination control
91. reverse transcription control
92. reverse transcription control
93. reverse transcription control
94. positive PCR control
95. positive PCR control
96. positive PCR control

### **3.9. Triple negative BC cell lines**

MDA-MB-231    Adenocarcinoma

MDA-MB-468    Adenocarcinoma

### **3.10. Study populations**

Within the multicentre GeparSixto trial from August 2011 to December 2012, BC patients were randomized to receive neoadjuvant treatment with paclitaxel (80mg/m<sup>2</sup>/week) and non-pegylated liposomal doxorubicin (20mg/m<sup>2</sup>/week) with or without addition of carboplatin (AUC 2.0-1.5/week) for 18 weeks. Hormone-receptor status, HER2 status, and Ki67 were centrally confirmed prior to randomization. Plasma samples of 211 HER2-positive and 224 TNBC patients were collected directly before therapy. After therapy, plasma samples of 4 HER2-positive and 5 TNBC patients were also available. Median age of BC patients was 47 years and ranged from 21 to 78 years. In addition, plasma samples were collected from 20 healthy women (median age 55, range 47 to 69) with no history of cancer and in good health based on self-report during 2016. Regarding blood processing, uniform management concerning the specific described protocols was performed.

## 4. Methods

### 4.1. Verification of hemolysis in plasma samples

To avoid quantifying exosomal miRNAs in hemolytic plasma samples that may influence the results, hemoglobin measurements by spectral analysis was performed (Kirschner et al., 2011). In 7 mL of whole blood, red blood cells were lysed using erythrocyte lysis buffer (containing 0.3 M sucrose, 10 mM Tris pH 7.5, 5 mM MgCl<sub>2</sub> and 1% Triton X100). A dilution series (1:1, 1:3, 1:4, 1:6, 1:8, 1:10, 1:12, 1:14, 1:18, 1:20) of lysed red blood cells in plasma was prepared that served as a standard curve for the measurement of hemolysis in all plasma samples. Fifty µl of each plasma sample (standard and plasma of interest) was measured in duplicates on a Microplate reader (Tecan, Männergdorf, Switzerland). The average values and standard deviations were calculated from the duplicates.

### 4.2. Isolation of total exosomes from plasma samples using ExoQuick

Total exosomes were isolated by ExoQuick (polyethylene glycol), according to the manufacturer's instructions. Briefly, 550 µL of plasma, removed from cells and debris by two centrifugation steps at 3 000 g for 15 min were incubated with 120 µL ExoQuick exosome precipitation solution at 4 °C, for 30 min. Following centrifugation at 1 500 g for 30 min, the exosomes were precipitated, and then resuspended in PBS (Phosphate-Buffered Saline) buffer.

### 4.3. Visualization of exosomes using confocal microscope

Exosomes isolated with ExoQuick were labeled by the Exo-GLOW Exosome Labeling Kit.

The Exo-Red exosome label is a nucleic acid selective fluorescent cationic dye. It is a cell-permeable reagent that interacts non-covalently with RNA by electrostatic attractions and with DNA by intercalation.

Briefly, 500  $\mu$ l resuspended exosomes and 50  $\mu$ L Exo-Red in PBS were incubated at 37°C for 10 min. The labeling reaction was stopped with 100  $\mu$ L ExoQuick-TC reagent at 4°C for 30 min. After centrifugation for 3 min. at 16 000 g, the labeled exosome pellet was resuspended in 500  $\mu$ L PBS and monitored under a confocal microscope Leica TCS SP5. For excitation and detection of the fluorescence light a 63x NA=1.4 oil objective lens was employed. The 460 nm laser excitation was used to excite the red (Exo-Red) .

### 4.4. ELISA

Exosomes were quantified by the Exosome Antibodies & ELISA Kit which is specific for the exosomal protein CD63. For performing ELISA, 400  $\mu$ L plasma was purified to remove fibrin pellet by adding 4  $\mu$ L thrombin at a final concentration of 5 U/mL. Following exosome extraction by ExoQuick, 50  $\mu$ L exosome resuspension in duplicate and CD63 protein standards (undiluted, diluted 1:2, 1:4, 1:8, 1:16, 1:32 and 1:64) were added to the micro-titer plate. The absorbance of the samples was measured at 450 nm on a spectrophotometric plate reader, and the amounts of CD63 protein were calculated according to the exosome protein standard curve.

#### 4.5. Western blotting

Western blotting is a method to identify specific proteins in a mixture of proteins. First, proteins are separated by size and charge on a polyacrylamide gel (SDS-PAGE) followed by a transfer to a membrane and incubation using a primary antibody against to the protein of interest and a secondary antibody. Given that the ionic detergent sodium dodecyl sulfate (SDS) denatures and binds proteins, SDS-PAGE is able to separate proteins based primarily on their size. Furthermore, SDS confers negative charge on the surface of the proteins it binds, therefore, when a current is applied, all SDS-bound proteins in a sample will migrate through the gel towards the positively charged electrode. Proteins of a smaller size migrate more quickly through the gel than those with a higher mass.

The protein concentrations were first measured with the DC Protein Assay Kit at a wavelength of 650 nm on a spectrophotometric plate reader. A standard curve of 0, 0.625, 1.25, 2.5, 5 and 10 mg/mL BSA (bovine serum albumin) was applied by the double-dilution method. Five  $\mu$ L of exosomes, exosome supernatant and BSA standard protein samples, all solved in RIPA buffer (Sigma-Aldrich, Munich, Germany) was added to 96-well plates according to the manufacturer's instructions. The protein concentrations were then calculated according to a linear equation by applying the regression method.

Thirty  $\mu$ g of exosome proteins and exosome supernatant, all dissolved in RIPA buffer, were electrophoretically separated. The gel consists of a stacking gel and a resolving gel (as outlined below). The stacking gel allows the loaded proteins to be concentrated into a tight band during the first few minutes of electrophoresis and guarantees proteins with different molecular weights to be separated from the same starting point when they enter the resolving gel.



Staking gel	Components
dd H <sub>2</sub> O	2.7 mL
30% PAA	670 $\mu$ L
1 M Tris pH 6.8	500 $\mu$ L
10% SDS	40 $\mu$ L
TEMED	5 $\mu$ L
10% APS	40 $\mu$ L

Resolving gel	10% CD63 and AGO2	15% CD81
dd H <sub>2</sub> O	5.9 mL	3.5 mL
30% PAA	5 mL	7.5 mL
1.5 M Tris pH 8.8	3.8 mL	3.8 mL
10% SDS	150 $\mu$ L	150 $\mu$ L
TEMED	6 $\mu$ L	5 $\mu$ L
10% APS	150 $\mu$ L	150 $\mu$ L

For gel electrophoresis, the XCell SureLock® Mini-Cell device and 1x Laemmli Running Buffer were used. PageRuler™ Plus Prestained Protein Ladder served as a standard indicator for the molecular weights of proteins. The running time was determined by the molecular weight of the protein being investigated. In the experiments outlined in this thesis, the running time was approximately 2 h at 125 V.

After gel electrophoresis, the separated proteins in the gel were transferred onto a 0.45  $\mu$ m for CD63 and AGO2 and 0.2  $\mu$ m for CD81 PVDF (polyvinylidene fluoride) membrane by the XCell II™ Blot Module. Prior to the transfer, the PVDF membrane was activated with methanol for 1 min, then incubated with double-distilled water for 3 min and soaked in transfer buffer for 5 min. Blotting pads and filter papers, presoaked with transfer buffer, were placed in the cathode core of the XCell II™ Blot Module as shown in Figure 9. The assembled chamber was filled with transfer buffer, and the outside of the chamber was surrounded with tap water for cooling. The transfer was carried out for 1 h at 25 V.

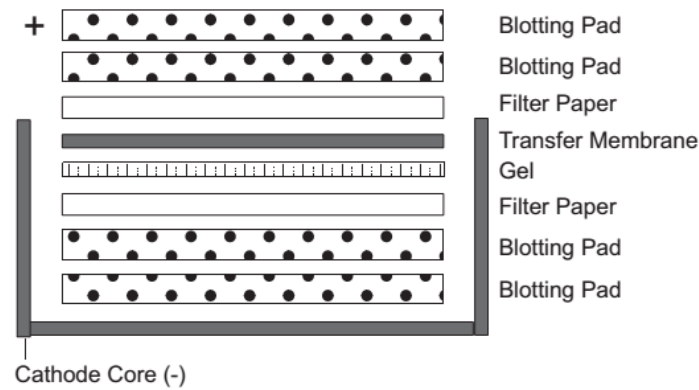


**Figure 9: Schematic representation of the gel membrane assembly** (taken from the original Invitrogen protocol).

The blotting pads sponges and filters ensure the continuous contact between gel and membrane. The negatively charged proteins run from the cathode (-) to the anode (+).

After transfer, the PVDF membrane was first blocked with 6% milk solution (6 g in 100 mL TBST buffer), at room temperature for 1 h, in a 50 mL-tube, to prevent non-specific antibody binding or non-specific signal on the final western blot. The washed PVDF membrane was subsequently incubated with antibodies specific for the exosomal markers CD63 (1:1000), CD81 (1:500) in 6% milk and AGO2 (1:2000) in 5% BSA overnight. Before and after incubation with a secondary antibody at room temperature for 1 h, the PVDF membrane was washed 3 times with TBST buffer each time for 10 min. For CD63 polyclonal swine anti-rabbit and for AGO2 and CD81 a polyclonal rabbit anti-mouse secondary antibody was used. Detection of the proteins was carried out using peroxidase-conjugated antibodies (1:2000) and a chemoluminescence detection solution. The chemiluminescent signals were detected on photosensitive X-ray films. Depending on the signal strength of the particular protein, the exposure time varied from 5 secs to 15 min. The films were developed in an X-ray film developer Curix60 and scanned with the EPSON perfection V750 PRO device.

#### 4.6. Extraction of miRNAs and conversion into cDNA

MiRNAs were extracted from exosomes lysed in 150  $\mu\text{L}$  lysis buffer by using the TaqMan miRNA ABC Purification Kit according to the manufacturer's recommendations. Briefly, 80  $\mu\text{L}$  of beads, bound by a unique set of 377 anti-miRNA oligonucleotides, were added to lysed exosomes to capture miRNAs. For isolation efficiency, 2  $\mu\text{L}$  of 1 nM cel-miR-39 was added as an exogenous spike in control. The beads with the bound miRNAs were washed with 100  $\mu\text{L}$  wash buffer 1 and 2, to remove DNA, proteins, contaminants and residual binding solution. The captured miRNAs were then eluted from the beads in 20  $\mu\text{L}$  of elution buffer. The extracted miRNAs were immediately reverse transcribed into cDNA using a modified protocol of TaqMan MiRNA Reverse Transcription kit. The 15  $\mu\text{L}$  reaction contained:

Component	Volume per Reaction
Custom RT primer pool	6 $\mu\text{L}$
100 mM dNTPs with dTTP	0.3 $\mu\text{L}$
50 U/ $\mu\text{l}$ MultiScribe Reverse Transcriptase	3 $\mu\text{L}$
10X RT buffer	1.5 $\mu\text{L}$
20 U/ $\mu\text{l}$ RNase Inhibitor	0.19 $\mu\text{L}$
miRNA	4 $\mu\text{L}$

The reverse transcription was carried out on a MJ Research PTC-200 Peltier Thermal Cycler under following conditions:

16 °C for 30 min

42 °C for 30 min

85 °C for 5 min

The cDNA samples were stored at -20 °C for future usage.

#### 4.7. Preamplification of miRNAs

To increase the input cDNA, a preamplification step was included. The preamplification step significantly enhance the detection of low-expressed miRNAs, enabling the generation of a comprehensive expression profile using as little as 1 ng of total RNA.

Five  $\mu\text{l}$  cDNA was preamplified in a 25- $\mu\text{l}$  reaction containing:

Component	Volume per Reaction
TaqMan PreAmp Master Mix	12.5 $\mu\text{L}$
Custom PreAmp Primer Pool	3.75 $\mu\text{L}$
Nuclease free water	3.75 $\mu\text{L}$

Preamplification reaction was run on a MJ Research PTC-200 Peltier Thermal Cycler under following conditions:

95 °C for 10 min

55 °C for 2 min

72 °C for 2 min

95 °C for 15 s

60 °C for 4 min

16 cycles

99.9 °C for 10 min

To avoid false positive data (e.g., primer dimer formation or unspecific PCR products), a negative control, without any templates, was reverse transcribed in parallel with the experimental samples.

#### 4.8. MiRNAs expression profiling

To identify differentially expressed miRNAs, real-time TaqMan PCR was at first carried out using the Custom TaqMan miRNA array cards containing 384 different miRNAs (as shown in Materials) from plasma samples of 15 TNBC patients treated with/without chemotherapy and with/without pathological response (pCR, defined as ypT0 or ypTis and ypN0).

Subsequently, miRNAs were quantified using TaqMan miRNA array cards mounted with the 45 most significant miRNAs derived from the quantification using the 384-array card. Two endogenous reference miRNAs (miR-92a and miR484), as well as 1 exogenous control miRNA (cel-miR-39), were included for data normalization. The plasma of 435 BC patients and 20 healthy women were then quantified by real-time TaqMan PCR. To carry out real-time TaqMan PCR, the Thermo Fisher Scientific protocol was modified. The 112.5- $\mu$ L PCR reaction containing 56.25  $\mu$ L TaqMan Universal Master Mix II and 2  $\mu$ l preamplification product was loaded on the array cards. PCR was run on a 7300 HT 384 block under following conditions:

95 °C for 10 min

95 °C for 15 s	} 40 cycles
60 °C for 1 min.	

Following 45 miRNAs were selected: snRNU6, let-7g, miR-16, miR-20a, miR-27a, miR-27b, miR-30c, miR-99b, miR-106b, miR-125b, miR-128a, miR-143, miR-145, miR-148a, miR150, miR-152, miR-155, miR-181a, miR-185, miR-193b, miR-199a-3p, miR-202, miR-301, miR-324-3p, miR-328, miR-335, miR-340, miR-365, miR-370, miR-374, miR-376a, miR-376c, miR-382, miR-410, miR-422a, miR-423-5p, miR-433, miR-489, miR-511, miR-598, miR-628-5p, miR-652, miR-660, miR-744, miR-891a.

As tested by the Genorm Algorithm software, miR-92a and miR-484 provided evidence for being the most stable and consistently expressed miRNA, thus making them suitable reference miRNAs for data normalization.

#### **4.9. Cell line cultures**

Two cell lines were used in this study, MDA-MB-231 and MDA-MB-468. Cell lines were cultured in DMEM supplemented with L-Glutamine 200 mM and Streptomycin/Penicillin (200 U/mL) at 37°C, 10 % CO<sub>2</sub>, humidified atmosphere. Cell lines with 90 % confluence were split twice a week. Briefly, cells were washed with PBS and de-attached with 37°C Trypsin-EDTA solution (0.05 %/0.02 %) and centrifuged for 3 min at 250 x g. Once a month, a mycoplasma test was performed to ensure cells were free from contamination.

#### **4.10. Identification of mRNA targets of miR-376c using MirTrap system**

The MirTrap System is a novel tool that helps identifying specific mRNA targets of miRNAs. By co-transfecting the miRNA mimic of interest with a pMirTrap vector, the RISC complex, expressed by the vector can bind the miRNA which subsequently binds to its target mRNA. This complex can then be pulled down using an antibody specific for this complex. The target mRNAs can, then be identified and quantified by quantitative PCR methods, using either mRNA arrays or next generation sequencing (Figure 10). In this study, identifying the mRNA targets of miR-376c was of interest

First, synthetic RNA oligos were designed in a way that the miRNA sequence of miR-376c contained additional 3' overhangs. The passenger strand oligo contained a non-complementary nucleotide near the 3' end to promote thermodynamic instability and facilitate incorporation into the RISC and the 5' ends of both oligo's are phosphorylated (as shown in Materials).

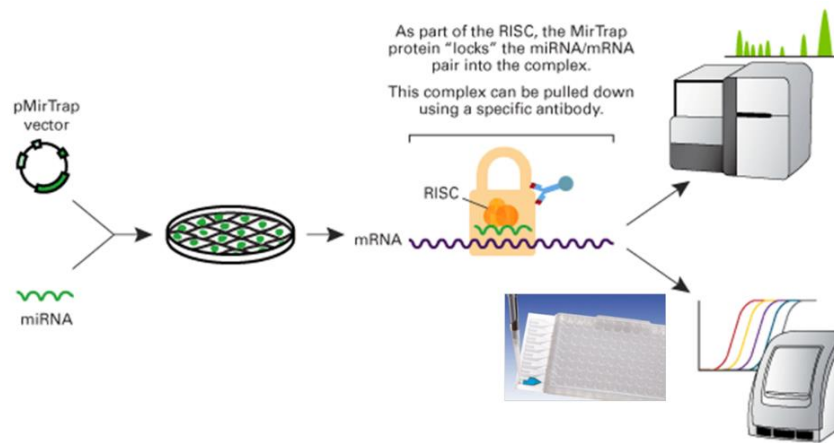


**Figure 10: MirTrap system** (taken from the original sheet of Clontech Laboratories).

First, the cells are transfected with the pMirTrap vector and miRNA. Next step includes binding of mRNA to miRNA inside of the RISC complex. The RISC complex is then isolated, and mRNA targets can be analysed using next generation sequencing or RT-PCR.

To hybridize the single miR-376c 5' with the 3' oligo strands, each oligo was resuspended in resuspension buffer (20 mM NaCl, 10 mM Tris, pH 8.0) to a final concentration of 200  $\mu$ M. Then the oligos were mixed in a 1:1 volume ratio, resulting in a concentration of 100  $\mu$ M. The hybridization was incubated on a peqSTAR 96 Universal Gradient under following conditions:

95°C for 2 min

10 min slope to 37°C

37°C for 60 min

5 min slope to 25°C

To confirm that the oligos were properly annealed, agarose gel electrophoresis was performed. Briefly, a 3% agarose gel was made, gel red was used to stain the double-stranded miRNAs and electrophoresis was carried out at 100V for 1 hour. The double-stranded miRNA mimic was now ready for transfection.

The MirTrap system consists of two parts:

1. A control reaction with the control miR-132
2. A reaction of concern with the miRNA of interest (miR-376c)

To cotransfect the control miR-132 and miR-376c together with the pMirTrap Control and pMirTrap vectors, MDA-MB-468 cells were seeded in a 10-cm dish and were 60-70% confluent at time of transfection.

For the transfection with control miRNA-132, two microcentrifuge tubes were prepared:

<b>Tube 1</b>
5 $\mu$ L (500 pmoles) miR-132
60 $\mu$ L (30 $\mu$ g) pMirTrap vector
20 $\mu$ L (10 $\mu$ g) pMirTrap control vector
515 $\mu$ L Xfect reaction buffer

<b>Tube 2</b>
12 $\mu$ L Xfect polymer
528 $\mu$ L Xfect Reaction buffer
Combined vortex and added
60 $\mu$ L Xfect miRNA transfection polymer

For the transfection with miR-376c, two microcentrifuge tubes were also prepared:

<b>Tube 1</b>
5 $\mu$ L (500 pmoles) miR-376c mimic
60 $\mu$ L (30 $\mu$ g) pMirTrap vector
535 $\mu$ L Xfect reaction buffer

<b>Tube 2</b>
10 $\mu$ L Xfect polymer
530 $\mu$ L Xfect Reaction buffer
Combined vortexed and added
60 $\mu$ L Xfect miRNA transfection polymer

Each tube was vortexed, the contents of tube 1 and 2 were mixed together and incubated for 20 min, to allow nanoparticles complex to form. These complexes were added dropwise to the cell culture and incubated at 37°C for 24 hours. Transfected cells were washed with 10 mL of cold PBS, and 1 mL of cold Lysis/Wash Buffer was added to the cell suspension, which was incubated on ice for 10 min with occasional rocking following cell lysis. Collected lysates were placed on ice for 10 min and centrifuged at 250 x g for 30 min at 4°C. Fifty  $\mu$ L of supernatant was stored at -80°C until the time of RNA isolation. The tube was labeled “Before IP”. The remaining supernatant was transferred to a separate tube and later added to the beads.



In parallel, immunoprecipitation anti-DYKDDDDK beads were prepared for each transfection. Forty  $\mu\text{L}$  of beads suspension was washed twice with 500  $\mu\text{L}$  of Lysis/Wash Buffer containing protease inhibitor cocktail, 10  $\mu\text{L}$  of 1M DTT and 25  $\mu\text{L}$  of RNase inhibitor. After centrifugation at 100 x g for 1 min, supernatant was discarded, and 350  $\mu\text{L}$  of Lysis/Wash buffer, 50  $\mu\text{L}$  of 10 mg/mL tRNA solution and 50  $\mu\text{L}$  of 10 mg/mL BSA solution were added to the bead pellet. The bead suspension was placed on a rotating platform at low speed for 3 hours at 4°C and washed twice with 500  $\mu\text{L}$  of Lysis/Wash Buffer, centrifuged at 100 x g for 1 min and the supernatant was discarded.

The remaining supernatant from above was added to the beads and this solution was placed on a rotation platform at low speed for 2 hours at 4°C. Following the centrifugation at 100 x g for 1 min, the supernatant was discarded. The beads now bound to the RISC complex were washed 3 times with 1 mL Lysis/Wash Buffer, centrifuged at 100 x g for 1 min, and the supernatant was removed. Tubes containing the beads were labeled “After IP” and stored at -80°C until time of RNA isolation.

RNA was isolated from the immunoprecipitated material bound to the anti-DYKDDDDK Beads “Before IP” and “After IP” using the Nucleo spin RNA XS kit according to the manufacturer’s instructions. Briefly, for “Before IP” samples, 150  $\mu\text{L}$  of lysis buffer and 3  $\mu\text{L}$  TCEP were added, whereas for “After IP” samples, 200  $\mu\text{L}$  of lysis buffer and 4  $\mu\text{L}$  TCEP were added. Samples were then vortexed, incubated for 2 min, vortexed and centrifuged for 1 min at 13 400 x g to collect supernatant. For both “Before IP” and “After IP” samples, 5  $\mu\text{L}$  proteinase K was added, lysates were mixed with 200  $\mu\text{L}$  of 70% ethanol, transferred to a NucleoSpin RNA columns and washed with 100  $\mu\text{L}$  MDB. Subsequently, 25  $\mu\text{L}$  of rDNase reaction mix was added to the columns and incubated at room temperature for 15 min. The columns were washed with washing buffers RA2 and RA3, RNA was eluted in 10  $\mu\text{L}$  of RNase free  $\text{H}_2\text{O}$ , and RNA concentration was measured with Qubit.

To validate the assay, the binding of the control miR-132 to its mRNA targets, which are known, was examined. Here, the One Step SYBR RT-PCR kit was used. MiRNA PCR reactions were performed for each of the three sets of primers AcGFP1 (known mRNA target - positive control), hPlod3 (not an mRNA target - negative control) and hGAPDH (internal control). The reactions were set up in triplicate for the “Before IP” sample, the “After IP” sample, and a “no template” control (NTC). NTC was used to avoid false positive data (e.g., primer dimer formation or unspecific PCR products).

For each primer a separate master mix was prepared as follows:

Component	Volume per Reaction
2X One Step SYBR RT-PCR Buffer 4	12.5 $\mu$ L
PrimeScript 1 step Enzyme Mix 2	1.0 $\mu$ L
PCR Forward Primer (10 $\mu$ M)	1.0 $\mu$ L
PCR Reverse Primer (10 $\mu$ M)	1.0 $\mu$ L
RNase-free PCR-grade water	7.5 $\mu$ L

Two  $\mu$ L of diluted (1:10) “Before IP” sample and undiluted “After IP” sample were added to the reaction. PCR was performed on a qPCR CFX96 device under following conditions:

42°C for 5 min

95°C for 10 secs

95°C for 5 secs

60°C for 30 secs

} 40 cycles

In order to determine whether the target mRNA (AcGFP1) is bound by miR-132,  $\Delta$ Ct was calculated by the average of triplicates normalized by the average value of GAPDH. Then the relative RNA amount was calculated by the formula  $2^{-\Delta$ Ct}. The fold enrichment was determined by dividing the  $2^{-\Delta$ Ct value of the “After IP” sample by the  $2^{-\Delta$ Ct value of the “Before IP” sample.

For the identification of mRNA targets of miRNA-376c, the RT<sup>2</sup> Profiler™ PCR Array Human Breast Cancer kits were used. The RT<sup>2</sup> Profiler PCR Array Human BC profiles the mRNA expression of 89 genes commonly involved in the dysregulation of signal transduction and other biological processes during breast carcinogenesis.

To avoid false positive results, a human genomic DNA contamination control with an additional reverse transcription control was included, as well as a positive PCR control.

Isolated RNA from samples “Before IP” and “After IP” was reverse transcribed into cDNA using the RT PreAMP cDNA Synthesis kit. Briefly 8µL of RNA was mixed with 2 µL buffer GE. The RNA was added to 10 µL of reverse transcription mix:

Component	Volume per Reaction
5x Buffer BC3	4 µL
Control P2	1 µL
cDNA Synthesis Enzyme Mix	1 µL
RNase Inhibitor	1 µL
RNase-free water	3 µL

The incubation was performed at 42°C for 30 min, and reaction was stopped at 95°C for 5 min.

Pre-amplification of cDNA was performed using the following components:

Component	Volume per Reaction
RT <sup>2</sup> PreAMP PCR Mastermix	12.5 µL
RT <sup>2</sup> PreAMP Pathway Primer Mix	7.5 µL

Five µL of cDNA were mixed with 20 µL pre-amplification mix. Cycling conditions were as follows:

95°C for 10 min  
 95°C for 5 secs  
 60°C for 2 min

} 12 cycles

The real time PCR was carried out using RT<sup>2</sup> Profiler PCR arrays and the following components:

Component	Volume per Reaction
2x RT <sup>2</sup> SYBR Green Mastermix	1275 $\mu$ L
PreAMP product	102 $\mu$ L
RNase-free water	1173 $\mu$ L

Cycling conditions were following

95°C for 10 min  
 95°C for 15 secs  
 60°C for 1 min

} 40 cycles

To determine the target mRNAs which are bound by miR-376c,  $\Delta$ Ct was calculated and normalized by the value of GAPDH. Then the relative RNA amount was calculated by formula the  $2^{-\Delta$ Ct}. The fold enrichment was calculated by dividing the  $2^{-\Delta$ Ct} value of the “After IP” sample with the  $2^{-\Delta$ Ct} value of the “Before IP” sample.

#### 4.11. Isolation of EVs from cell lines using ultracentrifugation

Ultracentrifugation-based EVs isolation is considered to be the gold standard and is one of the most commonly used and reported techniques of EVs isolation. Medium from 90-100% confluent cell lines was collected and centrifuged for 10 min at 300 x g to remove cell debris. The supernatant was collected and centrifuged for 10 min at 2000 x g to remove large vesicles and apoptotic bodies. After collecting the supernatant, a further centrifugation step was done for 10 min at 10 000 x g to remove bigger vesicles. A final centrifugation step was then carried

out at 100 000 x g for 1 hour. Supernatant was discarded, and the pellet was dissolved in 200  $\mu$ l of 1  $\mu$ M HEPES.

#### 4.12. Nanoparticle tracking analysis

Nanoparticle Tracking Analysis (NTA) is used to characterize nanoparticles from 10-2000 nm in solution. NTA utilizes the properties of both light scattering and Brownian motion, to determine the particle size distribution in liquid suspensions. A laser beam is passed through the sample chamber and the particles in suspension that move in the path of the beam scatter light can be visualized, via a long working distance, by a 20x magnification using a microscope onto which is mounted a video camera. The camera captures a video file of the particles moving under the Brownian motion. The NTA software tracks many particles individually and calculates their hydrodynamic diameters using the Stokes Einstein equation. Each particle is individually but simultaneously analysed by a direct observation and measurement of diffusion events.

Each sample isolated from the cell culture media by ultracentrifugation was diluted in pre-filtered HEPES, at final concentration between  $1 \times 10^9$  and  $10 \times 10^9$  particles/mL. Concentration, size and size distribution profiles of the EVs were measured using a NanoSight LM10 instrument and the NTA 3.0 software. Videos were recorded at camera level 15 with the minimal, expected particle size, minimum track length, and blur setting all set to automatic. For each sample, 6 videos of 30–60 s in duration were recorded and analysed in batch-processing mode.

#### 4.13. Live imaging of EV shuttle

For the live microscopy, EVs were isolated using ultracentrifugation and stained with red fluorescent dye PKH26. PKH lipophilic dyes are highly fluorescent and stain membranes by intercalating their aliphatic portion into the exposed lipid bilayer.

Briefly, 200  $\mu$ l resuspended EVs in HEPES were incubated with PKH26 dye solution for 5 min at room temperature. The reaction was stopped with 1 mL exosome depleted FCS, followed by ultracentrifugation step at 100 000 x g for 1 hour. To remove the excess of dye an additional centrifugation step at 100 000 x g for 1 hour was performed. The MDA-MB-468 cell line was stained with the EpCAM antibody. Briefly, cells were seeded in exosome depleted medium, and the next day stained with antibody diluted 1:50 in PBS and incubated with the cells for 45 min. Cells were washed with PBS to remove the excess of the dye. The stained EVs were added to the stained cells and visualised under the confocal microscope Leica TCS SP8. Live cell imaging was performed in a time range from 30 min to 6 hours after EVs addition. For excitation and detection of the fluorescence light a 63x NA=1.4 oil objective lens was employed. The 488 nm and 561 nm laser excitation lines were used to excite the green (EpCAM) and the red (PKH26) dye respectively. Three dimensional images were acquired in streaming mode. The image field of view was set to be 94 $\mu$ m. Image pixel size was (90/180nm) while the distance between imaging plane was set to be 300/500 nm. Each Image stack was containing an average of 13/14 frames and the acquisition speed was about 3/4 frames per second.

#### 4.14. Transient transfection of cell lines

The cell lines MDA-MB-468 and MDA-MB-231 were seeded in triplicates in a 96-well plate with 5000 cells per well for the MTT (3-(4, 5-Dimethylthiazol-2-yl)-2, 5-Diphenyltetrazolium Bromide) assay. For the apoptosis assays, 400000 cells were seeded per well in a 6-well plate. The cells were counted with an electronic Hemocytometer Vi-CELL™XR. For functional assays of miR-376c, the mimics, AllStars negative control siRNA, an inhibitor and an miScript inhibitor negative control were dissolved in serum-free culture medium to a final concentration of 15 nM for mimics and 75 nM for inhibitors per well. For transfection, 0.75 µl or 12 µl of HiPerFect Transfection reagent was added per well to a 96 well plate or 6 well plate, respectively. In order to determine whether the transfection reagent or process causes nonspecific or cytotoxic effects, a mock-transfection control was included in each analysis. Untransfected cells were also included in each analysis.

#### 4.15. MTT

The MTT colorimetric assay is an established method for determining viable cell number in proliferation and cytotoxicity studies. This assay is based on the cleavage of the yellow tetrazolium salt, MTT, to form a soluble blue formazan product by mitochondrial enzymes. The amount of formazan produced is directly proportional to the number of viable cells. The cell lines MDA-MB-468 and MDA-MB-231 were seeded in triplicate in a 96 well plate. For each analysis, 10000 cells per well were suspended in 200 µL of serum-free medium and transfected after 24 hours with mimic, AllStars Negative Control siRNA, inhibitor, miScript inhibitor negative control and mock-transfection control.

After 24, 48 and 72 hours incubation, 20 µL MTT solution was incubated for approximately 3 hours, followed by addition 150 µL lysis buffer to lyse the cells. For colorimetric detection,

the OD of each well was measured at 540 nm together with a reference at 650 nm on a microplate reader. Measurements were performed in triplicate.

#### **4.16. Apoptosis measured by FACS**

Apoptosis is a highly regulated process of programmed cell death, involving morphological and biological changes. One of the most common features of apoptosis that can be measured by flow cytometry is the externalization of phosphatidylserine (PS), a phospholipid found in the inner membrane of healthy cells. Annexin V binds to PS, and thus, Annexin V labeled with fluorophores allow apoptosis to be assessed, usually in combination with the viability dye 7-aminoactinomycin D (7AAD). Healthy cells are negative for both Annexin V and 7AAD, apoptotic cells are positive for Annexin V and late apoptotic and necrotic cells are positive for Annexin V and 7AAD.

Cell lines were seeded in a 6-well plate with 400000 cells per well and transfected the next day. On the 3<sup>rd</sup> day, apoptosis was induced by a final concentration of 7.5  $\mu$ M camptothecin topoisomerase I inhibitor. This inhibitor binds to the covalent complex of topoisomerase I and DNA resulting in a stable ternary complex. The inhibition of DNA re-ligation causes DNA damage leading to apoptosis. On the 4<sup>th</sup> day untransfected and transfected cells were harvested using trypsin and washed with 1x PBS. Centrifuged cell pellets were resuspended in 100  $\mu$ L binding buffer, stained with 5  $\mu$ L Annexin V and 5  $\mu$ L 7AAD, and incubated for 15 min at RT. In addition, three tubes (unstained cells in binding buffer, cells stained only with Annexin V and cells stained only with 7AAD) were used for setting gates of the FACS (fluorescence activated cell sorting) Canto II device and software. The FACS Canto II device stimulated cells by a laser at a wavelength of 488 nm. Annexin V stained cells were detected by a 585/42 filter (556 nm long pass filter) while 7AAD stained cells were detected by a 660/20 filter (650 nm long-pass filter). The data were analysed using the FACS Diva software.



#### 4.17. Data normalization and statistical analyses

The statistical analyses were performed using the Thermo Fisher Scientific Analysis Software, Relative Quantification Analysis Module, version 3.1 ([www.aps.thermofisher.com](http://www.aps.thermofisher.com)), SPSS software package, version 22.0 (SPSS Inc. Chicago, IL) and Statistical Programming Language R, version 3.3.2 (R Core Team 2016, Vienna, Austria).

All raw real-time PCR data were imported into the Thermo Fisher Scientific Analysis Software. First, the amplification curves were manually checked due to the shape of the curve. If a curve was atypical, the Cq value was omitted from the analysis. Second, Cq values with a Cq confidence score below 0.95 were discarded. Last, the Cq confidence score was calculated according to the algorithm implemented in the Thermo Fisher Scientific Analysis Software and describes the likelihood that an obtained Cq value comes from a amplification curve by assessing the quality of the exponential phase of the respective curve.

The cleaned data of the miRNA expression levels were calculated and evaluated by the  $\Delta Cq$  method as follows:  $\Delta Cq = \text{value Cq (miRNA of interest)} - \text{mean value Cq (reference miR-92a and miR-484)}$ . Surprisingly, snRNU6 was not detectable in most plasma samples and could not be used as a normalizer. According to the Genorm Algorithm software, the most suitable reference miRNAs for data normalization were miR-92a and miR-484. Thus, normalization of miRNAs of interest was performed with these reference miRNAs (Schwarzenbach et al., 2015). Exogenous cel-miR-39, which was spiked into the plasma samples, served as a control for the isolation process.

The Thermo Fisher Scientific Analysis software was used for performing hierarchical clustering (heat map) and Volcano plots. For the heat map, distances between samples and assays were calculated using unsupervised hierarchical clustering based on the  $\Delta Cq$  values and Pearson's correlation. The clustering method used was average linkage. The Volcano plot displays the p-value versus the fold change for each target in the patient group of interest (BC patient group,

HER2-positive or TNBC subgroups), relative to a reference group (healthy group or even HER2-positive subgroup). Here,  $\Delta\Delta Cq$  was calculated as mean  $\Delta Cq$  (miRNA of interest in the group of interest) - mean of  $\Delta Cq$  (miRNA of interest in the reference group). Then, the relative value (Rq or gene expression fold change) was calculated as  $2^{-(\Delta\Delta Cq)}$ .  $\Delta Cq$  values were used to calculate p-values using unpaired two-tailed student t-test, and assuming unequal variances. Subsequently, the relative expression data (Rq) and p-values adjusted for multiple testing by Benjamini and Hochberg method were log<sub>2</sub> and log<sub>10</sub>-transformed, respectively, and plotted as a volcano plot.

Box plots for the ELISA values of exosomes and miRNAs, as well as receiver operating characteristic (ROC) curves were carried out by the SPSS (version 22) software. For nonparametric comparisons of two dependent and independent variables, miRNA levels before and after therapy, and differences in group levels, were compared by Wilcoxon and Mann–Whitney-U tests, respectively.

Fisher's exact and Mann–Whitney-U tests were carried out for categorical variables (Table 4) and continuous variables (Table 5), respectively. Differences of miRNA levels among the (sub)-groups were calculated using the two-tailed student t-test (Table 6). Associations between miRNA levels and dichotomous clinical variables were analysed by calculating the difference of mean  $\Delta Cq$  values between the clinical groups and using an unpaired Student's t-test (Table 7). Correlations between miRNA levels and continuous clinical variables are presented by Pearson's correlation coefficients and corresponding p-values for the null hypothesis of no correlation (Table 8). No multiple test correction was applied to the p-values in Tables 7 and 8. The dependency of pCR on miRNA levels, represented by  $\Delta Cq$  values, was estimated from logistic regression models: For each miRNA and each subgroup (all patients, HER2-positive patients, TNBC patients and patients in the treatment arm) a univariate model as well as a multivariate model including the covariables age (continuous), nodal status (N0 vs. N+), tumor size (T1-2 vs. T3-4) and grading (G1-2 vs. G3) was calculated. The odd ratio with the 95%

confidence interval and the associated Wald p-value for the miRNA were presented (Table 9).

A p-value  $<0.05$  was considered as statistically significant. All p-values are two-sided.

All images acquired using confocal microscopy were processed with Leica Application Suite X (LAS X) version 3.3.0 (Wetzlar, Germany)

## 5. Results

### 5.1. Study workflow

Plasma samples from 435 BC patients and 20 healthy women were examined, and sample workflow is described below.

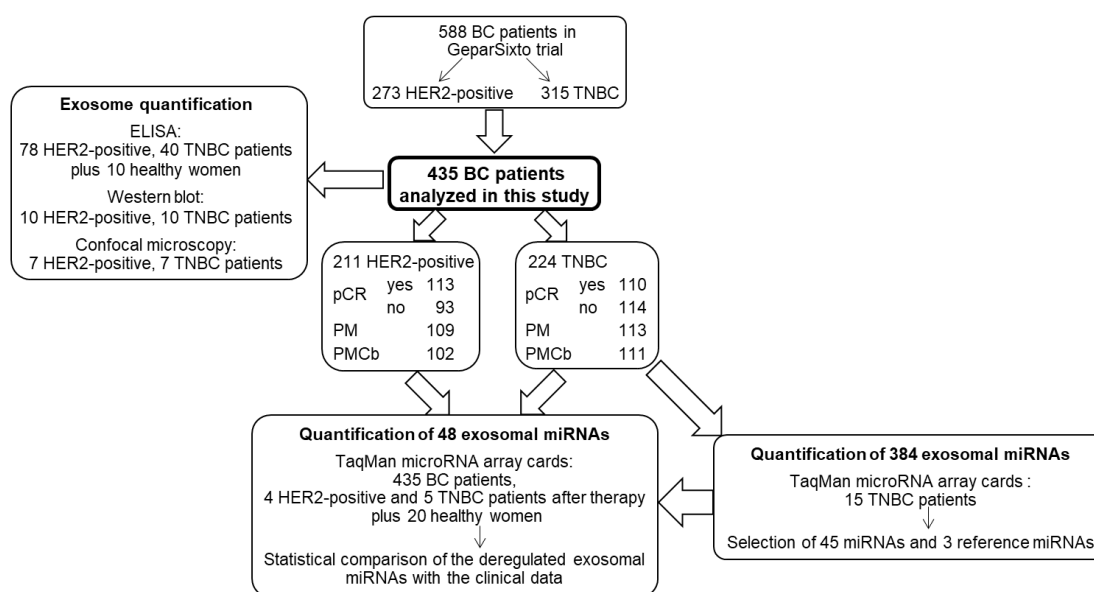


**Figure 11: Workflow of the study**

### 5.2. Measurement of hemolysis

Studies have shown that hemolysis occurring during blood collection has substantial impact on the miRNA content in plasma. To avoid quantifying exosomal miRNAs in hemolytic plasma samples that may influence the results, the level of hemolysis in plasma samples was assessed on a Microplate reader. Absorbance peaks at 414, 541 and 576 nm were indicative for free hemoglobin, with the highest peak at 414 nm. The higher the absorbance in samples is the higher is the degree of hemolysis. The average values and standard deviations were calculated from the duplicates (Figure 12).

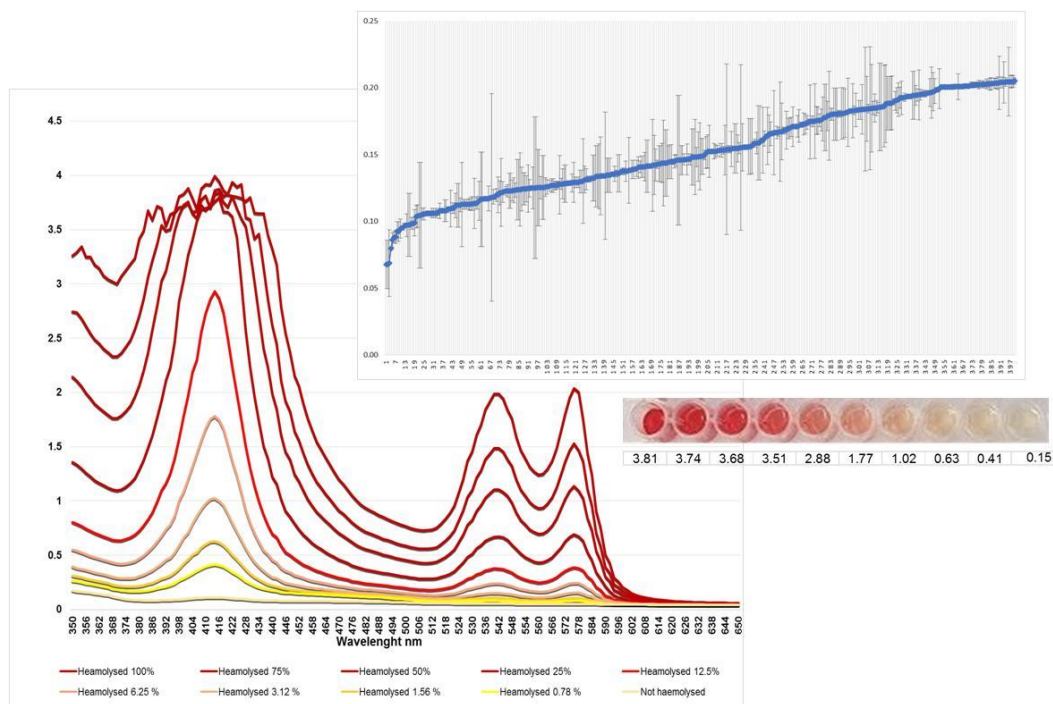


**Figure 12: Levels of free hemoglobin measured in plasma samples**

Hemolysis was assessed by spectrophotometry at wavelengths from 350 to 650 nm. A dilution series of lysed red blood cells in plasma was prepared (below the chart). The degree of hemolysis was determined based on the optical density (OD) at 414 nm (absorbance peak of free hemoglobin, called Soret band), with additional peaks at 541 and 576 nm. Samples were classified as being hemolysed if the OD at 414 exceeded 0.25. The integrated curve of plasma samples comprises values from 0.08 to 0.20 indicating that the samples were non-hemolysed.

### 5.3. Patient characteristics comprising categorial and continuous variables

In total, plasma samples from 435 BC patients and 20 healthy women were examined. Plasma samples of 211 HER2-positive and 224 TNBC patients were collected directly before neoadjuvant therapy. After therapy, plasma samples of 4 HER2-positive and 5 TNBC patients were available. Detailed patient characteristics are summarized in Table 4 (categorial variables) and Table 5 (continuous variables).

**Table 4: Breast cancer patient characteristics (categorical variables)**

Parameters		All BC patients analysed in this study	HER2-positive patients	TNBC patients	All BC patients in GeparSixto trial	p-value*
Total		435 (100.0%)	211 (100.0%)	244 (100.0%)	588 (100.0%)	
Subtype	HER2-positive patients	211 (48.5%)	Subgroups of all BC patients analysed in this study		273 (46.4%)	0.0909
	TNBC patients	224 (51.5%)			315 (53.6%)	
Age	<50	249 (57.2%)	120 (56.9%)	129 (57.6%)	341 (58.0%)	0.5684
	>=50	186 (42.8%)	91 (43.1%)	95 (42.4%)	247 (42.0%)	
Lymph node metastasis	N0	240 (56.1%)	106 (50.7%)	134 (61.2%)	338 (58.7%)	0.0333
	N+	188 (43.9%)	103 (49.3%)	85 (38.8%)	238 (41.3%)	
	missing	7	2	5	12	
Tumor size	T1-2	365 (84.3%)	167 (79.9%)	198 (88.4%)	499 (85.2%)	0.3570
	T3-4	68 (15.7%)	42 (20.1%)	26 (11.6%)	87 (14.8%)	
	missing	2	2	0	2	
Grading	G1-2	151 (34.7%)	93 (44.1%)	58 (25.9%)	207 (35.2%)	0.6944
	G3	284 (65.3%)	118 (55.9%)	166 (74.1%)	381 (64.8%)	
Lymphocyte predominant breast cancer	pos.	108 (25.1%)	44 (21.4%)	64 (28.6%)	142 (24.4%)	0.5825
	neg.	322 (74.9%)	162 (78.6%)	160 (71.4%)	439 (75.6%)	
	missing	5	5	0	7	
Therapy arm	PM**	222 (51.0%)	109 (51.7%)	113 (50.4%)	293 (49.8%)	0.3478
	PMCb***	213 (49.0%)	102 (48.3%)	111 (49.6%)	295 (50.2%)	
Pathological complete response (pCR)	yes	223 (51.3%)	113 (53.6%)	110 (49.1%)	296 (50.3%)	0.4540
	no	212 (48.7%)	98 (46.4%)	114 (50.9%)	292 (49.7%)	

\*Characteristics of patients were compared between patients with analysed samples and all patients of GeparSixto study (modified intend-to-treat population) using Fishers exact tests.

\*\*PM, non-carboplatin treatment arm.

\*\*\*PMCb, carboplatin treatment arm.

**Table 5: Patient characteristics at the time of primary diagnosis of breast cancer (continuous variables)**

Parameters		All BC patients analysed in this study	HER2-positive patients	TNBC patients	All BC patients in GeparSixto trial	p-value*
Ki67***	mean	46	32	59	47	0.4179
	std**	25	18	23	25	
	median	40	30	60	40	
	min, max	3, 95	3, 90	8, 95	2, 95	
Stromal lymphocytes, (strLy)***	mean	32	30	35	32	0.4678
	std**	25	25	24	25	
	median	30	20	30	30	
	min, max	0, 95	0, 95	0, 90	0, 95	
	missing	5	5	0	7	
Intratumoral lymphocytes, (iTuly)***	mean	9	6	12	9	0.5981
	std**	12	8	14	12	
	median	5	5	10	5	
	min, max	0, 70	0, 60	0, 70	0, 70	
	missing	7	7	0	9	
Body mass index	mean	25.3	25.3	25.3	25.4	0.9702
	std**	4.6	4.6	4.6	4.8	
	median	24.4	24.8	24.3	24.5	
	min, max	17.9, 47.4	17.9, 47.4	18.2, 42.2	16.7, 47.4	

\*Characteristics of patients were compared between patients with analysed samples and all patients of GeparSixto study (modified intend-to-treat population using Wilcoxon tests).

\*\*std, standard deviation.

\*\*\*measured % at baseline.

#### 5.4. Higher levels of exosomes in the blood circulation of breast cancer patients

First, we analysed the exosomes by confocal microscopy, Western blot and ELISA (Figure 13).

To visualize the exosomes by confocal microscopy, we stained them in plasma of 14 BC patients and healthy women with Exo-Red. As exemplarily shown in the wide-field fluorescence image, the labeled exosomes from a healthy woman, a BC patient and supernatant

are little red dots due to their sizes below the diffraction limit. Some more exosomes can be seen in the plasma of a BC patient than in a healthy woman. In the supernatant, we can also detect a few exosomes, but the level is very low (Figure 13A). However, it should be kept in mind that these images show only one frame of the pool of exosomes and one-time point. The extraction of exosomes from 20 BC patients was also verified on a Western Blot using antibodies specific for the exosomal markers CD63 and CD81, as well as for AGO2. The AGO2-specific antibody recognized cell-free miRNAs bound to AGO2 protein (103-kDa band) in the exosome supernatant but did not detect AGO2 in the non-lysed exosome pellet. These findings show that the exosome fraction may be pure and devoid of cell-free miRNAs. However, they do not exclude that exosomes may still contain traces of contaminations of cell-free AGO2-bound miRNAs that due to the sensitivity of the Western blot were not detectable. As expected in lysed exosomes, AGO2 protein could be detected, however, its band was at size of around 97 kDa and lower than its bands in the supernatant (Figure 13B). This discrepancy can possibly be explained due to the fact that supernatant was differently treated and not lysed, and a high concentration of other proteins and contaminants is still available which could produce a shift in size. As described by the company, the AGO2-specific antibody recognizes a band at size of 103 kDa which is detected in the supernatant. Moreover, Sharma et al. showed that the band is at size of 97 kDa corresponding to our findings in the lysed exosomes (19). However, further analyses have to be carried out to explain this inconsistency. As visible by the 45 and 29 kDa-bands, CD63- and CD81-specific antibodies recognized the non-lysed exosomes in the pellet, respectively, but did not detect any exosomes in the exosome supernatant (Figure 13C). In contrast to the wide-field fluorescence images that show some exosomes in the supernatant and not in Western blot, these findings indicate that Western blot is not sensitive enough. We also quantified circulating exosomes from plasma of 78 HER2-positive and 40 TNBC patients using an ELISA coated with antibodies against the exosomal marker CD63 and compared their exosome levels with those of 10 healthy women. The exosome levels were



significantly higher in HER2-positive ( $p=0.0001$ ) and TNBC patients ( $p=0.002$ ) than in healthy women, indicating an excessive, active secretion of exosomes in BC patients. Although the exosome levels were higher in HER2-positive patients than in TNBC patients, the difference between these two levels was not significant ( $p=0.086$ , Figure 13D).

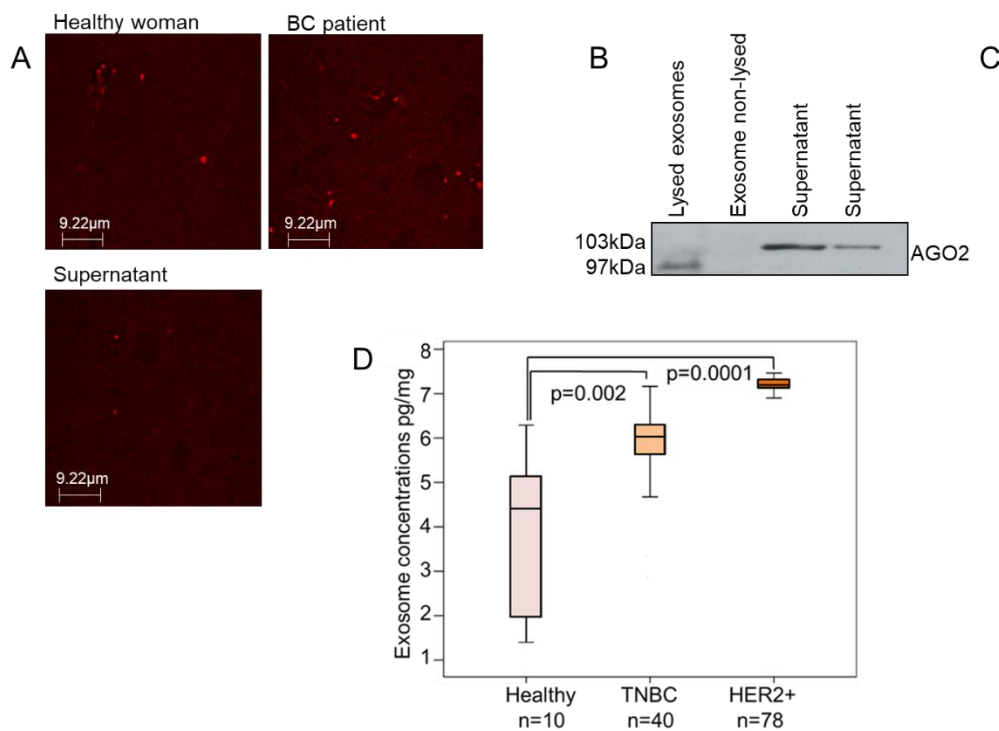


**Figure 13: Verification and quantification of exosomes**

Exosomes were precipitated from plasma of a healthy woman, a BC patient and supernatant by the agglutinating agent ExoQuick. Exosomes labeled by ExoRed are visible as red dots under the confocal microscope using 63x magnification with a scale bar presented in the picture (A). The extraction of exosomes from BC patients was also verified by Western blot using antibodies specific for the exosome proteins CD63 and CD81, and the miRNA-associated AGO2 protein. The Western blot shows a representative example of the supernatant, lysed and non-lysed exosomes where AGO2 protein was detected in lysed exosomes and supernatant (B). A further Western blot shows exosomes and supernatant, while in exosomes CD63 and CD81 proteins were identified (C). The box plot compares the exosome levels in the plasma of healthy women ( $n=10$ ), HER2-positive patients ( $n=78$ ) and TNBC patients ( $n=40$ ) as measured by an ELISA coated with CD63 antibodies (D).

### 5.5. Different exosomal miRNA signatures in HER2-positive and TNBC patients

Following the qualitative and quantitative analyses of exosomes, we determined the miRNA expression profiles in exosomes derived from plasma of 15 TNBC patients before neoadjuvant therapy using a quantitative TaqMan real-time PCR-based miRNA array card containing 384 different miRNAs. This group included 8 patients treated with carboplatin, (4 with pCR and 4 without pCR), and 7 patients from the non-carboplatin arm (4 with pCR and 3 without pCR). From the panel of 384 miRNAs it was aimed to select those exosomal miRNAs which are most differentially expressed between the respective subgroups defined by pCR and treatment arm. While the plasma levels of only one exosomal miRNA (miR-199a,  $p=0.036$ ) differed between patients with and without pCR, the levels of 4 exosomal miRNAs (miR-125,  $p=0.029$ ; miR-193b,  $p=0.029$ ; miR-365,  $p=0.029$ ; miR-370,  $p=0.016$ ) differed according to treatment arm. These 5 miRNAs and 40 additional miRNAs that were significantly associated with other clinical parameters (tumor size, nodal status, grading) were selected and further analysed in plasma from 435 BC patients before treatment and 20 healthy women (together with two references and one exogenous control miRNA). The complete list of miRNAs of this 48-miRNA array card is described in Materials and Methods. The  $\Delta Cq$  values of all 45 miRNAs vs. the mean of references miR-92a and miR-484 among all 455 samples were median-centered and clustered by unsupervised hierarchical clustering based on average linkage and Pearson's correlation as distance metric. The resulting heatmap shows conspicuously an integrated dark green color of some columns on left side referring to the mean levels of exosomal miRNAs detected in plasma of healthy women suggesting that there is no change in their miRNA expression in contrast to the patients. The color scale under the heat map represents  $\Delta Cq$  from the median of all data (Figure 14).

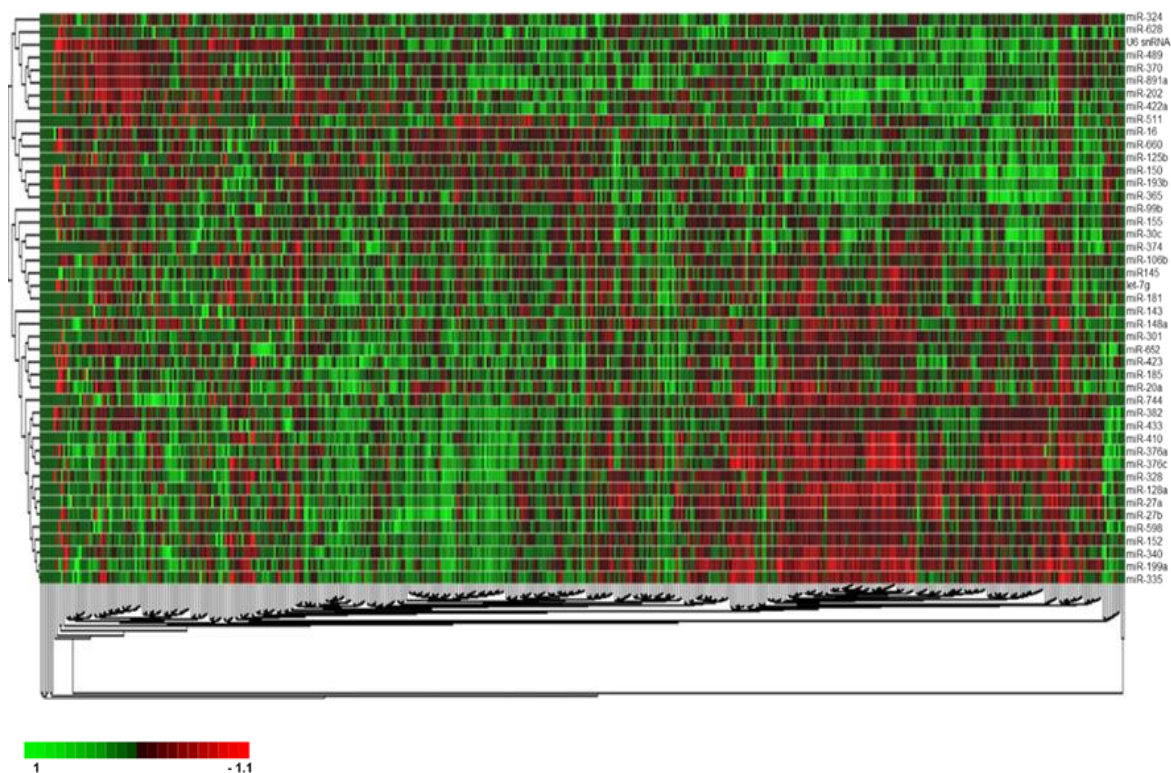


**Figure 14: Hierarchical cluster of 48 exosomal miRNAs**

A heat map of median centred  $\Delta Cq$  values of 45 exosomal miRNAs vs. the mean of references miR-92a and miR-484 (in rows) derived from plasma samples of 435 BC patients before treatment and 20 healthy women (in columns) is shown. Unsupervised hierarchical clustering of samples and miRNAs was based on average linkage and Pearson's correlation as distance metric. The red and green colors indicate that the  $\Delta Cq$  value is below (relatively high expression) and above (relatively low expression levels) the median of all  $\Delta Cq$  values in the study, respectively. Bottom: clustering of samples. Left: clustering of probes. The scale bar provides information on the degree of regulation.

The volcano plots with the Log<sub>2</sub> fold changes plotted on the x-axis and the negative log<sub>10</sub> p-values plotted on the y-axis show all down- (left side) and upregulated (right side) plasma levels of exosomal miRNAs in BC patients. As shown in Figure 15, the plots compare the expression levels of exosomal miRNA in plasma of all 435 BC patients (A) and the subgroups of 211 HER2-positive BC (B) and 224 TNBC patients (C) with those of 20 healthy women, as well as the levels between TNBC and HER2-positive BC patients (D). Compared with healthy women, we identified 8 up- (red dots) and 2 downregulated (green dots), 9 up- and 4 downregulated and

15 up- and 2 downregulated exosomal miRNAs in the entire cohort of BC patients (A), and in the subgroups of HER2-positive BC (B) and TNBC patients (C), respectively. The levels of 18 exosomal miRNAs differed between TNBC and HER2-positive BC patients, whereby 5 and 13 miRNAs were higher and lower in HER2-positive than in TNBC patients (D), respectively (Figure 15).

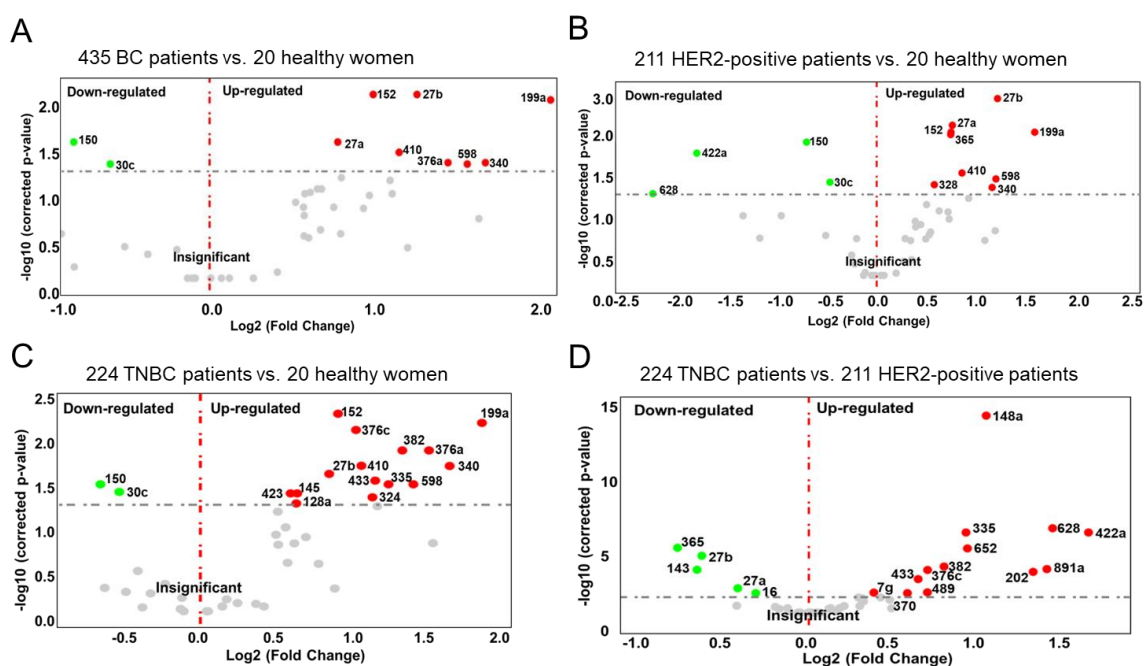


**Figure 15: Volcano plot of 45 exosomal miRNAs**

Volcano plots of p-values vs fold change for comparison of levels of exosomal miRNAs in 435 BC (A), 211 HER2-positive (B) and 224 TNBC patients (C) with those of 20 healthy women, as well as the comparison between HER2-positive and TNBC patients (D). The grey dashed line refers to the threshold value corresponding to a corrected p-value of 0.05. Significantly downregulated exosomal miRNAs are shown as green dots, whereas significantly upregulated exosomal miRNAs as red dots. Grey dots represent non-significant changes. P-values are calculated by student t-test and corrected according to Benjamini and Hochberg method.

**Table 6: Significantly deregulated exosomal miRNAs in plasma of HER2-positive and TNBC patients**

miRNAs	All patients analysed in this study vs. Healthy women	HER2-positive patients vs. Healthy women	TNBC patients vs. Healthy women	TNBC patients vs. Her2-positive patients
	p-value (fold change)			
let-7g	-	-	-	p=0.020 (1.3)
miR-16	-	-	-	p=0.023 (0.8)
miR-27a	p=0.020 (1.7)	p=0.004 (1.9)	-	p=0.009 (0.8)
miR-27b	p=0.010 (2.3)	p=0.001 (2.8)	p=0.021 (1.9)	p<0.0001 (0.7)
miR-30c	p=0.040 (0.7)	p=0.032 (0.7)	p=0.035 (0.7)	-
miR-128a	-	-	p=0.048 (1.6)	-
miR-143	-	-	-	p<0.0001 (0.6)
miR-145	-	-	p=0.036 (1.6)	-
miR-148a	-	-	-	p<0.0001 (2.0)
miR-150	p=0.020 (0.6)	p=0.007 (0.5)	p=0.028 (0.6)	-
miR-152	p=0.010 (1.9)	p=0.005 (1.9)	p=0.004 (1.9)	-
miR-199a-3p	p=0.010 (3.9)	p=0.005 (3.9)	p=0.005 (3.9)	-
miR-202	-	-	-	p=0.0001 (2.4)
miR-324-3p	-	-	p=0.040 (2.3)	-
miR-328	-	p=0.035 (1.6)	-	-
miR-335	-	-	p=0.028 (2.5)	p<0.0001 (1.8)
miR-340	p=0.040 (3.0)	p=0.039 (2.7)	p=0.017 (3.3)	-
miR-365	-	p=0.005 (1.9)	-	p<0.0001 (0.6)
miR-370	-	-	-	p=0.023 (1.5)
miR-376a	p=0.040 (2.6)	-	p=0.011 (3.0)	-
miR-376c	-	-	p=0.006 (2.1)	p<0.0001 (1.6)
miR-382	-	-	p=0.011 (2.7)	p<0.0001 (1.7)
miR-410	p=0.030 (2.1)	p=0.023 (2.1)	p=0.017 (2.2)	-
miR-422a	-	p=0.011 (0.2)	-	p<0.0001 (3.0)
miR-423-5p	-	-	p=0.036 (1.5)	-
miR-433	-	-	p=0.025 (2.3)	p=0.001 (1.5)
miR-489	-	-	-	p=0.007 (1.6)
miR-598	p=0.040 (2.8)	p=0.028 (2.8)	p=0.028 (2.8)	-
miR-628	-	p=0.049 (0.15)	-	p<0.0001 (2.6)
miR-652	-	-	-	p<0.0001 (1.9)
miR-891a	-	-	-	p=0.0001 (2.7)

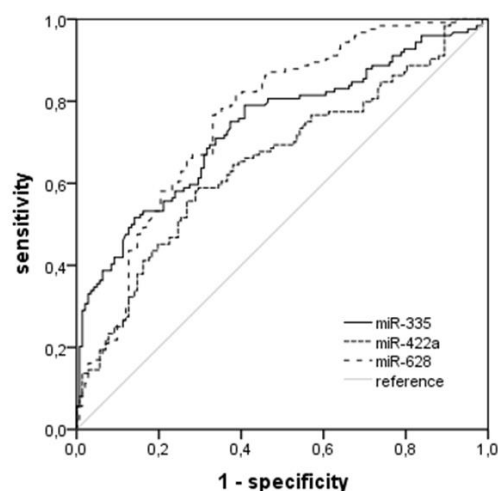
Cells filled with “-“ denote insignificant correlations.

Exosomal miRNAs levels which are deregulated in one or both subgroups and additionally differ between the two subgroups of HER2-positive and TNBC patients are marked in peach.

Table 6 summarizes the significant results with the adjusted p-values and fold changes of miRNAs as derived from volcano plots (Figure 15). From 45 miRNAs, 30 exosomal miRNAs

were either differentially expressed in the subgroups of HER2-positive and TNBC patients, or in all BC patients compared with those of healthy women. Of particular interest are the relative differences of exosomal miRNA levels between HER2-positive and TNBC patients. Of 18 exosomal miRNAs, those levels differed significantly between HER2-positive and TNBC patient subgroups, 9 miRNAs were also deregulated in one or both subgroups compared with healthy women.

With respect to the subgroup, the significant differences between TNBC and HER2-positive patients were reflected by AUC values of 0.737, 0.655 and 0.759 for miR-335, miR-422a and miR-628, respectively. To improve the discrimination, the concentrations of exosomal miR-335 and miR-628 as well as miR-335, miR-422a and miR-628 were combined by logistic regression. The combined scores of these exosomal miRNAs could discriminate between TNBC and HER2-positive patients with a sensitivity of 65% and 68% and a specificity of 84% and 81%, respectively (These numbers may be biased towards higher values, because the scores were fitted on the same data). Sensitivities and specificities were determined at the highest Youden index (sensitivity + specificity - 1) (Figure 16).



variables	AUC	specificity	sensitivity	p-value
miR-335	0.737	59%	79%	<0.001
miR-422a	0.655	71%	58%	<0.001
miR-628	0.759	66%	77%	<0.001
miR-335 and miR-628	0.807	84%	65%	<0.001
miR-335,miR-422a and miR-628	0.808	81%	68%	<0.001

**Figure 16: Exosomal miRNAs differ between HER2-positive and TNBC patients**

ROC analyses show the profiles of sensitivity and specificity of exosomal miR-335, miR-422a and miR-628 and their combinations to distinguish TNBC from HER2-positive BC patients. The table below summarizes the sensitivities and specificities of exosomal miR-335, miR-422a, miR-628 and their combinations.

## 5.6. Exosomal miRNA levels after neoadjuvant therapy

Plasma samples from only 9 BC (4 HER2-positive and 5 TNBC) patients were available directly after neoadjuvant therapy before surgery. To obtain information on changes in the plasma levels induced by the therapy, we compared the levels of exosomal miRNAs after therapy with those before therapy, and those of healthy women. Only 4 miRNAs (miR-27a, miR-155, miR-376a and miR-376c) significantly changed their levels after therapy. Since the levels of the other miRNAs differed hardly before and after therapy the box plot and the table (p-values) only show the dynamics of these 4 miRNAs (Figure 17). Although the data are not representative because of the small number of BC patients, they nevertheless show that the decrease in the levels of 4 exosomal miRNAs to normal (healthy) levels after therapy may be affected by

neoadjuvant therapy (Figure 17). Unfortunately, the cohort of 9 BC patients was too small to result in a robust statistical evaluation.

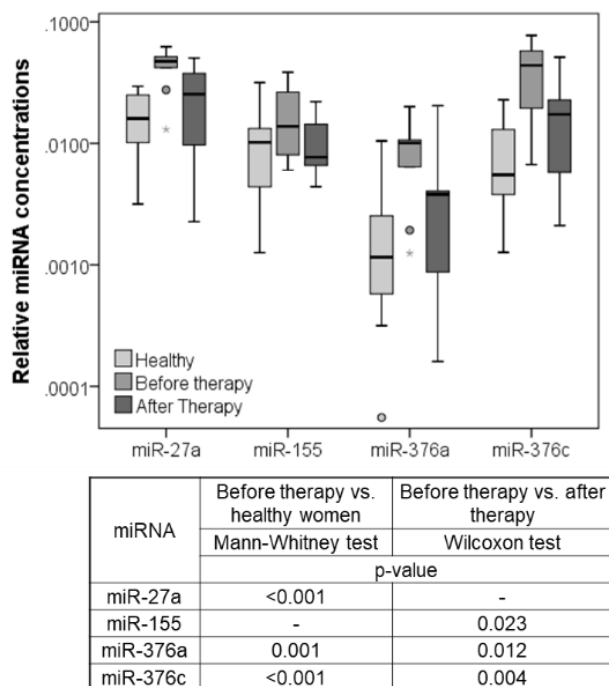


**Figure 17: Exosomal miRNA levels before and after neoadjuvant therapy**

The box blot shows the plasma levels of exosomal miRNAs of 9 BC patients before and after neoadjuvant therapy and 20 healthy women. P-values comparing the expression levels before and after therapy, and between patients and healthy women are indicated in the table below. Cells filled with “-“ denote insignificant correlations.

### 5.7. Associations of exosomal miRNA levels with the established risk factors

Tables 7 (categorical variables) and Table 8 (continuous variables) summarize the significant correlations between the exosomal miRNA levels and the clinicopathological risk parameters of BC patients. Strikingly, the levels of miRNAs in both subgroups (HER2-positive and TNBC) displayed a different preference to correlate with clinicopathological parameters: With only one exception (miR-152 and stromal lymphocytes, Table 8), no miRNA correlated with a clinical parameter, such as nodal status, tumor size, grading, lymphocyte predominant BC, Ki67 expression and intratumoral lymphocytes, in both subgroups. In particular, the levels of



exosomal miR-16 ( $p=0.23$ ), miR-328 ( $p=0.19$ ) and miR-660 ( $p=0.016$ ) were associated with lymph node status in HER2-positive patients (Table 7). Accordingly, the levels of exosomal miR-16 were lower in TNBC than in HER2-positive patients ( $p=0.023$ ), while those of miR-328 were only upregulated in HER2-positive patients compared to healthy patients ( $p=0.035$ , Table 5). In the subgroup of TNBC patients, only the levels of exosomal miR-374 were associated with higher tumor size, whereas in HER2-positive BC patients the levels of 6 exosomal miRNAs (miR-185, miR-376a, miR-382, miR-410, miR-433 and miR-628) were associated with the tumor size (Table 7). These findings show the heterogeneity of both BC subtypes that is reflected by the subtype-specific miRNA expression or packaging of miRNAs into exosomes or both, and the relationship of these unique exosomal miRNA patterns with the diverse clinical parameters.

**Table 7: Significant associations between the plasma levels of exosomal miRNAs and clinicopathological/risk parameters (categorical variables)**

Clinical/risk factors	miRNAs*	All BC patients	HER2-positive patients	TNBC patients
		p(t-test)**	p(t-test)**	p(t-test)**
Age (<50, >=50)	miR-20a	0.011	-	-
	miR-30c	-	-	0.038
	miR-99b	0.006	-	0.002
	miR-106b	0.024	-	-
	miR-145	0.015	-	0.040
	miR-150	0.008	-	0.015
	miR-185	0.035	-	-
	miR-202	0.046	-	-
	miR-301	0.019	0.032	-
miR-891a	0.007	-	0.010	
Nodal status (N0, N+)	miR-16	-	0.023	-
	miR-328	-	0.019	-
	miR-660	-	0.016	-
Tumor size (T1-2, T3-4)	miR-185	-	0.040	-
	miR-199a-3p	0.034	-	-
	miR-374	-	-	0.030
	miR-376a	-	0.004	-
	miR-382	0.031	0.014	-
	miR-410	-	0.038	-
	miR-433	-	0.037	-
miR-628-5p	-	0.041	-	
Grading (G1-2, G3)	miR-16	0.033	-	-
	miR-20a	0.024	-	0.032
	miR-30c	-	-	0.023
	miR-155	-	-	0.038
	miR-193b	-	-	0.028
	miR-422a	-	0.010	-
miR-628-5p	-	0.005	-	
Lymphocyte predominant breast cancer (neg, pos)	miR-148a	0.036	-	-
	miR-335	0.048	-	-
	miR-652	-	0.040	-
	miR-891a	0.050	0.022	-

Cells filled with “-“ denote insignificant correlations.

\*Only miRNAs are listed which significantly correlate with the clinical parameter in one of the (TNBC and HER2-positive) patient subgroups and/or all patients.

\*\* p(t-test), Student’s t-test.

**Table 8: Significant associations between the plasma levels of exosomal miRNAs and clinicopathological risk parameters (continuous variables)**

Clinical risk factor	miRNA*	All BC patients		HER2-positive patients		TNBC patients	
		Pearson**	p(Pearson)***	Pearson**	p(Pearson)***	Pearson**	p(Pearson)***
Ki67****	let-7g	-0.098	0.045	-	-	-	-
	miR-16	0.114	0.018	-	-	-	-
	miR-27b	0.115	0.021	-	-	-	-
	miR-99b	-0.121	0.013	-	-	-	-
	miR-145	-0.122	0.012	-	-	-	-
	miR-148a	-0.297	<0.001	-	-	-	-
	miR-155	0.121	0.014	-	-	0.211	0.002
	miR-202	-0.128	0.015	-	-	-	-
	miR-324-3p	-0.111	0.025	-	-	-	-
	miR-328	-	-	-	-	-0.141	0.042
	miR-335	-0.185	<0.001	-	-	-	-
	miR-365	0.149	0.002	-	-	-	-
	miR-370	-0.122	0.022	-	-	-	-
	miR-374	-0.109	0.038	-	-	-	-
	miR-376c	-0.149	0.002	-	-	-	-
	miR-382	-	-	0.148	0.033	-	-
	miR-422a	-0.220	<0.001	-	-	-	-
	miR-433	-0.118	0.015	-	-	-	-
	miR-489	-0.103	0.036	-	-	-	-
	miR-628-5p	-0.192	<0.001	-	-	-	-
miR-652	-0.160	0.001	-	-	-	-	
miR-660	-	-	-	-	0.157	0.022	
miR-744	-0.120	0.019	-	-	-0.141	0.047	
miR-891a	-0.106	0.041	-	-	-	-	
Intratumoral lymphocytes (iTuly)****	miR-27a	-0.147	0.003	-	-	-0.219	0.001
	miR-148a	-0.142	0.005	-	-	-	-
	miR-152	-0.110	0.026	-	-	-0.164	0.016
	miR-328	-0.098	0.047	-	-	-0.143	0.038
	miR-335	-0.143	0.004	-	-	-	-
	miR-365	-	-	-	-	-0.185	0.008
	miR-374	-0.112	0.035	-	-	-	-
	miR-376c	-0.103	0.038	-	-	-	-
	miR-423-5p	-0.102	0.039	-	-	-	-
miR-744	-0.155	0.026	-	-	-	-	
Stromal lymphocytes (strLy)****	miR-27a	-	-	-	-	-0.155	0.023
	miR-152	-	-	0.170	0.017	-0.135	0.048
	miR-365	-	-	-	-	-0.141	0.042
	miR-410	-	-	-	-	-0.142	0.046
	miR-511	-	-	-	-	-0.178	0.026
	miR-598	-	-	0.155	0.036	-	-
miR-652	-	-	0.195	0.005	-	-	

Cells filled with “-“ denote insignificant correlations.

\*Only miRNAs are listed which significantly correlate with the clinical parameter in one of the (TNBC and HER2-positive) patient subgroups and/or all patients.

\*\* Pearson, Pearson correlation coefficients.

\*\*\* p(Pearson), p-values.

\*\*\*\*measured % at baseline.

## 5.8. Associations of exosomal miRNA levels with pCR and treatment arm

Finally, univariate as well as multivariate (with covariables age, nodal status, tumor size and grading) logistic regression models for pCR were carried out in all patients and in the subgroups defined by TNBC patients, HER2-positive patients and patients in the carboplatin (pMCb) and non-carboplatin (pM) arm. Table 9 contains the unit odds ratio with 95% confidence interval and the corresponding Wald p-value for the miRNA variable in each model. Model results are only reported if the uni- or multivariate model showed a significant contribution of the miRNA to the model, and only miRNAs contributing to all or the single subgroups are reported. At the beginning of our study quantifying exosomal miRNAs in plasma of 8 patients treated with carboplatin, (4 with pCR and 4 without pCR), and 7 patients from the non-carboplatin arm (4 with pCR and 3 without pCR) using the miRNA array containing 384 different miRNAs, we detected that the plasma levels of miR-199a ( $p=0.036$ ) differed between patients with and without pCR, and the levels of miR-125 ( $p=0.029$ ), miR-193b ( $p=0.029$ ), miR-365 ( $p=0.029$ ) and miR-370 ( $p=0.016$ ) differed according to treatment arm. Now, in uni- and multivariate models comprising our large cohort of 435 patients including the single subgroups, the levels of exosomal miR-199a and the other 4 miRNAs did not correlate with pCR and treatment arm, respectively, any more, suggesting that our starting patient cohort of 15 patients was too small to establish a significance of these exosomal miRNAs with pCR or treatment arm. In addition, the concentrations of no miRNA in our set of 45 exosomal miRNAs were associated with the treatment arm, indicating that this set of miRNAs measured in pretreatment plasma samples cannot predict the treatment arm. However, 12 miRNAs could predict pCR in uni- or

multivariate comprising all patients or the single subgroups. Strikingly, the levels of miR-155 most significantly predicted pCR in uni- ( $p=0.002$ ) and multivariate model ( $p=0.003$ ) comprising all patients, as well as HER2-positive patients and TNBC patients (Table 9). This exosomal miRNA was also significantly downregulated in the 9 patients after therapy (Figure 17,  $p=0.023$ ). Furthermore, the levels of miR-301 were also most significantly associated with pCR in uni- ( $p=0.002$ ) and multivariate model ( $p=0.001$ ) comprising all patients, as well as HER2-positive patients. Both, the levels of miR-155 and miR-301 correlated somewhat better with pCR in the PMCb than PM arm (Table 9), indicating an improved response to carboplatin-based therapy.

**Table 9: Logistic regression models for pCR with p-values odd ratio and confidence intervals**

miRNAs	Patients	All BC patients		HER2-positive patients		TNBC patients	
	Model	univariate	multivariate	univariate	multivariate	univariate	multivariate
miR-20a	all	-	-	-	-	-	-
	in PM*	-	-	-	-	-	-
	in PMCb**	$p=0.020$ 1.39 (1.05-1.84)	$p=0.019$ 1.41 (1.06-1.89)	-	-	-	-
miR-27b	all	-	-	$p=0.035$ 1.30 (1.02-1.65)	$p=0.050$ 1.28 (1.00-1.63)	-	-
	in PM*	-	-	-	-	-	-
	in PMCb**	$p=0.038$ 1.27 (1.01-1.59)	$p=0.030$ 1.30 (1.03-1.64)	-	-	-	-
miR-99b	all	$p=0.103$ 1.14 (0.97-1.34)	$p=0.039$ 1.19 (1.01-1.41)	-	-	-	-
	in PM*	-	-	-	-	-	-
	in PMCb**	-	-	-	-	-	-
miR-155	all	$p=0.002$ 1.25 (1.08-1.44)	$p=0.003$ 1.24 (1.08-1.44)	$p=0.049$ 1.24 (1.00-1.53)	$p=0.035$ 1.26 (1.02-1.56)	$p=0.013$ 1.29 (1.05-1.57)	$p=0.018$ 1.29 (1.04-1.58)

	in PM*	p=0.033 1.26 (1.02-1.55)	p=0.049 1.24 (1.00-1.53)	-	-	-	-
	in PMCb**	p=0.032 1.24 (1.02-1.51)	p=0.023 1.27 (1.03-1.55)	-	-	-	-
miR-193b	all	p=0.039 1.13 (1.01-1.26)	p=0.055 1.12 (1.00-1.26)	p=0.010 1.26 (1.06-1.50)	p=0.012 1.26 (1.05-1.51)	-	-
	in PM*	-	-	-	-	-	-
	in PMCb**	-	-	-	-	-	-
miR-301	all	p=0.002 1.25 (1.08-1.44)	p=0.001 1.27 (1.10-1.46)	p=0.013 1.30 (1.06-1.60)	p=0.011 1.32 (1.07-1.64)	-	-
	in PM*	p=0.040 1.22 (1.01-1.48)	p=0.028 1.25 (1.02-1.52)	-	-	-	-
	in PMCb**	p=0.020 1.28 (1.04-1.57)	p=0.022 1.29 (1.04-1.6)	p=0.012 1.53 (1.10-2.12)	p=0.016 1.51 (1.08-2.12)	-	-
miR-365	all	-	-	-	-	-	-
	in PM*	-	-	p=0.052 1.35 (1.00-1.81)	p=0.038 1.39 (1.02-1.90)	-	-
	in PMCb**	-	-	-	-	-	-
miR-423	all	p=0.048 1.19 (1.00-1.42)	p=0.064 1.18 (0.99-1.41)	-	-	-	-
	in PM*	-	-	-	-	-	-
	in PMCb**	-	-	-	-	-	-
miR-511	all	-	-	-	-	-	-
	in PM*	-	-	-	-	-	-
	in PMCb**	-	-	-	-	p=0.239 0.90 (0.76-1.07)	p=0.043 0.78 (0.62-0.99)
miR-628	all	-	-	-	-	p=0.024 0.81 (0.67-0.97)	p=0.017 0.79 (0.65-0.96)
	in PM*	-	-	-	-	-	-
	in PMCb**	-	-	-	-	-	-
miR-660	all	-	-	p=0.044 1.35 (1.01-1.80)	p=0.027 1.40 (1.04-1.89)	-	-
	in PM*	-	-	-	-	-	-
	in PMCb**	-	-	-	-	-	-

miR-891a	all	p=0.063 1.07 (1.00-1.15)	p=0.036 1.08 (1.01-1.16)	-	-	-	-
	in PM*	-	-	-	-	-	-
	in PMCb**	-	-	-	-	-	-

Cells filled with “-“ denote insignificant miRNA contributions to the models. MiRNAs which do not show significant contributions in any population were omitted. For each miRNA variable and each patient group a univariate as well as a multivariate model with the covariables of age, nodal status, tumor size and grading were calculated.

The odd ratio with the 95% confidence interval and the associated Wald p-value for the miRNAs are presented.

\*PM, non-carboplatin treatment arm.

\*\*PMCb , carboplatin treatment arm

### 5.9. Identification of potential mRNAs targets of miR-376c

In this study one of the most deregulated exosomal miRNAs was miR-376c. In order to detect potential mRNA targets of miR-376c, we used an mRNA array containing 84 key genes involved in signal transduction, and other biological processes such as angiogenesis, adhesion, proteolysis, cell cycle and apoptosis. Using Mir Trap system and this mRNA array we have identified 31 potential mRNAs which can be bound by miR-376c.

**Table 10: Predicted mRNA targets with fold enrichments and function of the gene.**

mRNAs targeted by miR-376c	Fold Enrichment	Function
MMP9	1018	angiogenesis
BCL2	927	anti-apoptotic
VEGFA	669	angiogenesis
ABCB1	633	drug pump
CDKN2A	595	cell cycle inhibitor
Ki-67	572	cell proliferation
ATM	491	DNA repair
IGFBP3	302	cell proliferation
BRCA2	285	DNA repair
PTGS2	280	anti-apoptotic
CDKN1C	256	cell migration, invasion inhibitor
MYC	252	cell proliferation
ERBB2	250	cell proliferation
IL6	215	growth and metastasis
EGFR	195	cell proliferation
TMS1 (PYCARD)	182	apoptotic
IGF1R	164	metastasis
CDH1	158	metastasis
CSF1	156	tumor progression
BRCA1	153	DNA repair
THBS1 (Trombospondin)	129	angiogenesis inhibitor
CCNE1	116	cell cycle progression
CDKN1A	112	cell cycle inhibitor
KRT19 (CK19)	97	circulating tumor cells
ID1	96	tumor progression
MUC1	93	tumor growth
MAPK1	67	cell proliferation
AKT1	64	tumorigenesis, progression
TGFB1	49	metastasis
CDK2	47	cell progression
PTEN	46	tumorigenesis inhibitor



### 5.10. No impact of miR-376c on cell proliferation

Proliferation was measured using the MTT assay after overexpression or inhibition of miR-376c for 24, 48 and 72 hours in BC cell lines (MDA-MB-231 and MDA-MB-468). The results show that miRNA-376c did not affect cell proliferation in MDA-MB-231 and MDA-MB-468 cell lines (Figure 18).

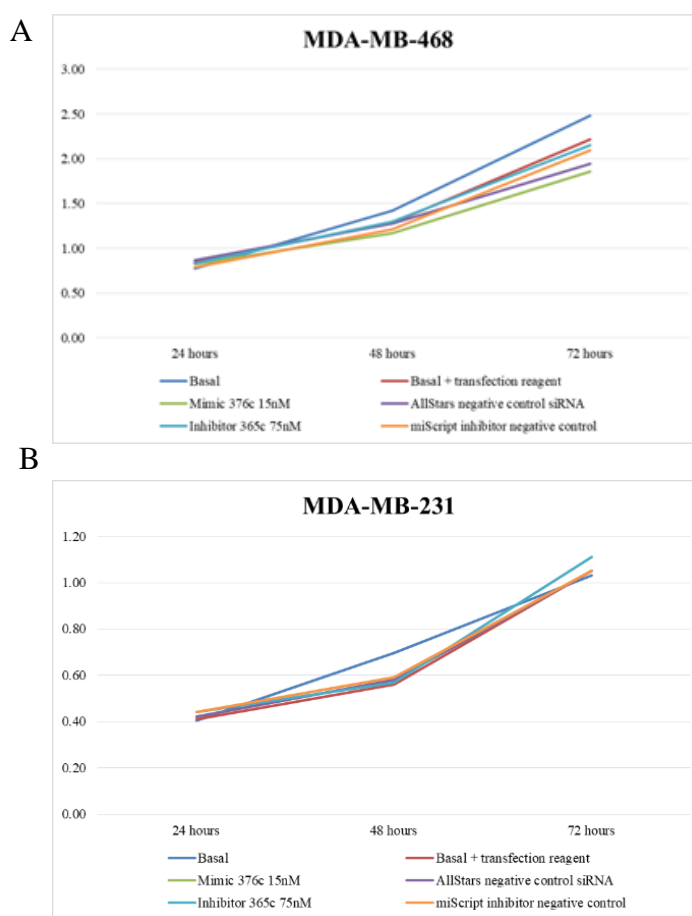


**Figure 18: MiR-376c has no effect on cell proliferation in BC cell lines**

Both cell lines were transfected with mimics, inhibitor, AllStars negative control siRNA, miScript inhibitor negative control. MiR-376c does not affect proliferation of MDA-MB-231 (A) and MDA-MB-468 cell lines (B).

### 5.11. No impact of miR-376c on apoptosis

The impact of miR-376c on apoptosis was measured by FACS in the two cell lines MDA-MB-231 and MDA-MB-468.

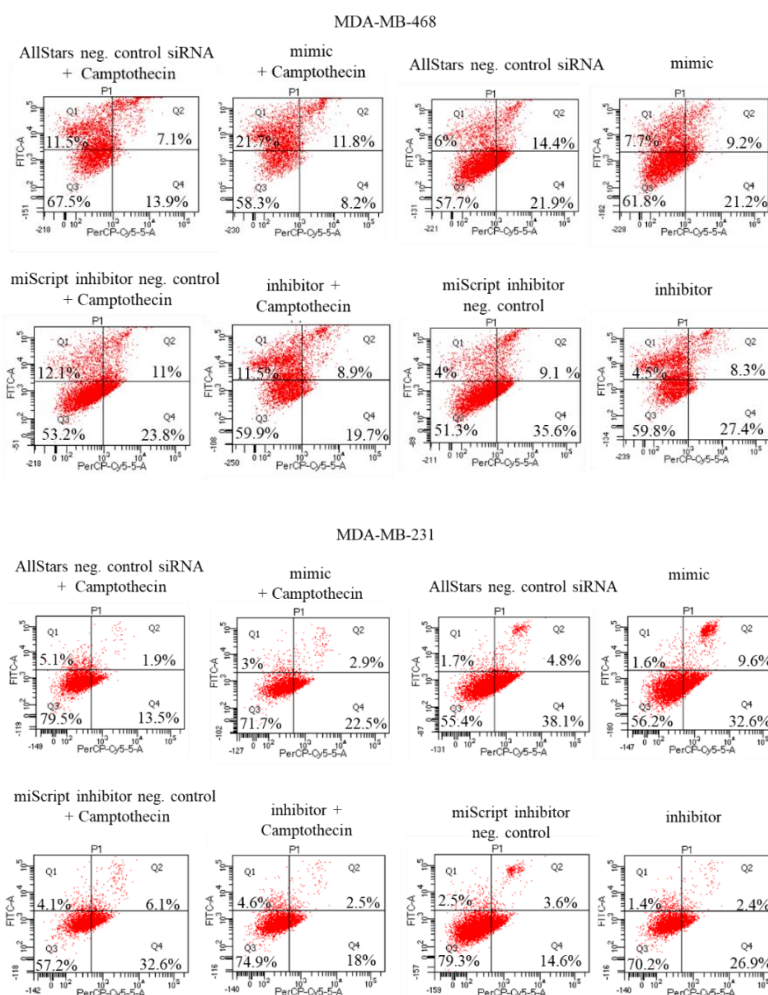


**Figure 19: miR-376c impact on apoptosis in MDA-MB-231 and MDA-MB-468**

Both cell lines were transfected with mimics, inhibitor, AllStars negative control siRNA and miScript inhibitor negative control. Additionally, cells were treated with topoisomerase I inhibitor camptothecin to induce apoptosis. The cells were labeled with Annexin-V-FITC and 7AAD and analysed on a FACS Canto II device. Apoptotic cells are positive for Annexin-V upper left corner (Q1), late apoptotic and necrotic cells are positive for both Annexin-V and 7AAD upper right corner (Q2), healthy cells are negative for Annexin-V and 7AAD lower left corner (Q3), and cell fragments only positive for 7AAD lower left corner (Q4). The size for each population (%) is given in the corresponding area.

Cells were transfected with mimics or inhibitors of miR-376c, AllStars negative control siRNA and miScript inhibitor negative control. As a control served the cell line was transfected only with transfection reagent. Additionally, cells were treated with the topoisomerase I inhibitor camptothecin, which is used in cancer chemotherapy and induces apoptosis. FACS analyses showed that miR-376c did not affect apoptosis in MDA-MB-231 and MDA-MB-468 (Figure 19).

### 5.12. Size distribution of EVs determined by nanoparticles tracking analysis

The size distribution and concentration of isolated EVs from cell cultured media were determined by nanoparticle tracking analysis (NTA) on a Nanosight device. The size of isolated EVs were in the range from 10 to 300 nm indicating that the sample also contains exosomes and microvesicles. However, majority of the isolated vesicles size was 120 suggesting that the majority of isolated vesicles are exosomes (Figure 20).

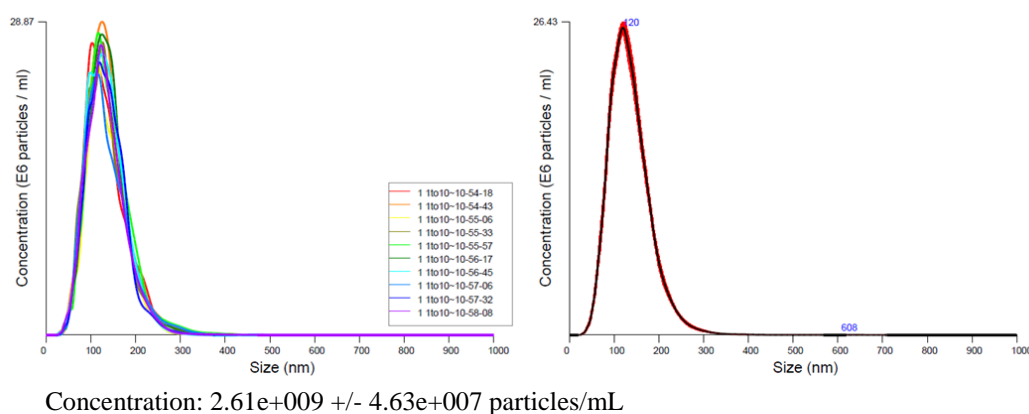


**Figure 20: Size distribution of EVs determined by NTA**

The chart on the left side comprises 10 measurements from the same sample, and shows the size distribution of EVs vs. concentration. The chart on the right side represents the mean of all 10 measurements with a peak that displays the size of 120 nm indicating that the majority of the measured EVs are exosomes.

### 5.13. Shuttle of EV visualized by confocal microscopy

To examine the shuttle of EVs, EVs isolated from MDA-MB-468 cells were stained and seeded onto MDA-MB-468 recipient cells. Approximately 20000000 EVs were added to the 30000 cells per well and incubated for 1 hour. In order to determine if the EVs are inside the cell and to remove the excess of the EVs that didn't enter inside the cells, cells were washed after 1-3 hours, and fresh exosome depleted medium was added. Using live-cell confocal microscopy, EVs were detected around or on the membrane of MDA-MB-468 cells. The time range required to observe EVs entering into a cell varied from 30 min up to 1 hour. Figure 21 shows the EVs 1 hour after their addition. In Figure 21 in red is depicted the signal arising from EVs and in green the signal coming from the cell membrane. As a result the EVs are localized around the cell membrane of both the displayed cells and there are no visible EVs in the surroundings.

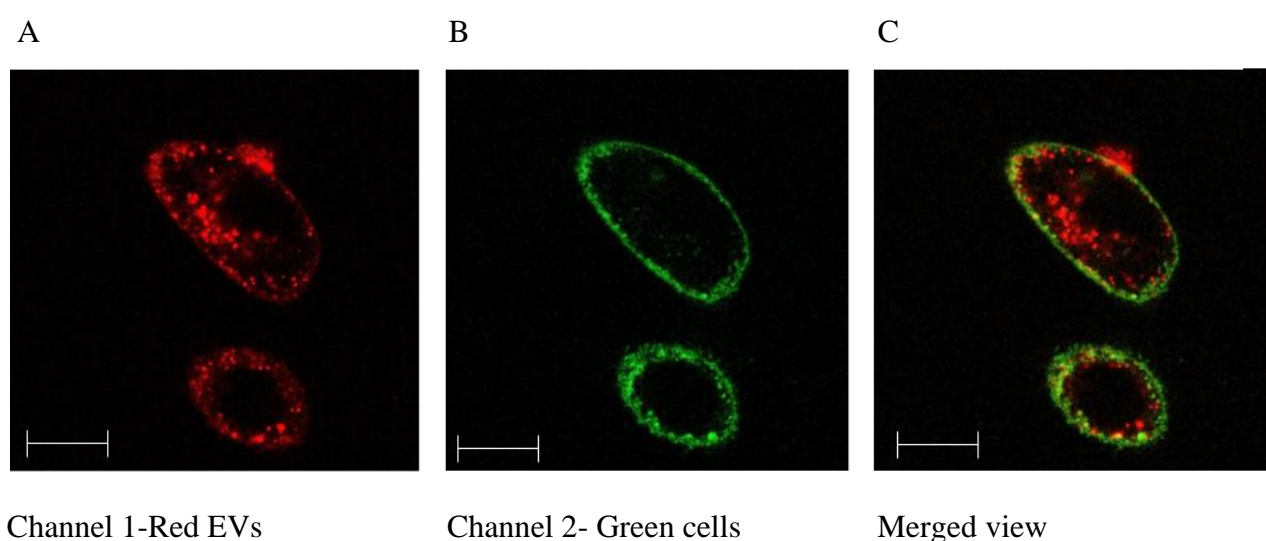


**Figure 21: EVs are localized in the cell membrane**

The scale bar is set to be 18.8  $\mu\text{m}$  in all the pictures. (A) Channel 1 EVs labeled with PHK26, (B) Channel 2 cell membrane stained with EpCAM antibody, (C) merged view. As shown in (C) EVs are localized around the cell membrane and most of EVs are inside of the cells.

The uptake of EVs into the cells can be seen in Figure 22, where some cells have uptake higher amounts of EVs than others. To see if cells can also release EVs and if there is a shuttle from cell to cell videos were recorded. Already 30 min after the addition of EVs it was visible that EVs were released from the cells (Figure 22). Also detectable were the different sizes of EVs that were uptaken by cells.

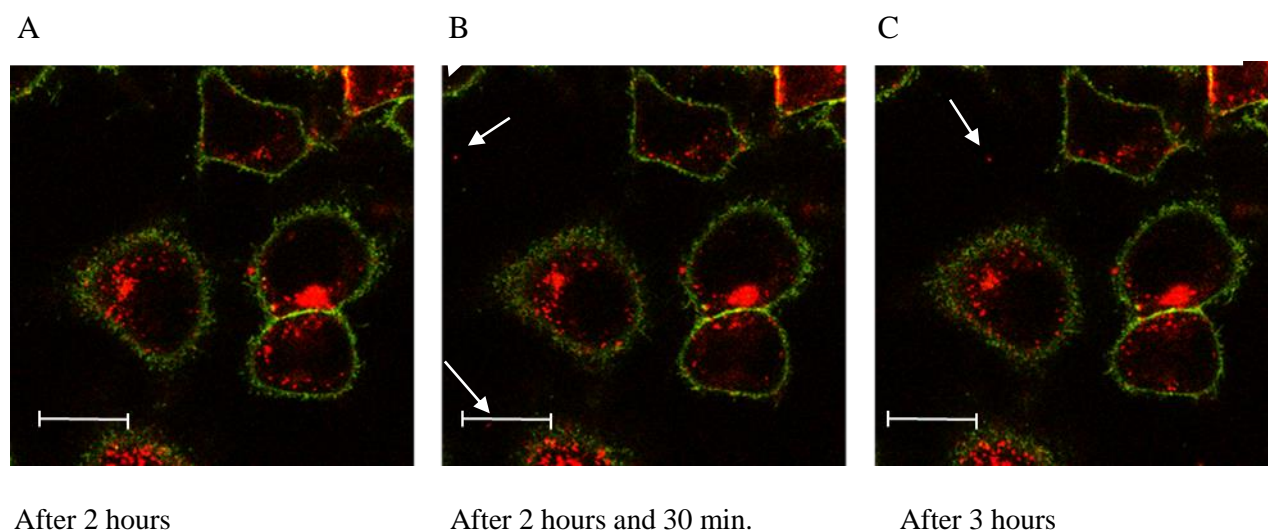


**Figure 22: EV released from cells**

The scale bar is set to be 18.8  $\mu\text{m}$  in all the pictures Red: EVs labeled with with PHK2. Green: cell membrane labeled with EpCAM antibody (A) as it is clearly shown after 2 hours the EVs were not detectible outside the cells, since the excess of EVs was removed with a washing step. (B, C) After waiting further 30 min a few EVs appeared outside the cells. The majority of the EVs were inside the cell over the period of 1 hour. However, there were also visible a few EVs outside the cells, as indicated by the arrow. Please note that fat red spots are clusters of EVs that couldn't dissolve.

To confirm that EVs are released from the cell a 30 min long time video was recorded.

As shown in Figure 23 the video shows that EVs are travelling from the inner side of the cell membrane to the outer part of the membrane. These data suggest that EVs are trafficking between the cells.

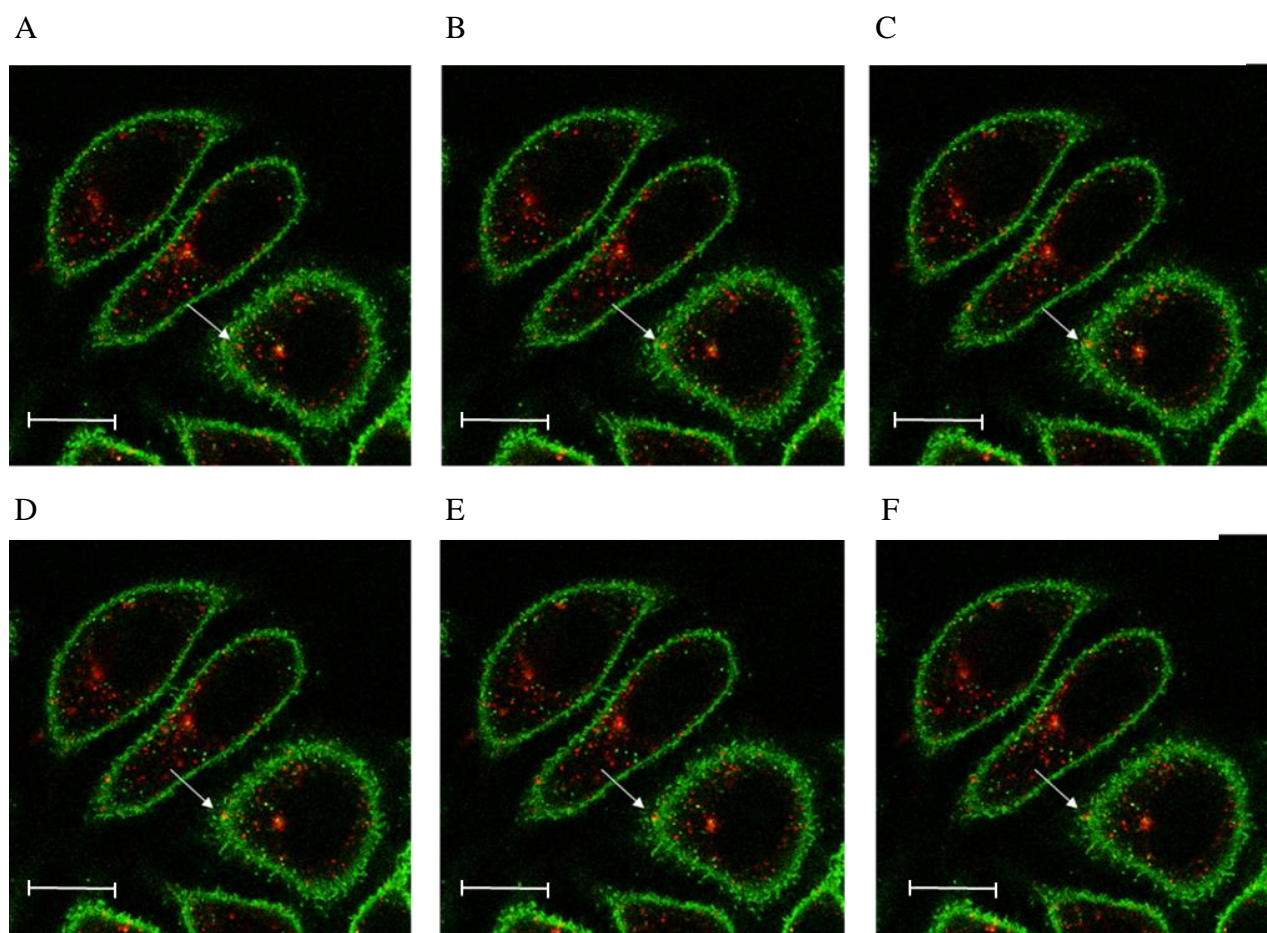


**Figure 23: EV shuttle from inside of the cell to outside**

The scale bar is set to be  $18.8 \mu\text{m}$  in all the pictures. Red: EVs labeled with PHK26, Green: cell membrane labeled with EpCAM antibody. A)-F) images of EVs taken at short time interval  $\text{dt} = 20\text{secs}$ . The moving of EV is indicated with an arrow.

## 6. Discussion

### 6.1. Quantification of exosomal miRNA in BC patients

Molecular classification of BC into HER2-positive and TNBC tumours is essential for optimal use of current therapies and for development of new drugs. Of interest is that exosomes participate in cell-to-cell communication between cancer cells and normal host cells, and thus, are crucial components for regulation of the tumor microenvironment (Zhao et al., 2015). In this regard, investigation of the involvement of exosomal miRNAs in these subtypes could provide new diagnostic/prognostic biomarkers and therapeutic target molecules, apart from a better understanding of tumor growth processes. In the current study, we identified miRNA signatures in exosomes specific to discriminate between HER2-positive and TNBC patients, indicating the different biology in these subgroups. Strikingly, different exosomal miRNA patterns were associated with the clinicopathological characteristics within the respective subgroups. As far as we know, this is the first study that measured a panel of 45 miRNAs in exosomes derived from a large cohort of 435 BC patients.

As we recently reported for ovarian cancer patients (Meng et al., 2016), we found that BC patients also had an excessive, active secretion of exosomes into their blood circulation. Although the levels of exosomes are somewhat higher in HER2-positive than TNBC patients, the difference is not significant. These findings suggest that a high secretion of exosomes may be a general feature of cancer patients. However, the exosomes differ in their content within both subgroups. Namely, we detected differently expressed miR-27a/b, miR-335, miR-365, miR-376c, miR-382, miR-422a, miR-433 and miR-628 in exosomes of either HER2-positive or TNBC patients compared with healthy women. This subtype-specific distribution of miRNAs in exosomes may indicate both, a different miRNA expression pattern and a selective

exosomal packaging process. Based on the ability of exosomes to communicate between cells, the detection of these miRNA panels in exosomes may be superior to the detection of cell-free miRNAs in plasma or serum. To date, the presence of these miRNAs has not yet been described in BC-derived exosomes.

In our study, we detected that in comparison with healthy women, the levels of exosomal miR-27a were only significantly upregulated in HER2-positive patients (but not in TNBC patients), whereas the levels of miR-27b were upregulated in both subtypes, but with a significantly higher exosomal occurrence in HER2-positive patients. MiR-27a was reported to activate the Wnt/ $\beta$ -catenin signaling pathway to promote the proliferation, migration and invasion of BC cells (Kong et al., 2017). So far, an association of miR-27a with HER2-positive BC has not been described. However, in contrast to our data an association of this miRNA with TNBC was revealed in a meta-analysis, but its quantification was carried out in tumor tissues and not in exosomes (Lu et al., 2017). These findings possibly point to a selective packaging of miRNAs in exosomes independent of their expression levels. Conversely, our findings on the higher levels of exosomal miR-27b in HER2-positive patients are supported and complemented by the data by Jin et al. (Jin et al., 2013) showing that HER2 stimulated miR-27b expression through the AKT/NF- $\kappa$ B signaling cascade. We also detected that the levels of exosomal miR-27b predict pCR in HER2-positive patients, indicating its narrow association with HER2-positive tumours. Despite the conventional role of miR-335 to act as a tumor suppressor in BC (Bertoli et al., 2015), our data demonstrate its significantly increased occurrence in exosomes from TNBC patients. Nevertheless, Martin et al. (Martin et al., 2017) reported that miR-335 may also act in an oncogenic way in BC, to repress genes involved in the ER $\alpha$  signaling pathway, and consequently, to enhance resistance to the growth inhibitory effects of tamoxifen. Contrary to our findings that show significantly upregulated levels of exosomal miR-365 in the subgroup of HER2-positive (but not in TNBC), miR-365 was reported to be downregulated and act as a tumor suppressor in BC. Kodahl et al. (Kodahl et al., 2014) showed that its expression levels



were lower in serum of ER-positive BC patients than healthy controls, whereas we show that its levels in HER2-positive patients who do not express ER are increased. In addition, miR-365 was also described to be oncogenic. Overexpression of miR-365 promoted cell proliferation and invasion through targeting ADAMTS-1 (a disintegrin and metalloproteinase with thrombospondin motifs) in BC cells (Li et al., 2015). In our study, significantly higher levels of exosomal miR-376c and miR-382 were observed in TNBC patients, but not in HER2-positive BC patients. Upregulated levels of miR-376c (Cuk et al., 2013b) and miR-382 (Mar-Aguilar et al., 2013) were also detected in plasma and serum of BC patients (regardless of the subtypes), respectively, by 2 previous studies. In BC, miR-382 targeted and repressed the Ras GTPase superfamily member RERG (Ras-related and estrogen-regulated growth inhibitor), to attenuate the inhibitory effects of RERG on the oncogenic Ras/ERK pathway. Thereby, miR-382 promoted BC cell viability, clonogenicity, survival, migration, invasion and *in vivo* tumorigenesis/metastasis. (Ho et al., 2017). Contrary, for example in oral squamous cancer, miR-376c seems to have tumor suppressive functions. Its overexpression in these cancer cells suppressed fission, proliferation, migration and invasion and induced cell apoptosis via targeting the transcription factor HOXB7 (Wang et al., 2017). Finally, we found that the levels of exosomal miR-422a are downregulated in HER2-positive BC patients, whereas the levels of exosomal miR-433 are upregulated in TNBC patients, but till now, quantitative data on these miRNAs have not been published for BC patients. It was reported that in BC stem cells, up-regulation of miR-422a attenuated microsphere formation, proliferation and tumor formation via suppressing the PLP2 (Proteolipid protein 2) expression (Zou et al., 2018). Moreover, miR-433 repressed Rap1a, a small G protein of the Ras guanosine triphosphatase (GTPase) superfamily, that activates the MAPK signaling pathway, and thus, repressed cell migration and proliferation, and induced apoptosis in BC (Zhang et al., 2018b). In addition, miR-433 targeted AKT3 in BC (Hu et al., 2018). These findings highlight miR-422a and miR-433 as tumor suppressor genes.

Not only, the miRNA patterns in exosomes differed between HER2-positive and TNBC patients, but they were also specifically associated with different clinicopathological parameters within the subgroups. For example, we identified a particular set of exosomal miRNAs (miR-16, miR-328 and miR-660) to be associated with lymph node status only in the subgroup of HER2-positive BC patients, but not in TNBC patients. In addition, we detected that miR-660 predicted pCR to neoadjuvant therapy in HER2-positive patients. Shen et al. already showed the potential of miR-660 as a therapeutic target for clinical treatment of BC and its role as a regulator of proliferation, migration and invasion of human BC cells (Shen et al., 2017). Moreover, our present findings on the association of the levels of exosomal miR-16 with lymph node status are substantiated by our previous data (Stuckrath et al., 2015), demonstrating such an association with cell-free miR-16 in plasma. Thus, our findings indicate a possible role of miR-16 in the development of lymph node metastases in BC. In the subgroup of TNBC patients, we discovered that only the levels of exosomal miR-374 were associated with a higher tumor size, whereas the levels of 6 exosomal miRNAs (miR-185, miR-376a, miR-382, miR-410, miR-433 and miR-628) showed such an association in HER2-positive BC patients. In addition, we revealed that miR-376a, those exosome-free plasma levels are also upregulated in BC (Cuk et al., 2013b), displayed a dynamic presence in exosomes. Aside from miR-376a, three further miRNAs (miR-27a, miR-155 and miR-376c) were also downregulated to normal levels after neoadjuvant therapy, suggesting that these miRNAs may be released from the primary tumor into the blood to some extent, and their changes may directly reflect cancer status. Especially, miR-155 is a well-known miRNA with both tumor suppressive and oncogenic character, targeting e.g., HER2 (He et al., 2016) and the transcription factor FOXO3a (Kong et al., 2010; Yamamoto et al., 2011) in BC, respectively. Along with miR-27a, there is also an association of miR-155 with the decreased expression of FOXO3a which is paralleled with the increased expression of RUNX2 (Jurkovicova et al., 2016).

In neoadjuvant settings, the early identification of non-responding BC is crucial to avoid ineffective treatments. In particular for aggressive TNBC and HER2-positive BC subtypes, achievement of pCR correlates with improved long-term outcome (von Minckwitz et al., 2014a; von Minckwitz et al., 2014b). Here, we show for the first time that the levels of exosomal miR-155 in all BC patients and their subgroups, as well as exosomal miR-301 with the exception of triple negative BC patients most significantly predicted pCR to neoadjuvant therapy. This information could be used for treatment stratification considering alternative treatment options. However, to introduce exosomal miR-155 and miR-301 as predictive markers, further prospective studies are necessary to confirm their predictive value. Particularly, the quantification of these exosomal miRNAs in a large cohort of plasma samples before, during and after chemotherapy is required. Since miR-301 regulates the PTEN/Akt and NF $\kappa$ B signaling pathways that are important in the progression of BC (Ma et al., 2014; Shi et al., 2011), and binds to estrogen receptor 1 leading to estrogen independence of BC (Lettlova et al., 2018), miR-301 may be an early therapeutic target molecule in BC.

To summarize, our findings suggest that certain miRNAs are selectively enriched in exosomes of HER2-positive and TNBC patients and are also associated with the clinicopathological parameters and pCR within the BC subtypes. Exosomal miRNAs may reflect the characteristics of their parental cells, and therefore, may offer a tumor-related profile. Recently, we found that the majority of miRNAs detectable in plasma is concentrated in exosomes (Eichelser et al., 2014). However, it is of note to mention that the plasma exosome population is a heterogeneous mixture of cancer and normal (wild type) exosomes, and may be derived from all cells types, especially from blood cells. This, of course, compromises the tumor specificity of the identified exosomal miRNA signatures. Therefore, methods to selectively enrich cancer exosomes from plasma or serum have to be advanced. Unfortunately, tumor-associated exosome markers allowing such an enrichment are poorly defined. In addition, our unpublished data show that the proportion of tumor-derived exosomes is small in comparison with normal, wild-type

exosomes impeding the isolation of low-abundant miRNAs. However, the extensive secretion of exosomes in BC patients triggered by the tumor, points to that the tumor also communicates with wild-type exosomes. Thus, we should keep in mind that not only exosomes derived from the primary tumor or metastases may be eligible for cancer personalized diagnostics, but also exosomes derived from other organs that are affected by tumor burden (Roccaro et al., 2013). Although our results show a different packaging of miRNAs into exosomes, and exosomal miRNAs as future diagnostic markers and therapeutic molecules, there are some aspects that may limit our study. Our analyses were carried out by miRNA array cards. We did not verify them by single real-time PCR assays, since the number of miRNAs was too high, and the population size too large in our study. However, our previous analyses in an independent cohort before starting the current study showed that the data were nearly congruent applying miRNA array cards and single real-time PCR analyses. In addition, the number of plasma samples collected directly after neoadjuvant therapy was too low, to make a statistical conclusion on the impact of therapy on the miRNA expression levels. However, the strength of our study is the number of miRNAs analysed and the size of our patient population before neoadjuvant therapy.

## **6.2. Potential mRNA targets of miR-376c**

One miRNAs is able to interact with hundreds of mRNAs (Cloonan, 2015) and hence, a miRNAs regulate numerous signal transduction pathways involved e.g. in tumor development, differentiation, proliferation and progression (Hwang and Mendell, 2007; Peng and Croce, 2016; Zhao et al., 2017). Unlike plant miRNAs, which usually bind to their targets with perfect complementarity (Zhang, 2005), animal miRNAs have limited complementarity which makes it more difficult to determine possible miRNA targets with high specificity (Ambros, 2004). Current computational methods for identifying miRNA targets do not adequately use the temporal information and thus miss important miRNAs and their mRNA targets (Schulz et al.,

2013). In our study we have focused on the binding affinity of miR-376c to 84 key mRNAs involved in BC. The list includes genes involved in tumor classification, commonly affected signaling pathways, such as apoptosis, angiogenesis, proliferation and processes such as adhesion, proteolysis, and cell cycle. The results showed 31 potential mRNA targets with potential binding capacity to miR-376c using mRNA arrays. Since the mRNA arrays used only contained 84 mRNAs the selection of potential mRNA targets for miR376c was of course limited alluding to the fact that some mRNAs with potential binding affinity to the miR-376c were missed. However, the most BC relevant mRNA could be screened based on the assembly of the array cards. Undeniably, the use of the next generation sequencing would be better due to its assessment of a much broader mRNA profile, but this method is time consuming and expensive.

### **6.3. Impact of miR-376c on cell proliferation and apoptosis**

MiR-376c was shown previously to be up-regulated in BC (Cuk et al., 2013a; Lasithiotaki et al., 2017; Zhou et al., 2015). In BC, acute myeloid leukemia, colon cancer, glioblastoma, ovarian cancer, and gastric cancer, miR-376c can promote tumorigenesis or metastasis by enhancing cell proliferation, migration and survival, indicating a complex role of this miRNA in different malignancies (Agrawal et al., 2014; Huo et al., 2016; Lasithiotaki et al., 2017; Vychytilova-Faltejskova et al., 2016). In our study it is also shown that miR-376c is upregulated however there was no indication that miR-376c has significant impact on cell proliferation or apoptosis.

#### 6.4. EV shuttle

In this part of the study experiments were dedicated to study the shuttle of EVs between cells. First, an EV sample was measured with NTA. The results showed that preparations contained a mixture of exosomes and bigger microvesicles with a size from 10 to 300 nm. The majority of the vesicles had a size of 120 nm. Recent publication identified two exosome subpopulations (large exosome vesicles of 90-120 nm and small exosome vesicles of 60-80 nm). The authors discovered a population of non-membranous nanoparticles and called them ‘exomeres’ (approximately 35 nm) (Zhang et al., 2018a). In this PhD study, the presence of both exosomes and bigger microvesicles and probably also exomeres were detected. The PHK26 dye stains membranes therefore exomeres as non-membranous vesicles couldn’t be detected. Moreover, current limitations are heterogeneity and the composition of secreted microvesicles and exosomes populations. The techniques to isolate and characterize EVs include differential ultracentrifugation, immuno-affinity capture, ultrafiltration and size-exclusion chromatography, polymer-based precipitation however, they are not able to separate the single of EV populations (Chen et al., 2010; Jorgensen et al., 2015; Merchant et al., 2010; Niu et al., 2017; They et al., 2006).

Horibe et al reported the capability of the cells to uptake exosomes and compared it in 3 human carcinoma cell lines, A549 (lung), HCT116 and COLO205 (colon). They found that DiO-labeled exosome uptake increased from cell line to cell line, independently of the donor cell type. They suggested results indicate that exosomes uptake capability depends on the recipient cell type and does not depend on the donor cell type (Horibe et al., 2018). In contrast in this PhD study we also observed differences in the EVs uptake by the same cell line. Recorded videos showed the EVs were release by the cells, localized in the cell membrane and up-taken by the cells. Therefore, it can be assumed that there is a EVs shuttle between the cells, however

in this study it was not recorded the shuttle of EVs going from the inside of the cell through the medium and the membrane to the inside of another cell.

## 7. Conclusion

The data shown in this study demonstrate differentially expressed and packaged miRNA sets in BC exosomes that could serve as potentially diagnostic and therapeutic markers for BC. These specific exosomal miRNA profiles that exclusively reflect HER2-positive and TNBC as well as the different clinical parameters of BC may provide insight into the exosome biology for monitoring the disease. Moreover, miR-376c has potential binding affinity to 31 mRNAs, in particular the apoptosis inhibitor BCL2, the DNA repair and cell cycle gene BRCA1, the adhesion molecule Cadherin 1 and the cyclin-dependent kinase inhibitor 1A. However, this binding affinity has to be verified by further analysis e.g. by Western blot. There was no impact of miR-376c on cell proliferation and apoptosis. Finally, the EVs shuttle was observed through the cell membrane in a video recorded by confocal microscopy.

To summarize, these findings show that exosomes with their selective packaging of miRNAs in the HER2-positive and TNBC subgroups with different clinical parameters are able to shuttle their cargo between the cells.



## 8. Future perspectives

Further analyses are planned to investigate whether BC-associated miRNAs panel can be used as a tumor marker for the treatment course and /or target molecules in signalling pathway. The significantly deregulated exosomal miRNAs should be analysed in a higher number of plasma samples collected after treatment as well as to analyse their clinical relevance in follow-up studies. A further detailed investigation on their association with pCR and treatment arms is also required.

It will be interesting which signalling pathways can be influenced by miR-376c and targeted to assess their oncogenic function in the treatment of BC.

Whether exosomes can transfer resistance against Carboplatin is planned to be investigated by a transfer of exosomes from a Carboplatin-resistant to a sensitive recipient cell line. Until now two carboplatin resistant cell lines were created. Identification of exosomal miRNAs involved in this horizontal transfer is also planned to be performed by miRNAs array cards. Besides, empty exosomes will be loaded with miRNA-155, miR-301, miR-365 and miR-376c that in this study showed strong significances with the clinical parameters of BC patients as well as predicted pathological complete response (pCR), to evaluate their ability to transfer resistance.

## 9. Summary

Exosomes, small membrane vesicles, mediate cell-to-cell communication. Released by a donor cell, they transfer proteins, lipids and nucleic acids to another cell, resulting in modulation of the recipient cell. Tumor-derived exosomes may transform normal, wild type cells into malignant cells. MiRNAs that inhibit post-transcriptionally protein expression of their target mRNAs are assumed to be selectively packaged into exosomes and may be functionally active in the recipient cell.

In this study, the first aim was to identify particular miRNA signatures in exosomes derived from plasma of 435 HER2-positive and triple negative BC patients. First, the miRNA expression profiles were determined in exosomes derived from plasma of 15 triple-negative patients before neoadjuvant therapy using quantitative TaqMan real-time PCR-based microRNAs array cards containing 384 different miRNAs. Derived from these results, 45 miRNAs associated with different clinical parameters were then selected and mounted on miRNAs array cards that served for the quantification of exosomal miRNAs in 435 BC patients before therapy and 20 healthy women. A network of deregulated exosomal miRNAs with specific expression patterns that were also associated with clinicopathological parameters was identified in exosomes from HER2-positive and triple-negative patients. In uni- and multivariate models, miR-155 and miR-301 best predicted pathological complete response (pCR). The levels of 4 exosomal miRNAs (miR-27a, miR-155, miR-376a and miR-376c) upregulated before neoadjuvant therapy decreased to normal healthy levels after therapy. These findings may improve the stratification of patients into different risk groups and future targeted therapies. One of these most deregulated miRNAs was miR-376c detected in exosomes from BC patients. Its targets mRNAs were determined by the MirTrap system which locks the miRNA/mRNA pair into the RISC complex which can be pulled down using an antibody

against this complex. Using an mRNA array, it was found that 31 mRNAs could be bound by miR-376c. The mRNAs mostly enriched in the RISC complex were the apoptosis inhibitor BCL2, the DNA repair and cell cycle gene BRCA1, the adhesion molecule Cadherin 1 and the cyclin-dependent kinase inhibitor 1A. Functional analyses showed that miR-376c had no impact on cell proliferation and apoptosis.

Western blot and ELISA showed significantly higher levels of exosomes in plasma of BC patients than in healthy women. These findings point to an excessive secretion of exosomes in cancer patients. In addition, the size and concentration of the EVs were measured using the Nanoparticle tracking analysis. The measurements revealed that the majority of particles had a size of 120 nm. Finally, EVs were stained by a red fluorescence dye and visualized by confocal microscopy. The videos showed that EVs were released by cells, localized in the cell membrane and uptake by cells.

In conclusion, these findings suggest a selective packaging of miRNAs in exosomes from HER2-positive and triple-negative breast cancer patients which is also associated with the different clinical parameters. It is hypothesized that these different miRNA profiles forming the cargo of exosomes may be shuttled from cell to cell.

## 10. Zusammenfassung

Exosomen, kleine Membranvesikel, vermitteln die Kommunikation von Zelle zu Zelle. Sie werden von einer Donorzelle freigesetzt und transportieren Proteine, Lipide und Nukleinsäuren in eine andere Zelle, was zu einer Modulation der Empfängerzelle führt. Vom Tumor befreite Exosomen können normale Wildtypzellen in bösartige Zellen umwandeln. Es wird angenommen, dass miRNAs, die die post-transkriptionelle Proteinexpression ihrer Ziel-mRNAs hemmen, selektiv in Exosomen verpackt werden und in der Empfängerzelle funktionell aktiv sein können.

In dieser Studie war das erste Ziel, bestimmte miRNA-Signaturen in Exosomen aus dem Plasma von 435 HER2-positiven und triple-negativen Brustkrebspatientinnen zu identifizieren. Zuerst wurden die miRNA-Expressionsprofile in Exosomen aus dem Plasma von 15 triple-negativen Patienten vor einer neoadjuvanten Therapie unter Verwendung quantitativer TaqMan real-time PCR-basierter mikroRNA-Array-Karten mit 384 verschiedenen miRNAs bestimmt. Basierend auf diesen Ergebnissen wurden dann 45 miRNAs, die mit den verschiedenen klinischen Parametern assoziiert waren, ausgewählt und auf miRNA-Array-Karten angebracht, die zur Quantifizierung exosomaler miRNAs bei 435 Brustkrebspatientinnen vor Therapie und 20 gesunden Frauen dienten. Ein Netzwerk von deregulierten exosomalen miRNAs mit spezifischen Expressionsmustern, die auch mit den klinisch-pathologischen Parametern assoziiert waren, wurde in Exosomen von HER2-positiven und triple-negativen Patientinnen identifiziert. In uni- und multivariaten Modellen prognostizierten miR-155 und miR-301 am besten die pathologische Response (pCR). Die Konzentrationen von 4 exosomalen miRNAs (miR-27a, miR-155, miR-376a und miR-376c), die vor der neoadjuvanten Therapie hochreguliert waren, verkleinerten sich auf normale gesunde Werte nach der Therapie. Diese Ergebnisse könnten die Stratifizierung von Patienten in verschiedene Risikogruppen und

zukünftige zielgerichtete Therapien verbessern. Eine dieser am häufigsten deregulierten miRNAs war miR-376c, die in Exosomen von Brustkrebspatientinnen nachgewiesen wurde. Seine Ziel-mRNAs wurden durch das MirTrap-System bestimmt, das das miRNA/mRNA-Paar in den RISC-Komplex aufnimmt, und der dann mithilfe eines Antikörpers gegen diesen Komplex isoliert werden kann. Unter Verwendung eines mRNA-Arrays wurden 31 mRNAs, die durch miR-376c gebunden werden konnten, gefunden. Die im RISC-Komplex meist angereicherten mRNAs waren der Apoptose-Inhibitor BCL2, das DNA-Reparatur- und Zellzyklus-Gen BRCA1, das Adhäsionsmolekül Cadherin 1 und der Cyclin-abhängige Kinase-Inhibitor 1A. Funktionelle Analysen zeigten, dass miR-376c keinen Einfluss auf Zellproliferation und Apoptose hatte.

Western Blot und ELISA präsentierten signifikant höhere Exosomen-Niveaus im Plasma von Brustkrebspatientinnen als bei gesunden Frauen. Diese Befunde weisen auf eine exzessive Sekretion von Exosomen bei Krebspatienten hin. Zusätzlich wurden die Größe und Konzentration der Exosomen unter Verwendung der Nanopartikel-Tracking-Analyse gemessen. Die Messungen zeigten, dass die Mehrzahl der Partikel eine Größe von 120 nm aufwies. Schließlich wurden die Exosomen durch einen roten Fluoreszenzfarbstoff gefärbt und durch konfokale Mikroskopie sichtbar gemacht. Die Videos zeigten, dass EVs von Zellen freigesetzt wurden, in der Zellmembran lokalisiert waren und von Zellen aufgenommen wurden.

Zusammenfassend schlagen diese Ergebnisse eine selektive Verpackung von miRNAs in Exosomen von HER2-positiven und triple-negativen Brustkrebspatientinnen vor, die ebenfalls mit den unterschiedlichen klinischen Parametern assoziiert ist. Es wird vermutet, dass diese verschiedenen miRNA-Profile, die die Fracht von Exosomen bilden, von Zelle zu Zelle transportiert werden können.

## 11. List of Abbreviations

%	Percent
°C	Celsius Degree
7AAD	7-Aminoactinomycin D
ac-pre-miR	Argonaute-2 Cleaved Precursor miRNA
AGO2	Argonaute-2
AJCC	American Joint Committee on Cancer
AKT	Protein Kinase B
ANOVA	Analysis of Variance
ATCC	American Type Culture Collection
AUC	Area under the curve
BC	Breast Cancer
BL1	Basal-like 2 subtypes
BL2	Basal-like 2 subtypes
BME	Basement Membrane Extract
bp	Basepair
BRCA1	Breast Cancer, early onset 1
BRCA2	Breast Cancer, early onset 2
BSA	Bovine Serum Albumin
cDNA	Complementary DNA
CK	Cytokeratin
CO <sub>2</sub>	Carbon Dioxide
Cq	Cycle of Quantification
DCIS	Ductal carcinoma <i>in situ</i>

DGCR8	DiGeorge Critical Region8
DSMZ	Deutsche Sammlung von Mikroorganismen und Zellkulturen GmbH
EE	Early endosomes
EGFR	Epidermal Growth Factor Receptor
EMT	Epithelial-Mesenchymal Transition
EMT	Epithelial to esenchymal transition
ERK1/2	Extracellular Signal-regulated Kinases
ESCRT	Endosomal sorting complex
EV	Extracellular vesicles
FACS	Fluorescence-activated Cell Sorting
FCS	Fetal Calf Serum
FOXM1	Forkhead Box Protein M1
G	Grading
g	Gram
GAPDH	Glyceraldehyde 3-Phosphate Dehydrogenase
h	Hour
H2O2	Hydrogen Peroxide
HCl	Hydrochloric Acid
HDL	High Density Lipoproteins
hnRNPA2B1	Heterogeneous Nuclear Ribonucleoprotein A2B1
HRP	Horseradish Peroxidase
HSC 70	Heat Shock Cognate 70kDa Kilodalton
IHC	Immunohistochemistry
ILV	Interluminal vesicles
IM	Immunomodulatory subtype
LAR	Luminal androgen receptor subtype

LCIS	Lobular carcinoma <i>in situ</i>
M	Mesenchymal subtype
M	Metastases
M0	No Distant Metastasis
M1	Distant Metastasis
MC	Mucinous Carcinoma
MET	Mesenchymal-Epithelial Transition
MET	Mesenchymal to epithelial transition
mg	Milligram
MHC	Major Histocompatibility Complex
min	Minute
miR	MicroRNA
mL	Milliliter
mM	Millimole
mRNA	Messenger Ribonucleic Acid
MSL	Mesenchymal stem-like subtype
MTT	3-(4, 5-Dimethylthiazol-2-yl)-2, 5-Diphenyltetrazolium Bromide
MVBs	Multivesicular Bodies
MVEs	Multivesicular Endosomes
N	Regional lymph nodes
N0	No Lymph Node Metastasis
N1	Lymph Node Metastasis
nm	Nanometer
NTA	Nanoparticles tracking analysis
OD	Optical Density
OS	Overall Survival



PBS	Phosphate Buffered Saline
PCR	Polymerase Chain Reaction
pCR	Pathological complete response
pH	Hydrogen Ion Concentration
PM,	Non-carboplatin treatment arm.
PMCb,	Carboplatin treatment arm.
pre-miRNA	Precursor microRNA
pri-miRNA	Primary microRNA
PVDF	Polyvinylidene Fluoride
qPCR	Quantitative Polymerase Chain Reaction
RIPA	Radioimmunoprecipitation Assay
RISC	RNA-Induced Silencing Complex
RNA	Ribonucleic acid
RNase	Ribonuclease
ROC	Receiver Operating Characteristic
RT	Reverse Transcription
SDS-PAGE	Sodium Dodecyl Sulfate-Polyacrylamide Gel Electrophoresis
Secs	Seconds
SPSS	Statistical Product and Service Solutions
SYBR	Synergy Brands
T	Primary tumor
Taq	Thermus Aquaticus
TBST	Tris-Buffered Saline Tween
TMB	3,3',5,5'-Tetramethylbenzidine
TNBC	Triple negative breast cancer
TRBP	Tar-RNA Binding Protein

UTR	Untranslated Region
V	Voltage
$\mu\text{g}$	Microgram
$\mu\text{L}$	Microliter
$\mu\text{M}$	Micromole
$\mu\text{m}$	Micrometer

## 12. References

- Abdelfattah, A.M., Park, C., and Choi, M.Y. (2014). Update on non-canonical microRNAs. *Biomolecular concepts* 5, 275-287.
- Adams, L. (2017). Non-coding RNA: Pri-miRNA processing: structure is key. *Nat Rev Genet* 18, 145.
- Agrawal, R., Pandey, P., Jha, P., Dwivedi, V., Sarkar, C., and Kulshreshtha, R. (2014). Hypoxic signature of microRNAs in glioblastoma: insights from small RNA deep sequencing. *BMC Genomics* 15, 686.
- Alderton, G.K. (2012). Metastasis. Exosomes drive premetastatic niche formation. *Nat Rev Cancer* 12, 447.
- Ali, S., and Coombes, R.C. (2002). Endocrine-responsive breast cancer and strategies for combating resistance. *Nat Rev Cancer* 2, 101-112.
- Ambros, V. (2004). The functions of animal microRNAs. *Nature* 431, 350-355.
- Bartels, C.L., and Tsongalis, G.J. (2009). MicroRNAs: novel biomarkers for human cancer. *Clin Chem* 55, 623-631.
- Bebelman, M.P., Smit, M.J., Pegtel, D.M., and Baglio, S.R. (2018). Biogenesis and function of extracellular vesicles in cancer. *Pharmacol Ther.*
- Bellingham, S.A., Guo, B.B., Coleman, B.M., and Hill, A.F. (2012). Exosomes: vehicles for the transfer of toxic proteins associated with neurodegenerative diseases? *Frontiers in physiology* 3, 124.
- Bertoli, G., Cava, C., and Castiglioni, I. (2015). MicroRNAs: New Biomarkers for Diagnosis, Prognosis, Therapy Prediction and Therapeutic Tools for Breast Cancer. *Theranostics* 5, 1122-1143.

Biswas, T., Efirid, J.T., Prasad, S., Jindal, C., and Walker, P.R. (2017). The survival benefit of neoadjuvant chemotherapy and pCR among patients with advanced stage triple negative breast cancer. *Oncotarget* 8, 112712-112719.

Bocker, W. (2002). [WHO classification of breast tumors and tumors of the female genital organs: pathology and genetics]. *Verh Dtsch Ges Pathol* 86, 116-119.

Borchert, G.M., Lanier, W., and Davidson, B.L. (2006). RNA polymerase III transcribes human microRNAs. *Nat Struct Mol Biol* 13, 1097-1101.

Calin, G.A., Dumitru, C.D., Shimizu, M., Bichi, R., Zupo, S., Noch, E., Aldler, H., Rattan, S., Keating, M., Rai, K., *et al.* (2002). Frequent deletions and down-regulation of micro-RNA genes miR15 and miR16 at 13q14 in chronic lymphocytic leukemia. *P Natl Acad Sci USA* 99, 15524-15529.

Calin, G.A., Sevignani, C., Dan Dumitru, C., Hyslop, T., Noch, E., Yendamuri, S., Shimizu, M., Rattan, S., Bullrich, F., Negrini, M., *et al.* (2004). Human microRNA genes are frequently located at fragile sites and genomic regions involved in cancers. *P Natl Acad Sci USA* 101, 2999-3004.

Chambers, A.F., Groom, A.C., and MacDonald, I.C. (2002). Dissemination and growth of cancer cells in metastatic sites. *Nat Rev Cancer* 2, 563-572.

Chen, C., Skog, J., Hsu, C.H., Lessard, R.T., Balaj, L., Wurdinger, T., Carter, B.S., Breakefield, X.O., Toner, M., and Irimia, D. (2010). Microfluidic isolation and transcriptome analysis of serum microvesicles. *Lab Chip* 10, 505-511.

Cloonan, N. (2015). Re-thinking miRNA-mRNA interactions: intertwining issues confound target discovery. *Bioessays* 37, 379-388.

Colombo, M., Raposo, G., and Thery, C. (2014). Biogenesis, secretion, and intercellular interactions of exosomes and other extracellular vesicles. *Annu Rev Cell Dev Biol* 30, 255-289.

Corcoran, C., Friel, A.M., Duffy, M.J., Crown, J., and O'Driscoll, L. (2011). Intracellular and extracellular microRNAs in breast cancer. *Clin Chem* 57, 18-32.

Cuk, K., Zucknick, M., Heil, J., Madhavan, D., Schott, S., Turchinovich, A., Arlt, D., Rath, M., Sohn, C., Benner, A., *et al.* (2013a). Circulating microRNAs in plasma as early detection markers for breast cancer. *Int J Cancer* *132*, 1602-1612.

Cuk, K., Zucknick, M., Madhavan, D., Schott, S., Golatta, M., Heil, J., Marme, F., Turchinovich, A., Sinn, P., Sohn, C., *et al.* (2013b). Plasma microRNA panel for minimally invasive detection of breast cancer. *PLoS One* *8*, e76729.

Curigliano, G., Burstein, H.J., E, P.W., Gnant, M., Dubsy, P., Loibl, S., Colleoni, M., Regan, M.M., Piccart-Gebhart, M., Senn, H.J., *et al.* (2017). De-escalating and escalating treatments for early-stage breast cancer: the St. Gallen International Expert Consensus Conference on the Primary Therapy of Early Breast Cancer 2017. *Annals of oncology : official journal of the European Society for Medical Oncology* *28*, 1700-1712.

Cutuli, B., De Lafontan, B., Kirova, Y., Auvray, H., Tallet, A., Avigdor, S., Brunaud, C., and Delva, C. (2015). Lobular carcinoma in situ (LCIS) of the breast: is long-term outcome similar to ductal carcinoma in situ (DCIS)? Analysis of 200 cases. *Radiat Oncol* *10*, 110.

Edge, S.B., and Compton, C.C. (2010). The American Joint Committee on Cancer: the 7th edition of the AJCC cancer staging manual and the future of TNM. *Ann Surg Oncol* *17*, 1471-1474.

Eichelser, C., Stuckrath, I., Muller, V., Milde-Langosch, K., Wikman, H., Pantel, K., and Schwarzenbach, H. (2014). Increased serum levels of circulating exosomal microRNA-373 in receptor-negative breast cancer patients. *Oncotarget* *5*, 9650-9663.

Ernster, V.L., Ballard-Barbash, R., Barlow, W.E., Zheng, Y., Weaver, D.L., Cutter, G., Yankaskas, B.C., Rosenberg, R., Carney, P.A., Kerlikowske, K., *et al.* (2002). Detection of ductal carcinoma in situ in women undergoing screening mammography. *J Natl Cancer Inst* *94*, 1546-1554.

Ferlay, J., Soerjomataram, I., Dikshit, R., Eser, S., Mathers, C., Rebelo, M., Parkin, D.M., Forman, D., and Bray, F. (2015). Cancer incidence and mortality worldwide: sources, methods and major patterns in GLOBOCAN 2012. *Int J Cancer* *136*, E359-386.

Filipowicz, W., Bhattacharyya, S.N., and Sonenberg, N. (2008). Mechanisms of post-transcriptional regulation by microRNAs: are the answers in sight? *Nat Rev Genet* *9*, 102-114.

Friedlander, M.R., Lizano, E., Houben, A.J., Bezdan, D., Banez-Coronel, M., Kudla, G., Mateu-Huertas, E., Kagerbauer, B., Gonzalez, J., Chen, K.C., *et al.* (2014). Evidence for the biogenesis of more than 1,000 novel human microRNAs. *Genome Biol* *15*, R57.

Friedman, R.C., Farh, K.K., Burge, C.B., and Bartel, D.P. (2009). Most mammalian mRNAs are conserved targets of microRNAs. *Genome Res* *19*, 92-105.

Fu, S.W., Chen, L., and Man, Y.G. (2011). miRNA Biomarkers in Breast Cancer Detection and Management. *J Cancer* *2*, 116-122.

Garzon, R., Marcucci, G., and Croce, C.M. (2010). Targeting microRNAs in cancer: rationale, strategies and challenges. *Nat Rev Drug Discov* *9*, 775-789.

Goldhirsch, A., Winer, E.P., Coates, A.S., Gelber, R.D., Piccart-Gebhart, M., Thurlimann, B., Senn, H.J., and Panel, m. (2013). Personalizing the treatment of women with early breast cancer: highlights of the St Gallen International Expert Consensus on the Primary Therapy of Early Breast Cancer 2013. *Annals of oncology : official journal of the European Society for Medical Oncology* *24*, 2206-2223.

Goldhirsch, A., Wood, W.C., Coates, A.S., Gelber, R.D., Thurlimann, B., Senn, H.J., and Panel, m. (2011). Strategies for subtypes--dealing with the diversity of breast cancer: highlights of the St. Gallen International Expert Consensus on the Primary Therapy of Early Breast Cancer 2011. *Annals of oncology : official journal of the European Society for Medical Oncology* *22*, 1736-1747.

- Hannafon, B.N., Carpenter, K.J., Berry, W.L., Janknecht, R., Dooley, W.C., and Ding, W.Q. (2015). Exosome-mediated microRNA signaling from breast cancer cells is altered by the anti-angiogenesis agent docosahexaenoic acid (DHA). *Mol Cancer* *14*, 133.
- Harbeck, N., and Gluz, O. (2017). Neoadjuvant therapy for triple negative and HER2-positive early breast cancer. *Breast* *34 Suppl 1*, S99-S103.
- He, X.H., Zhu, W., Yuan, P., Jiang, S., Li, D., Zhang, H.W., and Liu, M.F. (2016). miR-155 downregulates ErbB2 and suppresses ErbB2-induced malignant transformation of breast epithelial cells. *Oncogene* *35*, 6015-6025.
- Heman-Ackah, S.M., Hallegger, M., Rao, M.S., and Wood, M.J. (2013). RISC in PD: the impact of microRNAs in Parkinson's disease cellular and molecular pathogenesis. *Frontiers in molecular neuroscience* *6*, 40.
- Henne, W.M., Buchkovich, N.J., and Emr, S.D. (2011). The ESCRT pathway. *Dev Cell* *21*, 77-91.
- Hessvik, N.P., and Llorente, A. (2018). Current knowledge on exosome biogenesis and release. *Cell Mol Life Sci* *75*, 193-208.
- Hessvik, N.P., Phuyal, S., Brech, A., Sandvig, K., and Llorente, A. (2012). Profiling of microRNAs in exosomes released from PC-3 prostate cancer cells. *Biochim Biophys Acta* *1819*, 1154-1163.
- Ho, J.Y., Hsu, R.J., Liu, J.M., Chen, S.C., Liao, G.S., Gao, H.W., and Yu, C.P. (2017). MicroRNA-382-5p aggravates breast cancer progression by regulating the RERG/Ras/ERK signaling axis. *Oncotarget* *8*, 22443-22459.
- Horibe, S., Tanahashi, T., Kawauchi, S., Murakami, Y., and Rikitake, Y. (2018). Mechanism of recipient cell-dependent differences in exosome uptake. *BMC Cancer* *18*, 47.
- Hu, X., Wang, J., He, W., Zhao, P., and Ye, C. (2018). MicroRNA-433 targets AKT3 and inhibits cell proliferation and viability in breast cancer. *Oncol Lett* *15*, 3998-4004.

- Huo, D., Clayton, W.M., Yoshimatsu, T.F., Chen, J., and Olopade, O.I. (2016). Identification of a circulating microRNA signature to distinguish recurrence in breast cancer patients. *Oncotarget* 7, 55231-55248.
- Huotari, J., and Helenius, A. (2011). Endosome maturation. *EMBO J* 30, 3481-3500.
- Hwang, H.W., and Mendell, J.T. (2007). MicroRNAs in cell proliferation, cell death, and tumorigenesis. *Br J Cancer* 96 *Suppl*, R40-44.
- Jin, L., Wessely, O., Marcusson, E.G., Ivan, C., Calin, G.A., and Alahari, S.K. (2013). Prooncogenic factors miR-23b and miR-27b are regulated by Her2/Neu, EGF, and TNF-alpha in breast cancer. *Cancer Res* 73, 2884-2896.
- Johnstone, R.M., Adam, M., Hammond, J.R., Orr, L., and Turbide, C. (1987). Vesicle formation during reticulocyte maturation. Association of plasma membrane activities with released vesicles (exosomes). *J Biol Chem* 262, 9412-9420.
- Josse, S.A., Gorges, T.M., and Pantel, K. (2015). Biology, detection, and clinical implications of circulating tumor cells. *EMBO Mol Med* 7, 1-11.
- Jorgensen, M.M., Baek, R., and Varming, K. (2015). Potentials and capabilities of the Extracellular Vesicle (EV) Array. *J Extracell Vesicles* 4, 26048.
- Jung, T., Castellana, D., Klingbeil, P., Cuesta Hernandez, I., Vitacolonna, M., Orlicky, D.J., Roffler, S.R., Brodt, P., and Zoller, M. (2009). CD44v6 dependence of premetastatic niche preparation by exosomes. *Neoplasia* 11, 1093-1105.
- Jurkovicova, D., Magyerkova, M., Sestakova, Z., Copakova, L., Bella, V., Konecny, M., Krivjanska, M., Kulcsar, L., and Chovanec, M. (2016). Evaluation of expression profiles of microRNAs and two target genes, FOXO3a and RUNX2, effectively supports diagnostics and therapy predictions in breast cancer. *Neoplasma* 63, 941-951.
- Kirschner, M.B., Kao, S.C., Edelman, J.J., Armstrong, N.J., Vallely, M.P., van Zandwijk, N., and Reid, G. (2011). Haemolysis during sample preparation alters microRNA content of plasma. *PLoS One* 6, e24145.



Kodahl, A.R., Lyng, M.B., Binder, H., Cold, S., Gravgaard, K., Knoop, A.S., and Ditzel, H.J. (2014). Novel circulating microRNA signature as a potential non-invasive multi-marker test in ER-positive early-stage breast cancer: a case control study. *Mol Oncol* 8, 874-883.

Kong, L.Y., Xue, M., Zhang, Q.C., and Su, C.F. (2017). In vivo and in vitro effects of microRNA-27a on proliferation, migration and invasion of breast cancer cells through targeting of SFRP1 gene via Wnt/beta-catenin signaling pathway. *Oncotarget* 8, 15507-15519.

Kong, W., He, L., Coppola, M., Guo, J., Esposito, N.N., Coppola, D., and Cheng, J.Q. (2010). MicroRNA-155 regulates cell survival, growth, and chemosensitivity by targeting FOXO3a in breast cancer. *J Biol Chem* 285, 17869-17879.

Krek, A., Grun, D., Poy, M.N., Wolf, R., Rosenberg, L., Epstein, E.J., MacMenamin, P., da Piedade, I., Gunsalus, K.C., Stoffel, M., *et al.* (2005). Combinatorial microRNA target predictions. *Nat Genet* 37, 495-500.

Lamouille, S., Xu, J., and Derynck, R. (2014). Molecular mechanisms of epithelial-mesenchymal transition. *Nat Rev Mol Cell Biol* 15, 178-196.

Lasithiotaki, I., Tsitoura, E., Koutsopoulos, A., Lagoudaki, E., Koutoulaki, C., Pitsidianakis, G., Spandidos, D.A., Siafakas, N.M., Sourvinos, G., and Antoniou, K.M. (2017). Aberrant expression of miR-21, miR-376c and miR-145 and their target host genes in Merkel cell polyomavirus-positive non-small cell lung cancer. *Oncotarget* 8, 112371-112383.

Lee, Y., Kim, M., Han, J., Yeom, K.H., Lee, S., Baek, S.H., and Kim, V.N. (2004). MicroRNA genes are transcribed by RNA polymerase II. *EMBO J* 23, 4051-4060.

Lehmann, B.D., Bauer, J.A., Chen, X., Sanders, M.E., Chakravarthy, A.B., Shyr, Y., and Pietersen, J.A. (2011). Identification of human triple-negative breast cancer subtypes and preclinical models for selection of targeted therapies. *The Journal of clinical investigation* 121, 2750-2767.

- Lettlova, S., Brynychova, V., Blecha, J., Vrana, D., Vondrusova, M., Soucek, P., and Truksa, J. (2018). MiR-301a-3p Suppresses Estrogen Signaling by Directly Inhibiting ESR1 in ERalpha Positive Breast Cancer. *Cell Physiol Biochem* 46, 2601-2615.
- Li, M., Liu, L., Zang, W., Wang, Y., Du, Y., Chen, X., Li, P., Li, J., and Zhao, G. (2015). miR365 overexpression promotes cell proliferation and invasion by targeting ADAMTS-1 in breast cancer. *Int J Oncol* 47, 296-302.
- Lu, L., Mao, X., Shi, P., He, B., Xu, K., Zhang, S., and Wang, J. (2017). MicroRNAs in the prognosis of triple-negative breast cancer: A systematic review and meta-analysis. *Medicine (Baltimore)* 96, e7085.
- Ludwig, N., Leidinger, P., Becker, K., Backes, C., Fehlmann, T., Pallasch, C., Rheinheimer, S., Meder, B., Stahler, C., Meese, E., *et al.* (2016). Distribution of miRNA expression across human tissues. *Nucleic Acids Res* 44, 3865-3877.
- Ma, F., Zhang, J., Zhong, L., Wang, L., Liu, Y., Wang, Y., Peng, L., and Guo, B. (2014). Upregulated microRNA-301a in breast cancer promotes tumor metastasis by targeting PTEN and activating Wnt/beta-catenin signaling. *Gene* 535, 191-197.
- Makki, J. (2015). Diversity of Breast Carcinoma: Histological Subtypes and Clinical Relevance. *Clin Med Insights Pathol* 8, 23-31.
- Malhotra, G.K., Zhao, X., Band, H., and Band, V. (2010). Histological, molecular and functional subtypes of breast cancers. *Cancer Biol Ther* 10, 955-960.
- Mar-Aguilar, F., Mendoza-Ramirez, J.A., Malagon-Santiago, I., Espino-Silva, P.K., Santuario-Facio, S.K., Ruiz-Flores, P., Rodriguez-Padilla, C., and Resendez-Perez, D. (2013). Serum circulating microRNA profiling for identification of potential breast cancer biomarkers. *Dis Markers* 34, 163-169.
- Martin, E.C., Conger, A.K., Yan, T.J., Hoang, V.T., Miller, D.F., Buechlein, A., Rusch, D.B., Nephew, K.P., Collins-Burow, B.M., and Burow, M.E. (2017). MicroRNA-335-5p and -

3p synergize to inhibit estrogen receptor alpha expression and promote tamoxifen resistance. *FEBS Lett* 591, 382-392.

May, D.S., Lee, N.C., Richardson, L.C., Giustozzi, A.G., and Bobo, J.K. (2000). Mammography and breast cancer detection by race and Hispanic ethnicity: results from a national program (United States). *Cancer Causes Control* 11, 697-705.

McPherson, K., Steel, C.M., and Dixon, J.M. (2000). ABC of breast diseases. Breast cancer-epidemiology, risk factors, and genetics. *BMJ* 321, 624-628.

Meng, X., Muller, V., Milde-Langosch, K., Trillsch, F., Pantel, K., and Schwarzenbach, H. (2016). Diagnostic and prognostic relevance of circulating exosomal miR-373, miR-200a, miR-200b and miR-200c in patients with epithelial ovarian cancer. *Oncotarget* 7, 16923-16935.

Merchant, M.L., Powell, D.W., Wilkey, D.W., Cummins, T.D., Deegens, J.K., Rood, I.M., McAfee, K.J., Fleischer, C., Klein, E., and Klein, J.B. (2010). Microfiltration isolation of human urinary exosomes for characterization by MS. *Proteomics Clin Appl* 4, 84-96.

Narod, S.A., and Foulkes, W.D. (2004). BRCA1 and BRCA2: 1994 and beyond. *Nat Rev Cancer* 4, 665-676.

Niu, Z., Pang, R.T.K., Liu, W., Li, Q., Cheng, R., and Yeung, W.S.B. (2017). Polymer-based precipitation preserves biological activities of extracellular vesicles from an endometrial cell line. *PLoS One* 12, e0186534.

Omarini, C., Guaitoli, G., Pipitone, S., Moscetti, L., Cortesi, L., Cascinu, S., and Piacentini, F. (2018). Neoadjuvant treatments in triple-negative breast cancer patients: where we are now and where we are going. *Cancer management and research* 10, 91-103.

Peng, Y., and Croce, C.M. (2016). The role of MicroRNAs in human cancer. *Signal Transduct Target Ther* 1, 15004.

Ren, X., Kloer, D.P., Kim, Y.C., Ghirlando, R., Saidi, L.F., Hummer, G., and Hurley, J.H. (2009). Hybrid structural model of the complete human ESCRT-0 complex. *Structure* 17, 406-416.

- Rivenbark, A.G., O'Connor, S.M., and Coleman, W.B. (2013). Molecular and cellular heterogeneity in breast cancer: challenges for personalized medicine. *Am J Pathol* *183*, 1113-1124.
- Roccaro, A.M., Sacco, A., Maiso, P., Azab, A.K., Tai, Y.T., Reagan, M., Azab, F., Flores, L.M., Campigotto, F., Weller, E., *et al.* (2013). BM mesenchymal stromal cell-derived exosomes facilitate multiple myeloma progression. *The Journal of clinical investigation* *123*, 1542-1555.
- Santos, J.C., Lima, N.D.S., Sarian, L.O., Matheu, A., Ribeiro, M.L., and Derchain, S.F.M. (2018). Exosome-mediated breast cancer chemoresistance via miR-155 transfer. *Sci Rep* *8*, 829.
- Schulz, M.H., Pandit, K.V., Lino Cardenas, C.L., Ambalavanan, N., Kaminski, N., and Bar-Joseph, Z. (2013). Reconstructing dynamic microRNA-regulated interaction networks. *Proc Natl Acad Sci U S A* *110*, 15686-15691.
- Schwarzenbach, H. (2015). The clinical relevance of circulating, exosomal miRNAs as biomarkers for cancer. *Expert Rev Mol Diagn* *15*, 1159-1169.
- Schwarzenbach, H., Machado da Silva, A., Calin, G., and Pantel, K. (2015). Data Normalization Strategies for MicroRNA Quantification. *Clin Chem*.
- Schwarzenbach, H., Nishida, N., Calin, G.A., and Pantel, K. (2014). Clinical relevance of circulating cell-free microRNAs in cancer. *Nat Rev Clin Oncol* *11*, 145-156.
- Shen, Y., Ye, Y.F., Ruan, L.W., Bao, L., Wu, M.W., and Zhou, Y. (2017). Inhibition of miR-660-5p expression suppresses tumor development and metastasis in human breast cancer. *Genet Mol Res* *16*.
- Shenouda, S.K., and Alahari, S.K. (2009). MicroRNA function in cancer: oncogene or a tumor suppressor? *Cancer Metastasis Rev* *28*, 369-378.

- Shi, W., Gerster, K., Alajez, N.M., Tsang, J., Waldron, L., Pintilie, M., Hui, A.B., Sykes, J., P'ng, C., Miller, N., *et al.* (2011). MicroRNA-301 mediates proliferation and invasion in human breast cancer. *Cancer Res* 71, 2926-2937.
- Siegel, R.L., Miller, K.D., and Jemal, A. (2017). Cancer Statistics, 2017. *CA Cancer J Clin* 67, 7-30.
- Slaby, O., Svoboda, M., Michalek, J., and Vyzula, R. (2009). MicroRNAs in colorectal cancer: translation of molecular biology into clinical application. *Mol Cancer* 8, 102.
- Stuckrath, I., Rack, B., Janni, W., Jager, B., Pantel, K., and Schwarzenbach, H. (2015). Aberrant plasma levels of circulating miR-16, miR-107, miR-130a and miR-146a are associated with lymph node metastasis and receptor status of breast cancer patients. *Oncotarget* 6, 13387-13401.
- They, C., Amigorena, S., Raposo, G., and Clayton, A. (2006). Isolation and characterization of exosomes from cell culture supernatants and biological fluids. *Curr Protoc Cell Biol Chapter 3*, Unit 3 22.
- Tricarico, C., Clancy, J., and D'Souza-Schorey, C. (2017). Biology and biogenesis of shed microvesicles. *Small GTPases* 8, 220-232.
- Tsai, J.H., and Yang, J. (2013). Epithelial-mesenchymal plasticity in carcinoma metastasis. *Genes Dev* 27, 2192-2206.
- Untch, M., Rezai, M., Loibl, S., Fasching, P.A., Huober, J., Tesch, H., Bauerfeind, I., Hilfrich, J., Eidtmann, H., Gerber, B., *et al.* (2010). Neoadjuvant treatment with trastuzumab in HER2-positive breast cancer: results from the GeparQuattro study. *Journal of clinical oncology : official journal of the American Society of Clinical Oncology* 28, 2024-2031.
- Valadi, H., Ekstrom, K., Bossios, A., Sjostrand, M., Lee, J.J., and Lotvall, J.O. (2007a). Exosome-mediated transfer of mRNAs and microRNAs is a novel mechanism of genetic exchange between cells. *Nat Cell Biol* 9, 654-U672.

Valadi, H., Ekstrom, K., Bossios, A., Sjostrand, M., Lee, J.J., and Lotvall, J.O. (2007b). Exosome-mediated transfer of mRNAs and microRNAs is a novel mechanism of genetic exchange between cells. *Nat Cell Biol* 9, 654-659.

Venkitaraman, A.R. (2001). Functions of BRCA1 and BRCA2 in the biological response to DNA damage. *J Cell Sci* 114, 3591-3598.

Visvader, J.E., and Stingl, J. (2014). Mammary stem cells and the differentiation hierarchy: current status and perspectives. *Genes Dev* 28, 1143-1158.

von Minckwitz, G., Loibl, S., Untch, M., Eidtmann, H., Rezai, M., Fasching, P.A., Tesch, H., Eggemann, H., Schrader, I., Kittel, K., *et al.* (2014a). Survival after neoadjuvant chemotherapy with or without bevacizumab or everolimus for HER2-negative primary breast cancer (GBG 44-GeparQuinto) dagger. *Annals of oncology : official journal of the European Society for Medical Oncology* 25, 2363-2372.

von Minckwitz, G., and Martin, M. (2012). Neoadjuvant treatments for triple-negative breast cancer (TNBC). *Annals of oncology : official journal of the European Society for Medical Oncology* 23 Suppl 6, vi35-39.

von Minckwitz, G., Schneeweiss, A., Loibl, S., Salat, C., Denkert, C., Rezai, M., Blohmer, J.U., Jackisch, C., Paepke, S., Gerber, B., *et al.* (2014b). Neoadjuvant carboplatin in patients with triple-negative and HER2-positive early breast cancer (GeparSixto; GBG 66): a randomised phase 2 trial. *Lancet Oncol* 15, 747-756.

Vychytilova-Faltejskova, P., Radova, L., Sachlova, M., Kosarova, Z., Slaba, K., Fabian, P., Grolich, T., Prochazka, V., Kala, Z., Svoboda, M., *et al.* (2016). Serum-based microRNA signatures in early diagnosis and prognosis prediction of colon cancer. *Carcinogenesis* 37, 941-950.

Walsh, T., Lee, M.K., Casadei, S., Thornton, A.M., Stray, S.M., Pennil, C., Nord, A.S., Mandell, J.B., Swisher, E.M., and King, M.C. (2010). Detection of inherited mutations for

breast and ovarian cancer using genomic capture and massively parallel sequencing. *Proc Natl Acad Sci U S A* *107*, 12629-12633.

Wang, K., Jin, J., Ma, T., and Zhai, H. (2017). MiR-376c-3p regulates the proliferation, invasion, migration, cell cycle and apoptosis of human oral squamous cancer cells by suppressing HOXB7. *Biomed Pharmacother* *91*, 517-525.

Wen, C., Seeger, R.C., Fabbri, M., Wang, L., Wayne, A.S., and Jong, A.Y. (2017). Biological roles and potential applications of immune cell-derived extracellular vesicles. *J Extracell Vesicles* *6*, 1400370.

Willms, E., Cabanas, C., Mager, I., Wood, M.J.A., and Vader, P. (2018). Extracellular Vesicle Heterogeneity: Subpopulations, Isolation Techniques, and Diverse Functions in Cancer Progression. *Front Immunol* *9*, 738.

Winter, J., Jung, S., Keller, S., Gregory, R.I., and Diederichs, S. (2009). Many roads to maturity: microRNA biogenesis pathways and their regulation. *Nat Cell Biol* *11*, 228-234.

Wolf, P. (1967). The nature and significance of platelet products in human plasma. *Br J Haematol* *13*, 269-288.

Wuerstlein, R., and Harbeck, N. (2017). Neoadjuvant Therapy for HER2-positive Breast Cancer. *Reviews on recent clinical trials* *12*, 81-92.

Yamamoto, M., Kondo, E., Takeuchi, M., Harashima, A., Otani, T., Tsuji-Takayama, K., Yamasaki, F., Kumon, H., Kibata, M., and Nakamura, S. (2011). miR-155, a Modulator of FOXO3a Protein Expression, Is Underexpressed and Cannot Be Upregulated by Stimulation of HOZOT, a Line of Multifunctional Treg. *PLoS One* *6*, e16841.

Yoshikawa, M., Iinuma, H., Umemoto, Y., Yanagisawa, T., Matsumoto, A., and Jinno, H. (2018). Exosome-encapsulated microRNA-223-3p as a minimally invasive biomarker for the early detection of invasive breast cancer. *Oncol Lett* *15*, 9584-9592.

Zhang, H., Freitas, D., Kim, H.S., Fabijanic, K., Li, Z., Chen, H., Mark, M.T., Molina, H., Martin, A.B., Bojmar, L., *et al.* (2018a). Identification of distinct nanoparticles and subsets

of extracellular vesicles by asymmetric flow field-flow fractionation. *Nat Cell Biol* 20, 332-343.

Zhang, J., Li, S., Li, L., Li, M., Guo, C., Yao, J., and Mi, S. (2015). Exosome and exosomal microRNA: trafficking, sorting, and function. *Genomics Proteomics Bioinformatics* 13, 17-24.

Zhang, T., Jiang, K., Zhu, X., Zhao, G., Wu, H., Deng, G., and Qiu, C. (2018b). miR-433 inhibits breast cancer cell growth via the MAPK signaling pathway by targeting Rap1a. *Int J Biol Sci* 14, 622-632.

Zhang, Y. (2005). miRU: an automated plant miRNA target prediction server. *Nucleic Acids Res* 33, W701-704.

Zhao, L., Liu, W., Xiao, J., and Cao, B. (2015). The role of exosomes and "exosomal shuttle microRNA" in tumorigenesis and drug resistance. *Cancer Lett* 356, 339-346.

Zhao, M., Ang, L., Huang, J., and Wang, J. (2017). MicroRNAs regulate the epithelial-mesenchymal transition and influence breast cancer invasion and metastasis. *Tumour Biol* 39, 1010428317691682.

Zhong, S., Chen, X., Wang, D., Zhang, X., Shen, H., Yang, S., Lv, M., Tang, J., and Zhao, J. (2016). MicroRNA expression profiles of drug-resistance breast cancer cells and their exosomes. *Oncotarget* 7, 19601-19609.

Zhou, J., Gong, G., Tan, H., Dai, F., Zhu, X., Chen, Y., Wang, J., Liu, Y., Chen, P., Wu, X., *et al.* (2015). Urinary microRNA-30a-5p is a potential biomarker for ovarian serous adenocarcinoma. *Oncol Rep* 33, 2915-2923.

Zou, Y., Chen, Y., Yao, S., Deng, G., Liu, D., Yuan, X., Liu, S., Rao, J., Xiong, H., Yuan, X., *et al.* (2018). MiR-422a weakened breast cancer stem cells properties by targeting PLP2. *Cancer Biol Ther* 19, 436-444.



### 13. Acknowledgments

The list of people I feel grateful to is endless, but I would like to start with my supervisor PD Dr. Heidi Schwarzenbach for providing me with an interesting PhD topic as well as her continuous support of my PhD study.

I would like to thank Prof. Dr. Klaus Pantel for all of his precious support and help as well as for giving me an opportunity to join the Institute, and use the laboratory and research facilities whenever needed.

I also owe a debt of gratitude to Prof. Dr. Seitz for the selfless support he offered me at the very beginning of my PhD study and helping me with my first steps in Hamburg.

Besides my supervisor, I would like to thank my co-supervisor Prof. Dr. Julia Kehr for her support, as well as the rest of my thesis committee: Prof. Wim Walter, Prof. Dr.med Friedrich Koch-Nolte and PD Dr. Harwig Lüthen for their insightful comments.

During the early stages of this project, it became quite clear to me that a researcher cannot complete a PhD thesis on their own. Although the list of individuals I wish to thank extends beyond the limits of this format, I would still like to emphasize my gratitude to my colleagues from the Dr. Schwarzenbach lab, Chi and Qintao, especially to Bettina, Christine, Magda, Sara and Silke who have been extremely helpful during all these years. Working with you was a great pleasure, but your advice, friendship and all those wonderful times outside of the lab is what I am thankful for the most.

I want to express my eternal gratitude to all the staff at the Institute of Tumor Biology for being there for me and their helpfulness, technical, professional and moral support, as well as consistent encouragement. Thank you for everything, Sandra, Roswitha, Antje, Connie, Desiree and Anna.

Special thanks go to Prof. Dr. Sonja Loges for all of her help and motivational talks we had.

Also I owe one my gratitude to Linda who helped me with writing and proofreading, and all of her kind advice, suggestions and words of encouragement during these past years.

I cannot go without thanking my friends at the Institute for their unconditional friendship, talks, and all the great moments we shared. A special thanks to my ITB girls Pari, Katharina, Svenja, Lena, Sonja, Johanna, Jana, Leonie and our only boy Sebastian. It was a great pleasure to spend these years with you. When I thought I could not reach my goals, you always supported me and kept me going. All your love made me feel like at home.

I also feel the need to express my appreciation for the people who worked with me on all of my experiments as I could always rely on the kind and professional assistance of Dr. Christian Pick who helped me with data analysis, the group of Prof. Dr. Tanja Zeller and the unconditional patience of Tim who constantly changed the PCR block for me, as well as Susanne Roscher and the entire FACS core facility for helpful advice and useful guidelines that helped me conduct my experiments.

Live imaging experiments would not have been possible without Dr. Antonio Virgilio Faila and Dr. Bernd Zodiak and their ongoing support, advice, patience and generous help. Jill, Sabrina and Alexander Hartman, I greatly appreciate all the input and help you have given me regarding the ultracentrifuge and nanoparticle tracking analysis.

Last but not least, I would like to thank my dear parents and brother for all their unconditional love and endless support, especially my mother for all the things she has done for me since day one. Without her, I would not be the person I am now. I cannot thank her enough for encouraging me throughout this experience.

## **14. Eidesstattliche Versicherung**

Hiermit erkläre ich an Eides statt, dass ich die vorliegende Dissertationsschrift selbst verfasst und keine anderen als die angegebenen Quellen und Hilfsmittel benutzt habe.

Hamburg, den 28.09.2018

## **15. Declaration on oath**

I hereby declare, on oath that I have written the present dissertation by my own and have not used other than acknowledged resources and aid.

Hamburg, 28.09.2018